# Armed Services Technical Information Agency

AD 30192

## UNIVERSITY OF CALIFORNIA

### INSTITUTE OF ENGINEERING RESEARCH

### BERKELEY CALIFORNIA
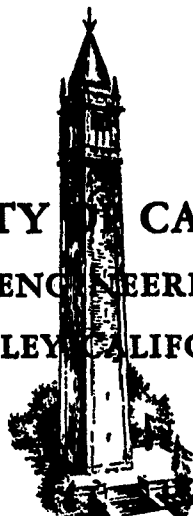
---

AN EXPERIMENTAL MOLECULAR BEAM INVESTIGATION
OF THE SCATTERING OF MOLECULES FROM SURFACES

---

by

F. C. HURLBUT

SERIES NO. ........... 20 ...........

ISSUE NO. ........... 98 ...........

DATE ........... DECEMBER 1, 1953 ...........

FLUID FLOW AND
HEAT   TRANSFER
AT LOW PRESSURES
AND TEMPERATURE

---

# AN EXPERIMENTAL MOLECULAR BEAM INVESTIGATION OF THE SCATTERING OF MOLECULES FROM SURFACES

---

By

F. C. HURLBUT

FACULTY INVESTIGATORS:

S. A. SCHAAF, ASSOCIATE PROFESSOR OF ENGINEERING SCIENCE

R. M. DRAKE, JR., ASSOCIATE PROFESSOR OF MECHANICAL ENGINEERING

L. TALBOT, ASSISTANT PROFESSOR OF MECHANICAL ENGINEERING

Approved by:

*S a Schaaf*

Note: This report was condensed from a Ph.D. thesis, University of California
Berkeley, 1953.

## List of Figures

# ABSTRACT

A molecular beam apparatus was used to investigate the scattering of air and $N_2$ molecules from surfaces of polished low carbon steel, etched low carbon steel, polished aluminum, unpolished window glass, and polished window glass. A beam of molecules was directed against the surface at representative angles of incidence. Polar flux distributions of the scattered molecules were measured by a movable detector. An ionization gage beam detection system was devised to accomplish this measurement.

Spatial polar plots of these measured flux distributions were found to approximate closely the form of the cosine scattering distribution for the cases of the steel and aluminum surfaces. Similar plots in the case of the glass surfaces were found to have well defined but small bulging deviations from the cosine scattering shape on the side away from the incident beam.

In order to illustrate one aerodynamic application of scattering data obtained by molecular beam techniques, a procedure was devised for the computation of the coefficient of specular reflection, $f$, ($f$ being that fraction of the total incident tangential momentum which is transferred to a surface in interaction with a flowing gas) and values of this coefficient were calculated for the case of an unpolished glass surface oriented tangentially to the direction of mass motion in a free molecule flow. These values were calculated as a function of the parameter $s$, the molecular speed ratio ( the ratio of the gas mass speed to the most probable thermal speed of the gas molecules). If all scattered molecules are assumed to have the distribution in speed in a particular direction which they would have had had they issued from a gas in equilibrium at the temperature of the surface, $f$ takes on values of $\sim 0.97$ as $s$ approaches $0$ to $\sim 0.99$ at $s = 10$. Alternatively, if those molecules contributing to the deviations from cosine scattering are assumed to issue from the surface with their incident speed while the remainder are assumed to be diffusely scattered, (a modified Maxwell model), $f$ takes on values of $\sim 0.97$ as $s$ approaches $0$ to $\sim 0.93$ at $s = 10$. These values do not correspond closely to the published values for air on glass of $0.89$ ($s \sim 0$).

## NOMENCLATURE

$a$ = tube or orifice area. (Subscripts 1, 2, 3, etc. denote association of $a$ with regions of the beam as required in section 2.31 and 2.32. Subscripts a, b, etc., denote the a or b end of a certain tube as required in sections 2.31 and 2.32).

$A$ = constant = $\dfrac{\beta^3}{\pi^{3/2}}$ (Subscripts r and f, if used, relate $A$ to reflected molecules or to molecules issuing from a fictitious gas respectively as described in section 4.2).

$A(\theta_i, \theta', \phi')$ = reflected beam signal amplitude in arbitrary units for incident molecules having direction $\theta_i$ and detector axis having direction $\theta', \phi'$.

$A_D$ = constant representing the diameter of the assumed cosine scattering shell.

$A_S(\theta_i, \theta', \phi')$ = beam signal amplitude differences defined by

$$A_S(\theta_i, \theta', \phi') = A(\theta_i, \theta', \phi') - A_D \cos \phi'$$

$a_1, a_2$ = radii of tubes or orifices

$b$ = $s \sin \theta_i$

$c$ = magnitude of the total molecular velocity (molecular speed) (subscripts i and r denote incident and reflected molecules respectively. Subscript f denotes molecules issuing from a fictitious gas as described in section 4.2).

$c_x, c_y, c_z$ = components of the total molecular velocity.

$\bar{c}$ = mean molecular speed referred to coordinate system fixed to the flowing gas = $\sqrt{\dfrac{8 \mathcal{R} T}{\pi m}} = \dfrac{2}{\sqrt{\pi} \beta}$ (Subscripts , 1, 2, 3, etc., denote specific mean speeds as required in section 2.31 and 2.32).

$\bar{c}_r$ = mean molecular speed of molecules issuing diffusely from a surface = $\dfrac{3}{4} \dfrac{\sqrt{\pi}}{\beta_r}$

$E_i, E_r, E_w$ = molecular energy fluxes incident, reflected and diffusely reflected.

$F_U$ = Maxwellian distribution function, Eq. 4.3.

$f$ = coefficient of specular reflection, section 1.2 and Eq. 4.1

$G_i$ = magnitude of the net tangential momentum incident on unit surface per unit time.

$G_i(\theta_i)$ = magnitude of the net tangential momentum incident on unit surface per unit time and unit solid angle having direction $\theta_i$, Eq. 4.25.

$G_r$ = magnitude of the net tangential momentum imparted by the surface to the issuing molecules per unit area per unit time, Eq. 4.1 (the addition of the subscript 2 indicates the application of assumption E-2 in the calculation of Gr).

$G_r(\theta_i)$ = issuing momentum function defined Eq. 4.15.

$g_r(\theta_i)$ = function defined in Eq. 4.10.

$I_0, I_1$ = modified Bessel function of zero and first order.

$k$ = Boltzmann's constant

$m$ = molecular mass

$N$ = number of beam molecules entering gage per unit time.

$N_i$ = number of molecules of all velocities striking unit surface area per unit time, Eq. 4.2.

$N_i(C_i,\theta_i,\phi_i)$ = number of incident molecules per unit speed range and solid angle having the speed $C_i$ and incident direction $\theta_i, \phi_i$ striking unit surface area per unit time.

$N_f$ = number of molecules per unit solid angle and unit speed range crossing a unit plane in a gas in a particular direction.

$n$ = molecule number density (the absence of a subscript denotes the free-stream density. Subscripts 1, 2, 3, etc., denote specified regions. Subscript f denotes number density of a fictitious gas).

$n(t)$ = instantaneous value of molecule number density in gage at time t, Eq. 2.321.

$P_1(C_i,\theta_i,\phi_i,C_r,\theta_r,\phi_r)$ = distribution function denoting the probability per unit solid angle and speed range that a molecule with incident speed $C_i$ and direction $\theta_i, \phi_i$ will be scattered with speed $C_r$ in direction $\theta_r, \phi_r$ (If present, the subscript D identifies the probability distribution function with the diffusely scattered molecules while the subscript S identifies that associated with the specularly scattered molecules).

$P_2(\Theta_i, \Theta', \phi')$ = distribution function denoting the probability per unit solid angle that a molecule with incident direction $\Theta_i$ ($\phi_i$ unspecified) will be scattered in direction $\Theta'$, $\phi'$ (the subscripts D and S perform the same function as above).

$P_3(C_r)$ = distribution function denoting the probability per unit speed range that a molecule will issue from a surface with the speed $C_r$.

$P, \Delta P$ = pressure and pressure increment (subscripts if used denote specified regions).

$R$ = surface - detector separation (Fig. 7)

$\lambda$ = beam path length (Fig. 7)

$\mathcal{S}$ = function defined Eq. 4.27

$$\mathcal{S}' = \frac{b\, e^{b^2}}{2\sqrt{\pi}} \mathcal{S}$$

$S$ = molecular speed ratio = $\dfrac{U}{V_m}$

$T$ = free-stream temperature, Kelvin (subscripts 1, 2, 3, etc. if applied refer to specified regions. Subscript f refers to fictitious gas. Subscript w refers to wall temperature).

$U$ = magnitude of the mass velocity

$V$ = detector gage volume

$V_m$ = molecular most probable speed = $\sqrt{\dfrac{m}{2 \& T}}$ = $\dfrac{1}{\beta}$

(Subscripts r, f, if used, associate Vm with $T_w$, $T_f$ respectively).

$W$ = probability that a molecule striking the plane of the end of a tube of specified shape from a gas at rest will pass through without returning to the entrance plane (subscripts 1,2,3, etc., when used, denote specific tubes).

$X, Y, Z$ = coordinate system of incident momentum considerations, Fig. 41

$X', Y', Z'$ = coordinate system of issuing momentum considerations, Fig. 42.

GREEK SYMBOLS

$\alpha$ = accommodation coefficient, section 1.2

$\beta = \dfrac{1}{V_m}$ (subscripts perform the same function as for $V_m$ )

$\theta_i, \phi_i, \theta_r, \phi_r$ = incident and reflected molecule direction in unprimed coordinate system, Fig. 41.

$\theta', \phi'$ = reflected molecule directions in primed coordinate system, section 4.4.

$\lambda$ = mean free path

$\mu$ = microns Hg = 0.001 mm Hg, a measure of pressure.

$\xi, \eta, \zeta$ = coordinate system fixed in a gas.

$\psi$ = polar angle as measured from $\zeta$ axis in above coordinate system.

$d\Omega$ = element of solid angle in above coordinate system.

$d\omega, d\omega'$ = element of solid angle in unprimed and primed X,Y,Z, coordinate systems.

## SYMBOLS USED IN SECTIONS 2.33 and 2.34 ONLY

$A$ = amplifier loop gain

$E_i$ = potential across control resistor, emission regulator.

$E_0$ = reference potential, emission regulator.

$e_o$ = error signal, emission regulator

$e_{out}$ = signal to meter, difference amplifier.

$e_{in}$ = signal current, difference amplifier.

$R_1, R_2$ etc. = circuit resistances.

$T_1, T_2$ etc. = circuit transformers.

$V_1, V_2$ etc. = circuit vacuum tubes.

# AN EXPERIMENTAL MOLECULAR BEAM INVESTIGATION
## OF THE SCATTERING OF MOLECULES FROM SURFACES

## 1.0 INTRODUCTION

### 1.1 General

Since the time of Maxwell and extending through the first
third of this century there have been many investigation in the field
of rarefied gases. In recent times there has been a resurgence of
interest, stimulated in part by the need for a wider understanding
of aerodynamic conditions met by bodies in high speed travel through
the upper atmosphere. Of the many investigations in this field only
a small portion have been concerned directly with the interaction of
gas and surface. It was the objective of the program of this report
to investigate one aspect of these gas-surface interactions by mole-
cular beam technique.

### 1.2 Low Density Flow Investigation as a Technique of Gas-Surface Interaction Study

Historically the problems of the interaction of gas and sur-
face were first investigated following the realization by Kundt and
Warburg that the gas was not at rest at the boundaries of rarefied
gas flows (Ref. 1). This mass motion is determined, in part, by the
detailed behavior of the molecules in interaction with the surface.
Considerations relating to these phenomena, therefore, have been of
great interest to aerodynamicists and have played an important role
in the formulation of rarefied gas flow boundary conditions. Con-
versely, from experimental investigations of rarefied gas flows for which
model boundary conditions have been formulated, some deductive under-
standing of the gas surface interactions has been gained. Summaries
of the major concepts and results of rarefied gas flow theory and ex-
periment are contained in references 2 and 3.

Maxwell in 1879, (Ref. 4) proposed a hypothetical model for the
gas-surface interaction with respect to momentum transfer which was
consistant with the available data and which has been used in part in
the formulation of boundary conditions to this date. If some molecules
are assumed to be scattered diffusely from the surface at some tempera-
ture as yet unspecified such that the scattered flux distribution is

in accordance with Lamberts law of diffuse scattering without regard to incident angle or speed, and if the remainder are supposed to be reflected specularly, then one can define $f$ , termed the "coefficient of specular reflection", as that fraction of all molecules which is diffusely scattered. Since only this fraction contributes to the tangential momentum transfer to the surface, one is led immediately to an alternative definition of $f$ ,

$$f = \frac{G_i - G_r}{G_i}$$

where $G_i$ is the total incident tangential momentum brought to the surface by all molecules and $G_r$ is that carried from the surface. Only those molecules which are specularly reflected in the Maxwell model contribute to $G_r$ . The coefficient $f$ can be restated, then, as being that fraction of the total incident tangential momentum which is transferred to the surface. It is in this sense that $f$ is most reasonably defined since it can be applied to a macroscopic experiment without the making of assumptions regarding the detailed interaction. It is this definition which will be employed in this report.

In its past application $f$ has been assumed to be constant of the surface and the gas independent of gas mass velocity or gas and surface temperature in the absence of more comprehensive data.

As a result of somewhat analogous reasoning applied to the development of a theory of heat conduction in gases, Knudsen in 1911 (Ref. 5) proposed a coefficient $\alpha$ , the accommodation coefficient, defined as

$$\alpha = \frac{E_i - E_r}{E_i - E_w}$$

where $E_i$ is that energy brought up to the surface by the incident molecules, $E_r$ is that which is carried away by them as they are scattered from the surface, and $E_w$ is that energy which would be carried away by the issuing molecules if they had come from a gas in Maxwellian equilibrium at the temperature of the wall. The accommodation coefficient has been in use to the present in the formulation of boundary conditions. As with $f$ it has been assumed to be constant of the surface and the gas.

There exists a small body of literature pertaining to theoretical and experimental determinations of $f$ as a result of studies of macroscopic flows. A table of all known values of $f$ from such determinations may be found in Table I.

Although the work of this report is applicable only in consideration of momentum transfer, a table of experimental values of $\alpha$ is included in Table II. Many important investigators whose names do not appear in the body of this report are referenced in these tables and so appear in the bibliography.

It can readily be seen from these tables that our knowledge of either of these quantitites is not extensive. More objectionable than this is the likelihood that the values as reported are valid only for flow conditions approximating those of the experimental determinations. The chief deficiency of these determinations, however, lies in the fact that they yield very little insight into the physical nature of the gas-surface interaction beyond the essential fact that by and large the molecules "forget" their past history upon interaction with a surface.

## 1.3 Detailed Investigations of Gas-Surface Interactions

Soon after the first concepts of the gas-surface interactions were formulated investigations were undertaken to study these phenomena in more detail. Some variation of the molecular beam technique was almost invariably used. These investigations, that is, involved a directed stream of molecules in interaction with a plane surface element. Measurements of the flux of scattered molecules at one or more positions about the scattering surface were obtained. A considerable body of literature exists devoted to the description of these experiments and to theories of the interaction. Two very comprehensive surveys of the techniques and results of experiment are contained in Refs. 2, and 6. A summary table of the best known of these investigations can be found in Table III. Those investigators not specifically mentioned in the body of the report are referenced in that table. Beyond pointing out certain salient features of these investigations it would not further this report to elaborate on them in greater detail.

Of these many investigations the most definitive was clearly that of I. Estermann and O. Stern (Ref. 7) in their classical experiments on the diffraction of He and $H_2$ from cleavage planes of LiFl and NaCl. The location of the observed diffraction maxima was found to be in strict accordance with the prediction of the optics of cross gratings.

The majority of the remainder of the investigators also worked with cleaved surfaces of natural crystals. For the most part the mode of molecular beam detection dictated the use of various metallic atoms, more or less readily condensible at the temperature of the scattering surface, for the parent beam material. These experiments did not in general permit such a clear and unambiguous interpretation of results as did the work of Estermann and Stern.

Only one group of tests on surfaces other than crystal cleavage planes appears appropriate to this present report. These were performed by Knauer and Stern (Ref. 8) on polished speculum metal. An optical criterion for the specular reflection of transverse waves is that the irregularities of the reflecting surface be less than a wave-length in extent as measured normal to the axis of wave propagation. This condition was believed to occur at glancing angles of 0.001 radian and less for $H_2$ and the polished metal. Experiment verified these predictions. Above 0.001 radian no detectable amount of specular reflection was observed.

On the basis of the foregoing remarks and Table III the state of knowledge of the surface interaction may be summarized as follows:

(1) He and $H_2$ interact with cleavage planes of simple crystals in a fashion predicted by wave mechanics.

(2) Gases having high forces of interaction with the crystal surface apparently scatter diffusely from it. For example, Li, Na, Cs, from NaCl.

(3) Apparently there is a tendency for some metallic gases to undergo a classical elastic specular reflection at a crystal surface where the interaction forces are low in a manner not readily understood in wave mechanical terms.

(4) Gas-surface interactions involving surfaces which are "liquid",

micro-crystalline or man-formed by polishing have been studied
hardly at all. The past findings in this area suggest that the
scattering is largely diffuse at least wherever the criterion
for optical specular reflection is not satisfied.

There is, however, experimental evidence from the determination
of values of $f$ that some interactions are not entirely diffuse.
For example, Millikan reported a value of $f = 0.89$ for air on glass.
Clearly it is here in these areas of diffuse or semif-diffuse scat-
tering that our understanding of the molecule-surface interaction
is most meager.

## 1.4 Objectives of the Experiment

In most general terms it is the objective of the molecular beam
program to study the fundamental nature of the gas-surface inter-
actions by molecular beam techniques. More specifically the present
experiment was designed to enable the measurement of the issuing flux
distributions of atmospheric constituent molecules scattered from sur-
faces of certain ordinary materials oriented at arbitrary angles to
the incident molecular beam.

It was recognized that the work herein reported could constitute
only a beginning to a systematic inquiry into the nature of the mole-
cule-surface interaction. Therefore, in establishing the choice of
gas and surface, experiment geometry and resolution, an attempt was
made to be guided by consideration of what should constitute a logi-
cal first step in such an investigation. The details of the experi-
mental technique and of the test program will be dealt with in the
appropriate sections of this report.

In addition to reporting the results of the experimental pro-
gram and discussing these findings, it was a further objective
of this paper to suggest by analysis the desirability of restating
the rarefied gas flow boundary condition for momentum transfer in
terms of a more general transfer ratio than the constant $f$. In
connection with this analysis a technique was developed for computing
the value of $f$, subject to certain assumptions to be discussed
later in this report, for a Maxwellian gas with superimposed mass
velocity tangentially directed relative to a surface. This compu-
tation was carried through for the $N_2$-glass interaction on the basis

of data obtained as a portion of the experimental work of this report.

## 2.0 DESCRIPTION OF THE APPARATUS

### 2.1 Introductory Remarks

The majority of molecular beam devices in existence, and those most familiar to physicists today, have been constructed for the study of the fundamental properties of the atom or nucleus as revealed by the interaction of these particles with electromagnetic fields. Since it might be expected that a molecular beam apparatus constructed for the study of the scattering of molecules from surfaces would differ slightly from these other equipments, a brief description of the equipment of this program will be given.

The molecular beam is formed by the thermal effusion of molecules through an orifice or tube from a small source chamber. The effusing molecules travel rectilinear diverging paths to the plane of the defining orifice. Those traveling in the proper direction pass on through and constitute the molecular beam. The remainder (the vast majority) are stopped and become removed by the source pump.

The molecular beam downstream from the defining orifice travels through a region of high vacuum ($P \sim 10^{-6}$ mm Hg; mean free path, $\lambda \sim$ 50 meters) until it strikes the scattering surface oriented at an externally variable angle of incidence to the beam axis. Those molecules issuing from the surface into a small solid angle $\Delta \omega'$ at $\Theta'$ and $\phi'$ measured from coordinate axes fixed in the surface (Figure 1) pass into the detector and create a beam signal by producing a small pressure increment within that gage. By moving the detector through all values of the coordinates one can obtain the relative distribution of molecular flux into all elements of the hemisphere at a fixed value of the incident angle. By repeating the measurements for representative values of the incident angle a description of the scattering of the molecules of a given gas from a given surface can be obtained. The data of this report were obtained in this fashion. Note, however, that this description gives a picture of scattering behavior which is by no means complete, since it applies to one incident gas temperature only, one surface temperature

only, and makes no measurement of the distribution in speed of the scattered molecules.

A description of the molecular beam apparatus is most logically divided into two principle sections, one concerning the physical apparatus, and the other concerning the molecular beam detection system.

## 2.2 The Physical Apparatus

In briefest terms the physical apparatus consisted of the beam forming and detecting elements supported within vacuum envelopes which were in turn associated with an evacuating system. Figure 2 is a schematic of the pumping system showing the source and detector regions of the apparatus and attached pumps, valves and refrigeration components. Figure 3 is a photograph of the complete equipment. The principle vacuum envelopes (source region and detector region) were of stainless steel. Other parts were variously of cold rolled steel, aluminum, copper, or brass. Nearly all gasketing was by means of rubber "O" rings for fixed as well as rotating seals. With the exception of the quarter swing valves between the main envelopes and the refrigerated traps, all valves were equipped with Teflon seats. Under beam-on conditions typical detector chamber pressures were of the order of $10^{-6}$ mm Hg or less while the source chamber pressures were of the order of $2 \times 10^{-5}$ mm Hg or greater.

All parts of the molecular beam forming and detecting equipment were designed to be supported on an optical bench which in turn was supported by the plate dividing the source vacuum envelope from the detector envelope. The mounted elements were, in order of their appearance in the beam forming or detecting process, the source chamber and source orifice, the defining orifice (carried by the bench support plate), the shutter, the secondary defining orifice, the detector mechanism (with test surface and detector gage), and the comparator gage. Attached to the downstream end of the optical bench was a plate (the "apron") carrying coordinate counters and screw driver tipped fittings linking the moveable parts on the optical bench with the rotating shafts piercing the detector envelope and plate. Figure 4 shows the optical bench and all mounted components.

The source chamber was mounted on a slide providing adjustment of the source orifice center by means of lead screws and ways. The source "orifice" was a tube mounted so as to make possible precise allignment of the beam axis with the source tube axis. A pair of auxiliary optical bench carriages with transverse and vertical slides and coordinate counters and mounting a Point-o-lite and a telemicroscope respectively were used for the beam alignment throughout. The source chamber was connected to the source gas supply system and manometer system shown in Figure 5.

The most complex of the various components of the beam forming and detecting system was the detector mechanism. Basically, this mechanism was a mounting device for holding two elements of the molecular beam system; i.e., test surface, and detector gage, in the desired mutual geometrical relationship. The test surface was mounted normal to the axis of the azimuth rotation axis by means of a shaft along that axis. (See Fig. 6). The test surface and all other elements above the transverse carriage could be rotated in a horizontal plane about a vertical line element in the test surface face by means of exterior controls. Thus the incident angle of the beam with respect to the test surface was variable. The upper elements of the detector mechanism supported the detector gage. These elements were rotatably mounted to provide adjustment of the polar and azimuth angles of the gage entrance tube referred to the polar axis normal to the test surface. Azimuth angle control was made by internal adjustment. The polar angle was controlled externally by means of flexible shafting and swiveling miter gear linkages. The gage support system was terminated by a small ground bar way which carried the gage holder. The gage holder provided adjustment of gage-to-surface separation and rotational and vertical allignment. All motions not considered "set-up" were provided with coordinate indicators in the form of 5 place Veeder Root counters. Angular position settings were determined to have a reproducibility of 0.015°. On the basis of guaranteed minimum gear quality the total cumulative error in angular setting was estimated to be approximately. 0.05°. For the incident and polar angle gear trains the counters rotated 38.519 units per degree.

Directly associated with the physical apparatus were certain items of general instrumentation including pressure monitors, source gas regulation and pressure measurement devices, and protective devices. Three Pirani type vacuum gages were employed to monitor pressures in the appropriate range, one being connected to the fore pressure line, one between the booster pump and the diffusion pumps, and one to the source pressure manifold. Both the source and detector sections of the main vacuum envelope were provided with Alpert type ionization gages for base pressure monitoring. Each was connected to a standard Low Pressures Project design power supply and metering circuit. This device is provided with an over-pressure protection circuit which removes filament power if the pressure should exceed the maximum pressure of the range selected. At the same time power is removed from a control line which may be connected to other devices. In this way the detector and comparator gages were also protected against the effects of over-pressure conditions.

The source pressure manometer indicated in Figure 5 was an early forerunner of the present Low Pressures design precision oil manometer (Ref. 25). While it lacked certain mechanical and optical refinements of the present models, oil column height differences were easily read to within 0.001 inches. The reliability of readings in calibration experiments with a precision McLeod have been found to be $\pm$ 1 micron. A more detailed discussion of the design consideration leading to the present equipment may be found in Ref. 36.

## 2.3 The Molecular Beam Detection System

### 2.31 Preliminary Considerations

A portion of the molecular beam apparatus necessitated by the present experimental program was a beam detection system for atmospheric constituent molecules. Such a system must include a gage which collects a number of directed molecules and measures the resultant increment in molecule number density within its volume.

Referring to Figure 7, with the gage set to receive the direct beam and with the test surface withdrawn, let the molecular beam shutter be opened suddenly, the molecule number density within the gage having been at equilibrium with the

residual gas within the vacuum shell. Then $N$ directed molecules per second pass into the gage volume. At equilibrium with this new influx $\frac{m_3 \bar{c}_3 a_{3b}}{4}$ molecules per second strike the area $a_{3b}$ from within the gage, where $\bar{c}_3$ is the molecule mean speed at the temperature of the gas and $m_3$ is the incremental molecule number density. Of these $\frac{m_3 \bar{c}_3 a_{3b} W_3}{4}$ succeed in emerging from the entrance tube, where $W_3$ is the probability that a molecule striking the area $a_{3b}$ will emerge through the area $a_{3a}$ without re-entering the gage.

$W_3$ depends upon the shape of the entrance tube only. At equilibrium, then,

$$m_3 = \frac{4N}{\bar{c}_3 \, a_{3b} W_3} \tag{2.311}$$

Since this adjustment takes place under free molecule flow conditions it is assumed to be independent of other similar adjustments taking place simultaneously as a result of small changes in instrument base pressure, for example. It has also been assumed that no thermal gradients exist along the entrance tube.

In order to fix ideas of the orders of magnitude involved in the detection of a diffusely scattered beam, consider the idealized schematic of a scattering experiment, Figure 7.

When the length of the beam path, $\lambda$ , very greatly exceeds $a_1$ , the radius of the source orifice, point source geometry affords a good approximation in the calculation of beam intensity. The number of molecules effusing from the source orifice under conditions of free molecule flow is $\frac{m_1 \bar{c}_1 a_1}{4}$ , where $a_1$ is the area of the source orifice, $\bar{c}_1$ is the mean speed of the source molecules, and $m_1$ is the source molecule number density. Let the beam cross sectional area be chosen as $a_2$ at $\lambda$ and the defining slit size adjusted to permit this. The number of molecules crossing $a_2$ per second becomes

$$N_2 = \frac{m_1 \bar{c}_1 a_1 a_2}{8 \pi \lambda^2} \tag{2.312}$$

Let these molecules be intercepted by the scattering surface.
For an unambiguous determination of the flux of molecules through
the area $a_3$ at angle $\theta'$ as measured from the normal to the
scattering surface, let $a_3$ be an orifice in the wall of the
detector gage $(W = 1)$.

If there is perfectly diffuse scattering at the surface,
the number of molecules crossing $a_3$ into the gage is
$\dfrac{m_1 \bar{c}_1 a_1 a_2 a_3 \cos \theta'}{16 \pi^2 \lambda^2 R^2}$ . At equilibrium then
$\dfrac{m_3 \bar{c}_3 a_3}{4} = \dfrac{m_1 \bar{c}_1 a_1 a_2 a_3 \cos \theta'}{16 \pi^2 \lambda^2 R^2}$ since $\dfrac{\bar{c}_3}{\bar{c}_1} = \sqrt{\dfrac{T_2}{T_1}}$
and this ratio is of order 1 for moderate gage temperatures.
Thus:

$$m_3 = \frac{m_1 a_1^2 a_3^2 \cos \theta'}{4 \lambda^2 R^2} \qquad (2.313)$$

where $m_3$ is the incremental molecule number density in the gage
due to the scattered beam.

The desired angular resolution of the experiment, the physi-
cal size of various components of the beam forming and detect-
ing system, and the available pumping speeds on source and de-
tector sides of the plane of the defining orifice all play a part
in limiting the choice of the parameters on the right hand side
of equation 2.313. For the present experiment, typical values

$$a_1 = 0.25 \text{ mm}$$
$$a_2 = 1.5 \text{ mm}$$
$$\lambda = 25 \text{ cm}$$
$$R = 3 \text{ cm}$$
$$m_1 = 3.6 \times 10^{11} \text{ molecules cm}^{-3} \text{ at a maximum}$$

then $m_3 = 2.25 \times 10^7 \cos \theta'$ . The pressure increment cor-
responding to this density increment is

$$\Delta p = 0.63 \times 10^{-9} \text{ mm Hg}$$

An entrance cone of taper such that no molecule can hit the
side wall before entering the gage volume (Figure 7) can be
constructed to have a value of $W_3$ of the order 0.2. The
scattered beam pressure increment may thus be raised to the
order of $3.1 \times 10^{-9}$ mm Hg.

A pressure increment of this small size would not be difficult to detect were it not for the presence of the background gas. This residual gas, existing in the detector region at a mean pressure of $10^{-6}$ mm Hg, suffers rapid random fluctuations in pressure as a result of uneven diffusion pump operation. These pressure fluctuations under operating conditions are of the order of $3 \times 10^{-8}$ mm Hg. This gas also suffers slower "drifts" in pressure in response to minor changes in diffusion pump efficiency or system outgassing rate. These changes in turn may be caused by changes in pump heater current, ambient temperature, cooling water temperature or cold-trap temperature. A background pressure change of $5 \times 10^{-8}$ mm Hg may occur in a few seconds, of $10^{-7}$ mm Hg in several minutes or $5 \times 10^{-7}$ mm Hg in the course of a few hours.

Thus the atmospheric constituent detection system must include a second gage known as the "comparator". This gage must measure the background pressure, responding to its fluctuations with the same sensitivity and with the same time of response as that of the detector. If the comparator provided a perfect replica of the signal from the detector in response to the background pressure fluctuations, a subtraction of the total signal from each gage would leave a net signal representing only those pressure increments due to the beam. This condition of perfect compensation is never quite realized in practice.

An important requirement for good compensation is that the time response of comparator and detector gages be equal. The time response of either gage to a stepwise increment of molecular flow into the gage, $N$ molecules per unit time, is given by

$$m(t) = \frac{4N}{\bar{c}_3 W_3 a_3} \left( 1 - e^{-\frac{\bar{c}_3 W_3 a_3 t}{4V}} \right) \quad (2.314)$$

where $m(t)$ is the incremental number density of molecules in the gage volume at time $t$ after initiation of the incremental flow, $\bar{c}_3$ is the mean molecular speed of the molecules within the gage, $a_3$ is the area of the entrance tube opening, and

$W_3$ is the probability that a molecule will pass on out of the
tube without returning to the gage volume. $V$ is the volume of
the gage. If $N$ is due to a stepwise increase in molecule number
density $m_o$ within the vacuum shell of the detector region,

$$m(t) = \frac{m_o \bar{c}_o}{\bar{c}_3} \left( 1 - e^{-\frac{\bar{c}_3 W_3 a_3 t}{4V}} \right)$$

(2.315)

Clearly, if the response times of detector and comparator
are to be made equal, the factors $\frac{\bar{c}_3 W_3 a_3}{4V}$ must be
made equal. This was most conveniently achieved by providing
the comparator gage with a telescoping entrance tube which
was then adjusted by trial and error for minimum time response
difference.

Although the fundamental concepts of the detector-com-
parator form of measurement have been widely applied in other
fields (and referred to in other terms) they are believed
to have been first applied to a molecular beam detection system
by O. Stern, I. Estermann and their associates.

## 2.32   The Ionization Gage Detector

As has been remarked earlier in this report, the ioni-
zation gage was chosen for development as a molecular beam
detector. The Pirani gage appeared to have been brought close
to the limit of its potential by earlier workers (again Ester-
mann, Stern, et. al). It did not seem that their work could
be bettered by one or two orders of magnitude.

In its most common form the ionization gage employs three
major elements, contained within and supported by a glass envelope.
The heated filament, operating temperature-limited, supplies

electrons for the ionization of neutral molecules in the grid-
anode region. The grid accelerates the electrons and ultimately
collects them after they have made several passes from grid-
cathode to grid-anode region and back. Such ions as are formed
by electron collision in the grid-anode region are collected
at the anode. Electrode potentials and field configuration
are such as to permit this action. The magnitude of the ion
current is linearly proportional to the number density of
molecules in the gage at pressures below one micron Hg and to
the electron emission current. It is also a function of grid
potential and gage geometry, and is inherently very insensitive
to changes in ambient temperature.

An emitting tungsten filament continuously loses mass to
its surroundings. Ultimately, conducting films of tungsten
become deposited on the gage walls. At the same time diffusion
pump oils are broken down to elemental constituents or to
resinous molecules and also become deposited on the walls.
A complex film is built up having conduction properties of
varied and sometimes repidly fluctuating character. Leakage
paths and fluctuating charge distributions have a very dis-
turbing effect on the stability of the ion current when that
current must be known to a few parts in $10^5$, although for or-
dinary pressure monitoring these deposits are of little interest.

In designing an ion gage for use as a molecular beam de-
tector, particular care must be taken to insure that electrical
leakage paths between the various elements or from them to
ground have virtually no opportunity of formation. The gage
must also be exceptionally rugged and physically compact.

By February of 1949, the major design features of a satis-
factory ion gage for molecular beam detection were well estab-
lished. A detailed record of this development is presented in
Ref. 26. The ion gage had improved itself in two experimental
programs (Refs. 27 and 28) and it had been established that
signals at least as small as those encountered in the work of
earlier experimenters could be resolved from the noise.

In 1952 a major change was made in the molecular beam detector as a result of the publication of the work of D. Alpert and others at Westinghouse Research Laboratory (Ref. 29). While the major advantage of the Alpert gage (i.e. the measurement of extremely low absolute pressures) was thought not to be of interest at this time its configuration allowed a cleanness and ruggedness of structure which was regarded as very desirable. On the basis of the Alpert design and on the previously achieved design of this project, the ion gage detector of the present investigation was constructed (see Figure 8).

The sensitivity and other performance characteristics of these gages were discovered to be very similar to those of the Alpert gage. In spite of the attention given to the prevention of film formation this still constituted a serious problem. One month was found to be about the maximum running time before conducting films made the gage inoperable for molecular beam use. A thorough cleaning with dilute hydrofluoric acid was found to be necessary to restore a dirty gage to usefulness.

## 2.33 The Emission Regulator

For the proper operation of the ionization gage detector a stable source of gird potential must be supplied. Also a source of filament power must be provided which is so regulated as to permit an unvarying flow of emission current within the gage. It was a requirement of the experiment that this current be regulated to a few parts in $10^5$. Similarly the source of grid potential was required to possess a very high order of stability. The device which supplied both filament and grid was termed the emission regulator. Two such devices were constructed, one for the detector gage and one for the comparator. (Beam detector system schematic, Figure 9).

This filament emission regulator was of a type in which the total emission current develops a signal $E_1$ across the control resistor R. (Figure 10). The potential $E_1$ is compared with a reference potential $E_0$. The difference $e_0$ ($E_1-E_0 = e_0$) constitutes an error signal whish is then minimized by the

regulator action. In a total feed-back circuit of this type $\frac{E_1}{E_0} = \frac{A}{1 + A}$ where A is the loop gain of the circuit. All minor

fluctuations in regulator performance, supply voltage, filament emissivity, etc., can be considered equivalent to changes in loop gain. In principle the ratio $\frac{E_1}{E_0}$ can be made to remain as constant as desired by providing a sufficiently high loop gain. In particular if variations in effective loop gain of 10% A are to be expected, and if the ratio $\frac{E_1}{E_0}$ is to remain constant to 1 part in $10^5$ then A must have the value of 10,000. Variations in the reference potential $E_0$ and variations in input stage quiescent point are excluded from this argument, of course.

It is a matter of experimental record, however, that the achievement of a loop gain of this order is not feasible in the straight forward D.C. amplifier type of emission regulator design. If the voltage output of the regulator is sinusoidal the resultant emission current will have a ripple component superimposed on the D.C. level. This ripple component is the result of the response of the temperature limited emission current to the periodic fluctuation of the impressed power. A high gain D.C. amplifier normally becomes blocked by this signal in a final stage. Attempts to reduce the magnitude of this ripple component by brute force filtering are met with very limited success because of the attendent phase shift around the loop and the resultant low frequency hunting.

A point at which phase shift is unavoidably introduced is at the filament of the ionization gage itself as a result of the thermal capacity of the filament. This highly non-linear element makes the realization of extremely precise regulation more difficult than in the case of a pure resistive load.

The design of the ion gage detector regulator followed an approach suggested by Greenough, Williams and Taylor (Ref. 30) and applied by them to a low voltage power supply for electrolysis. The essential feature of the Greenough, Williams approach was the use of a square wave as the regulator output signal. The application of power in this form to the filament

results in a great reduction in the emission current ripple component and a consequent increase in the feasible loop gain.

Schematic diagrams of the complete regulator and power supply circuits are presented in Figures 11 and 12. Referring to the schematic of Figure 11 the emission current entering at point A develops a signal voltage across precision resistors R. This voltage is compared with reference battery $E_0$ and the resultant difference signal is applied to the grid of the first amplifier $V_2$. $V_1$ compensates the signal for small changes in contact potential originating from filament emission changes in $V_2$. $V_4$ and $V_5$ comprise a multivibrator pair serving as the plate load of the control tube $V_3$. A square wave of acceptable quality is electron coupled out through a loop gain control dual potentiometer to a high grain AC amplifier adapted from the Childs circuit (Ref. 31). The output transformer $T_1$ was chosen to have $\frac{1}{2}$ db band pass of 20-20,000 cycles, to insure good transfer of the square wave to the ion gage filament. Provision was made for balancing the plate currents in the push-pull power output stage. It was found necessary to include the variable RC network $R_1$ $R_2$ $R_3$ $C_1$ $C_2$ as an anti-hunt control. Highest performance of the regulator was achieved by adjusting anti-hunt, loop gain, and various balance controls.

The power supply units (Figure 12) were rebuilt from Signal Corps. SCR 545A mobile Radar "standard" power supplies.

Using a precision voltage divider, biasing batteries and a 0-20 millivolt strip chart recorder, determinations of the stability of the regulator and of its loop gain were made. After a short initial warm up period the "drift" was of the order of one part in $10^4$ per minute. This was a matter of no concern since after warm up the drifts had been ascertained to be less than 1% per day except under conditions of excessive ambient temperature change. (The reference potentials were supplied by ordinary dry cells). The noise was of the order of 2 parts in $10^5$ of the total signal in amplitude, permitting adequate gage operation. The loop gain was variously checked at between 10,000 and 20,000 under good operating conditions.

While long time stability of the highest order was not a requirement of the program of this report, it could have been approached more closely by making two simple changes in the equipment. The reference potential could have been supplied by a mercury cell having a low temperature coefficient of e.m.f., and the heaters of the tubes of the input stage could have been powered from the regulated supply.

## 2.34 The Difference Amplifier

At some point in the detection process, in order that meaningful data can be obtained from the molecular beam detector, the signals from detector and comparator must be compared and a difference signal noted. The apparatus which performed this function in the molecular beam detector system was known as the difference amplifier.

In order to understand the nature of the problem it is useful to recall the orders of magnitude of the current involved. The background pressure current was of the order of $10^{-8}$ to $10^{-7}$ amperes. Random current fluctuations of the order of $10^{-9}$ amperes in amplitude were superimposed on this as a result of the background pressure flucutuations. The beam signal current was of the order of $10^{-10}$ amperes. It was thought desirable to resolve this signal to at least one part in 10. The conditions of the experiment required therefore that currents from detector and comparator be amplified and subtracted in such fashion as to yield difference signals of as little as one part in $10^4$ of the total.

Systems for performing a similar function have been devised in the past for use in mass spectrometer isotope abundance studies (see for instance, Ref. 32). These systems normally used one complete amplifier for each signal, the subtraction being performed directly preceeding the indicating device. It was thought, in view of the special circumstance of having nearly identical input signals, that the two amplifiers could be joined in a single push-pull circuit minimizing the opportunity for unequal phase shift through two amplifiers and for other inequalities of response possible with two complete amplifiers. This and more specialized design considerations led to the difference amplifier circuit shown in Figure 13. Power supplies for this

unit are shown in Figure 14.

If circuit sections of Figure 13 including $V_1$, $V_2$ and $V_3$, are considered alone, it can be seen that these together form a basic feed back electrometer circuit for which $e_{out} = i_{in} R_1 \left(\frac{A}{1+A}\right)$ where $e_{out}$ is the signal potential to the metering circuit, $i_{in}$ is the signal current in, $R_1$ is the high resistance range determining resistor and A is the effective gain of the amplifier section. As with the emission regulator, if gain variations of 10% A are to be expected, A must have a value of the order of $10^4$ for the ratio $\frac{e_{out}}{i_{in} R_1}$ to remain constant to one part in $10^5$. If a shunting resistance to ground is present (as for instance $R_2$ in Figure 14) the product $A R_2$ must be very much greater than $R_1$ in order for this shunt to have a negligible effect on the output signal. The gain of the amplifier in the difference amplifier circuit was somewhat greater than $10^4$.

Referring again to the schematic of Figure 13, the signals from detector and comparator are conducted to $V_1$ and $V_5$ housed in the pick up head. This section of the unit was adapted with minor modification from the National Research Corporation Alphatron vacuum gage. Selected 954 type vacuum tubes connected as shown have been found to show grid currents of less than $10^{-14}$ amperes (Ref. 33). The pairs $V_2$, $V_6$ and $V_3$, $V_7$ were connected with common cathode resistors to minimize the effects of variation in plate supply voltage and to afford a means of balancing the gain of each stage. The balanced cathode follower output stage provided a low impedance drive for the strip chart recorder.

With an input range resistor of $10^8$ ohms the least output difference signal distinguishable on the strip chart recorder was of the order of $10^{-12}$ amperes. Drift and noise appeared to be absent at this sensitivity. Larger values of the input range resistor were not employed because of the magnitude of the voltage which would have been developed across them by the large background pressure current.

All heaters were supplied from the regulated supply of Figure 14. This supply was also modified from the Signal Corps.

SCR545A "standard" power supply.

# 3.0 THE EXPERIMENTAL PROGRAM

## 3.1 Test Surfaces and Geometries

In view of the survey nature of this experimental program, it was regarded as of first importance to choose test surface and beam geometries in such a way as to allow an overall determination of the scattering behavior with a minimum of ambiguity. The results of the first design choices are shown in Figure 15. The beam was axially symmetric as was the gage entrance cone. The surface was circular and of approximately the same area as that of the entrance end of the gage entrance cone. At normal incidence the beam umbra illuminated somewhat less than the total surface area. However, low intensity elements of the penumbra overlapped the surface slightly. The gage entrance cone was designed to accept approximately 1% of the total hemisphere solid angle. This was a "low resolution" geometry, chosen, on the basis of beam intensity calculations and available signal-to-noise ratio, so as to provide a reasonable expectation of yielding detectable signals for the case of diffuse scattering.

Three surfaces were tested using this test geometry. These surfaces and the test surface holder are illustrated in Figure 16. A summary of this portion of the testing program follows.

### 3.11 Cold Rolled Steel

This specimen was of common cold rolled steel of low carbon content, lathe turned from a 1/4" diameter rod. The specimen was mounted in lucite and polished using standard metallurgical laboratory techniques. Examination revealed a uniform mat of fine polish marks of the order of 1/4 micron in depth. The surface appeared to the naked eye to have a high polish. After insertion into the specimen holder in the molecular beam apparatus, the surface was thoroughly washed with absolute alcohol and dried with tank nitrogen. Polar traverses were made both in the incident plane and out of the incident plane with the beam incident at a variety of representative incident angles. Room air served as the test gas. The surface temperature was very slightly above room temperature. About 250 data points were obtained in the period Feb. 12, 1953 to March 2, 1953.

Following the completion of this sequence the surface w
heated to 250 degrees centigrade and a series of incident pl
polar traverses were made at this temperature in order to di
cover any possible change in the scattering behavior as a re
of the outgassing of organic films or other adsorbed layers.

A final polar traverse was made again at room temperatu

## 3.12 Cold Rolled Steel, Etched

A specimen of the same material as that of item 3.11 wa
polished in the same fashion. It was then given a light etc
in a standard 10% nitol solution. Microscopic examination s
the characteristic grain structure of a low carbon steel. N
polish marks were visible. Room air was again used as the b
gas. This specimen was tested as before, first at room temp
erature, then at elevated temperature, and again at room tem
ture. Incident plane polar traverses only were made. It wa
thought not worthwhile to spend the time on the exhaustive t
of the first section unless significant changes in the scatt
ing behavior developed. In all, about 200 data points were
tained in the period March 5, 1953 to March 13, 1953.

## 3.13 Aluminum

This specimen was lathe turned from S02, a commercially
grade of aluminum. It was polished in the same manner as th
steel specimen. This specimen was tested as in item 3.12.
together, some 120 data points were obtained in the period
March 23, 1953 through April 8, 1953.

Examination of the data of these first tests revealed t
deficiences of the experimental geometry which were correcte
in part before proceeding with the glass surfaces. It was o
served that at angles of incidence moderately close to glanc
the edge of the specimen intercepted a portion of the beam.
detector positions back of the test surface normal, the edge
scattered molecules contributed in part to the detector sign
making difficult an interpretation of the scattering data in
those directions. Secondly, direct beam molecules were dete
at incident and exit angles both close to grazing as a resul

of finite beam breadth. While such conditions are ultimately met in any beam geometry it was thought that in this geometry the limitation on large incident angle measurement was excessive.

The correction of both of these imperfections could have been accomplished by changing to a narrow ribbon geometry but only at the sacrifice of out-of-the-incident-plane information. It was thought better to retain the overall survey approach at this stage, but to narrow the beam by replacing the circular secondary defining orifice by a 1 mm x 5 mm slit. It had been ascertained that the signal to noise ratio was sufficiently high to permit this attenuation of the beam. At the same time, edge scattering was minimized by increasing the test surface length. This change also made the preparation and mounting of the glass surfaces less difficult. This beam geometry is illustrated in Figure 15. The glass test surfaces are included in Figure 16.

### 3.14 Unpolished Glass Surface

This specimen was obtained from a pane of single strength window glass. It was thoroughly cleaned, given a final rinse in absolute alcohol, and dried with tank nitrogen. The surface as viewed by the naked eye showed no defects and appeared free of film. The structure of the surface was presumably "as cooled".

It was this specimen which was chosen for the second exhaustive scattering examination, the results of which were later to be used in the determination of f, the coefficient of specular reflection. This choice was in part determined by the reported value $f = 0.89$ for air on glass as remarked in Section 1 of this report. In all, during the period April 17, 1953 to June 21, 1953, more than 400 data points were obtained. Tank nitrogen (99.5% $N_2$) was used as the test gas. The tests were run with the surface essentially at ambient temperature. Since it was mounted on a rod which was warmed by conduction through parts connected to the detector ion gage, the test surface was maintained at about 10°C above the temperature of the surrounding walls.

### 3.15 Polished Glass Surface

This specimen was cut from the same stock as the unpolished glass surface. It was then sent to a manufacturing optical laboratory for polishing. The polished specimen was cleaned and rinsed in the same fashion as before. For purposes of comparison with the unpolished glass plate it was necessary to observe scattering in the incident plane only. Approximately 100 data points were obtained. The experimental program of this report was completed with the conclusion of these tests July 23, 1953.

### 3.2 The Experimental Data

Each polar traverse made at fixed incident and azimuth angles yielded several data points representing the flux of scattered molecules into the detector gage. Each datum point resulted from the averaging of a number of beam on-off traces as recorded by the strip chart recorder. A reproduction of such a record is presented in Figure 17. For each day's run the beam source pressure was held constant as was the gage emission current, and hence the overall system sensitivity. When possible, in each run a record of the normal incidence scattering was taken and also a record of the direct beam strength. These last records afforded a means of comparison of one run with another.

It was found most convenient to represent the data in polar plot form, scaling the data of each run up or down to bring data of all runs of a given sequence into register.

In the case of the steel and aluminum surfaces two additional problems in data interpretation must be mentioned. As a result of the width of the shutter mechanism and of the detector ion gage the polar traverses could be continued to within about 40° of the reverse beam axis only. This conditions was improved only slightly in the glass plate tests. In these it was possible for the detector axis to come within 30 degrees of the reverse beam axis. The second problem resulted as a consequence of the small test surface size in relation to the beam diameter. As the angle of incidence was increased, an increasing percentage of beam molecules failed to strike the surface. The intensity of illumination per unit of surface area thus

fell off and in consequence the signal amplitude.

In view of the bulk of the experimental data and its general similarity in the case of the steel and aluminum surfaces no attempt will be made to present it in its entirety. However, representative polar plots for the steel plate are given in Figures 18 through 21 and for the aluminum plate, Figures 22 through 25.

Referring to the figures for the steel surface one can see unfortunate gaps appearing in the data at each angle of incidence. However, these gaps are somewhat filled by data obtained at other angles of incidence. The most striking aspect of these plots is the remarkable adherence of the data to a cosine distribution. The plots of data taken out of the incident plane still exhibit the same degree of circularity. No discernible change in the character of the scattering was made by outgassing the surface or running traverses at elevated temperature. For these surfaces undistorted representations of forward scattering were obtained to incident angles of about 70 degrees. The back scattering data at this incident angle was, however, seriously distorted by edge scattering. At larger angles of incidence (to 82 degrees) no evidence appeared of marked specular scattering, although, has such occurred close to 90 degrees, detection would have been masked by the signal of the direct beam.

A simple comparison of these data with the reference circles (introduced to aid in bringing the plots into register) suggests that the amplitude resolution of the experiment under these conditions was of the order of two to three percent of the maximum diffusely scattered signal.

Considering now Figures 22 through 25 for the aluminum surface one can observe that most of the remarks applying to the discussion of steel surfaces might also be applied to the aluminum. This work was not as complete as that on the steel surfaces, being done in the incident plane only and at fewer angles of incidence. While there seemed to be some deterioration in the signal amplitude resolution over this period, one must infer that the data indicates only slight deviations if any from the cosine distributions. There does, however, seem to be an indication of small bulges in the plots of the data of March 23, 1953, incident angles 53.65° and 81.83°.

The plots of the distribution of flux from the glass surfaces show a somewhat different character. Representative data are illustrated in Figures 26 through 32 for the unpolished glass surface and Figures 33 through 40 for the polished glass surface. On these plots one can readily observe bulges in the forward scattering direction, increasing in importance as the angle of beam incidence increases. These bulges are of the same general magnitude and shape for the two surfaces. Thus there would appear to be some interesting but undramatic deviations from the pure cosine distribution. While scattering data was taken at an angle of beam incidence as great as 84.82° no large specular peaks were observed. The plots at this angle of incidence show the influence of edge scattering and of direct beam detection at the extremes of the polar traverse.

One further obstacle to the quantitative interpretation of the data appeared in the observed flattening of the scattering patterns at the poles. This flattening arises as a consequence of the elongation of the beam spot on the extended test surface at large angles of incidence. Where the gage entrance tube also makes a large angle with the test surface normal the illuminated spot is entirely "seen" by the gage. As the tube approaches normal incidence, however, the gage can only "see" a portion of the illuminated area. If completely diffuse scattering were present the entire pattern would lie within the scattering circle established at normal incidence and would be flattened at the pole but symmetrically disposed about the test surface normal.

In order to compare the phenomenological results of the scattering tests with the reported value of f for air on a glass surface, an attempt was made to organize the data for this surface into complete "shells", each shell representing the distribution of scattered flux for all values of the exit coordinates at one angle of incidence. This work resulted in the construction of the smoothed figures of Figures 29 through 32. The outermost line of each figure represents the flux as measured in the incident plane. The inner lines represent the flux in the other meridian planes, taken at 10 degree intervals.

Since the data was quite incomplete in many areas it was necessary

to fill in the shells on the basis of certain reasonable assumptions. It was assumed that the shell area directly intersected by the incoming beam had no sharp cavity or protuberance. It was further assumed that the "back scattering" section of the shell followed the cosine distribution. This assumption was supported by observed data as far as it went. This assumption is further supported by Zahl in his observations of the scattering of Hg from NaCl cleavage planes. (Ref. 35). This means that the surplus of molecules forming the bulge on the "forward scattering" side were assumed to be withdrawn from the total number of molecules striking the surface, leaving the remainder to be scattered in totally diffuse fashion. Finally, it was assumed that the fall-off of the non-diffuse component away from the incident plane proceeded in the same gradual fashion as did the observed fall-off of this component about the specular ray axis. This assumption was again supported by such data as was obtained out of the incident plane.

Four such shells were completed in detail for the incident angles 53.65 degrees, 66.63 degrees, 79.62 degrees, and 84.82 degrees. Data for incident angles at 0.00 degrees, 29.10 degrees and 40.67 degrees yielded completely spherical shells or, in the 40.67 degree case, a shell so nearly spherical as to make uneconomical the rather laborious numerical computations to be described in section 4.0.

## 3.3 A Discussion of Errors

The usability of the data of this experimental program was not dependent upon a knowledge of the absolute value of a pressure or a current, but rather upon the stability of the experimental condition over the period of one data sequence. A data sequence would be any group of related polar traverses including some trace suitable for relating this sequence to another. It was also dependent upon the short time stability of the signal over the period of a beam on-off cycle.

The factors influencing the long time stability of the experimental conditions were the source pressure, the ion gage sensitivity, and the difference amplifier sensitivity. Of these, only the source pressure variation produced a measurable change in the ultimate signal amplitude over the period of a run. The source pressure responded somewhat to ambient temperature changes as a result of differential expansion in the source needle valve. In the operating range (400 to 800 microns

Hg) the slope of the source pressure-beam flux curve varied from
$\sim$ 0.3 to $\sim$ 0.1 chart units per micron. However, only on rare
occasions were the fluctuations within the period of a data sequence
important enough to warrant a correction. A one percent variation in
ultimate signal amplitude from one end of a run to the other, was
typical and was regarded as of no significane for the quantitative
or interpretive purposes of this program.

Less can be said about changes in inherent gage sensitivity
except that these changes (apparently due to film formation on the
gage walls) occurred slowly and did not significantly influence the
self consistency of the data.

The ultimate assurance of satisfactory long time system stability
arose from the comparison of direct beam signal strength at the begin-
ning and end of a data sequence. Such checks showed the direct beam
signal strength variation to be usually smaller than one percent of
the total beam. Occasionally, the variation was no greater than this
over a period of several days.

A much more serious problem was that of achieving a satisfactory
short time fluctuation level. This had been discussed in section
2.3 on instrumentation. However, it is worth considering the experi-
mentally observed signal-to-noise ratio in relation to the reliability
of the data. In the normal observing range the difference amplifier
sensitivity was $10^{-11}$ amperes per chart unit. One chart unit for
this recorder was equivalent to 0.1 millivolt and occupied approxi-
mately 0.05 inches of the recorder scale. At normal gage sensitivity
a deflection of one chart unit would be produced by a pressure change
in one ion gage of the order $10^{-10}$ mm Hg. On this scale the typical
direct beam signal was of the order of 900 chart units while the
diffusely scattered signal produced a plotted amplitude circle of
the order of 18 chart units in diameter. This is consistent with
the acceptance solid angle of the detector entrance tube.

At times when the observing conditions were exceptionally good
(· for instance as represented in Fig. 17) repeated points frequently
reproduced themselves to 0.1 chart units and polar traverses showing
cosine scattering behavior appeared to have an internal consistency
allowing a scatter of 0.1 to 0.3 chart units from the reference circle.

Root mean square deviations of the signal trace amplitude under these conditions were of the order of 0.2 chart units. Observing conditions were regarded as too poor for the taking of interpretable data when the r m s deviations exceeded 2.0 chart units. The bulk of the data was obtained under conditions lying in between these extremes. From observation of the polar traverses it was judged that over 90% of the experimental points lay within one half chart unit of a faired curve. Least square curve fittings were not attempted, since it was clear that the shapes of the scattering plots were well defined. Unfortunately, there remained those whose scattered experimental points led to curve fitting judgements which may have been in error by as much as 10%.

## 3.4 Physical Interpretation of the Data

The salient geometrical features of the data may be reviewed as follows:

(1) The most characteristic shape of all the scattering flux shells was that of a sphere. In the case of the glass surfaces the shells showed a bulging distortion of the forward hemisphere. The spherical shape (cosine distribution) was nearly perfect in the case of the metal surfaces tested.

(2) No shell possessed a "lobe" or dramatic protuberance. There were no cusps, cavities or reversals of curvature, i.e., the local curvature was always inward.

(3) The back scattered hemisphere appeared to be spherical surfaces without distortions in so far as could be determined.

(4) The distortion of the shells in the case of the glass surfaces increased with increasing angle of incidence. The point of maximum distortion occurred close to the intersection point of the specular ray.

(5) The scattering behavior for the unpolished and polished glass surfaces was very similar.

(6) There was no discernable effect on the scattering distributions for the metal surfaces as a result of outgassing

the surfaces either during or following the period of elevated surface temperature.

These data provide a confirmation in some degree of what is already known or what might be guessed regarding the interaction of air or nitrogen with the surfaces tested. That is, it is shown that by far the greatest fraction of air molecules incident to these surfaces scatter from them according to a cosine distribution. Values of f for air on steel and aluminum have not yet appeared in the literature. On the basis of these measurements $f = 1.0$. If all scattering shells in a sequence were figures of revolution about the polar axis but not necessarily spheres, f would also turn out to be 1. It is intuitively satisfying to conclude that probably most other surfaces for which f equals 1 would yield cosine distribution scattering shells in test.

Still, little understanding is gained of the basic mechanism of the scattering. It was not discovered, for example, whether the interactions of the single molecules at the surface were more elastic or more inelastic in nature. A perfectly rough surface might well give rise to the cosine scattering distribution even if every individual molecule-surface interaction were perfectly elastic. One would suspect from published values of the energy accomodation coefficient that this is not the case. On the other hand, one would also suspect from these published values of $\alpha$ that the interactions are not entirely inelastic. For example, $\alpha$ for air on polished cast iron has values of 0.87 to 0.88, although $f$ for polished cold rolled steel has the value 1.0. However, if multiple impacts with the surface irregularities are not excluded, the individual interactions might be quite elastic and still result in the above values of $f$ and $\alpha$. (Ref. 34). Thus, while the results of these experiments give issuing flux distributions, it must again be emphasized that they tell us little about the energy exchange at the surface and hence little about the individual molecule-surface interaction mechanism.

One important uncertainty in the physical interpretation of these results is that relating to the adsorbed films which might lie on the test surface. In the case of the metal surfaces the removal of superficial surface films (if present) by heating had no

effect on the test results as noted in item (6) above. Since the metal surface scattering distributions differed from those of the glass surface one might imagine that some essential properties of the underlying surface were reproduced in the adsorbed films. However, the extent to which the basic properties of the surface were obscured by the surface films remained largely undetermined as did the composition or extent of the surface films themselves. Since oil diffusion pumps were employed, it is quite possible that oil mono-layers formed on all test surfaces in spite of efficient cold trapping. It is also quite possible that nitrogen and other residual gas molecules were adsorbed on the surfaces. The point of view which was therefore adopted as a result of the preceeding consideration was that the effects of surface contamination on the angular flux distributions were small (as suggested by the results of item (6) above) but that some reservation must be retained in predicting behavior for surfaces of absolute cleanness on the basis of the present tests. A modification of the apparatus which would make future experiment less ambiguous in this respect would be the substitution of mercury vapor pumps for the oil diffusion pumps. Mercury vapor does not possess, as strongly as oil vapor, the tendency to stick to metal or glass surfaces.

The scattering behavior evidenced by the glass surfaces suggests strongly that a not-negligible minority of the incident molecules suffered elastic impacts with tilted surface elements, thus smearing out the "specular" component. Since the majority of molecules might still be considered to have undergone a cosine scattering one might imagine that here and there the local field contours have joined to form elastic scattering regions, standing like islands in a jumbled sea of unjoined fields. This model of the inelastic inter-action for the majority of incident molecules with a smeared out specular reflection for the remainder is interestingly close to the original Maxwell model. This particular picture will be referred to as the "modified Maxwell hypothesis".

This picture is by no means the only one permissible as an interpretation of the observed scattering distributions. As was remarked earlier in this section, many hypotheses concerning the

energy exchange between molecule and surface could be made
which would be consistant with the observed scattered flux distribu-
tions. One such is that all molecules are completely accommodated in
energy to that of the surface and are re-emitted from the surface
with a speed distribution in a given direction as though they had
originated from a gas in equilibrium at the temperature of the sur-
face.

The tests on the polished glass surface suggest that the ele-
mentary scattering elements retain their basic character in spite of
the polishing operation. Some substantiation of this is found in the
observations of lens makers that the polishing operation results in
some local melting and flow of the glass surface.

Certainly there is a vast amount of work to be done before much
more understanding of the gas surface interaction with such surfaces
as these could be claimed. However, one of the most promising avenues
of future discovery would appear to be in the use of a velocity se-
lector. Such a device could certainly tell whether or not the
"specular" component was accommodated to the surface temperature, and
at the same time of course, it could yield data leading to an evalu-
ation of the accommodation coefficient.

There are other experiments also likely to yield interesting
results. What are the effects of raising or lowering the mean in-
cidient momentum? At what angles of incidence on complex polished
surfaces do sharp reflection (if any) occur? What can be deduced
about complex surfaces and their associated gas surface  interactions
from careful  experiments on pure single crystals? These questions
suggest only a few of the problems. It is hoped that time and
further experiment will provide an understanding that is still lack-
ing with the completion of this report.

## 4.0  A QUANTITATIVE EXAMINATION OF THE DATA

### 4.1  Introduction

It is of interest to consider the application of the experimental
scattering distribution to the calculation of $f$, the coefficient of
specular reflection. In performing this analysis the surface under
consideration will be regarded as bounding a hypothetical free mole-
cule flow having mass velocity directed tangentially to the surface.

Incident and issuing momentum calculations will be made, subject to various assumptions enumerated below. The issuing momentum calculations will, in part, be dependent upon the form of the experimental scattering distributions. From the incident and issuing momentum calculations, values of f will be obtained in accordance with the definition of that coefficient.

The following assumptions will be applied to these calculations:

A.  For the molecule-surface interaction the element of surface is assumed to be isotropic, i.e., molecules entering at $\ominus$ and $\varphi$ exhibit a characteristic scattering behavior independent of $\varphi$ (see Fig. 41). This assumption does not apply to cleaved surfaces of regular single crystals. It would seem reasonable, however, to apply it to the present case of a cooled liquid surface or to the case of "man-finished" surfaces of micro crystalline or amorphous materials.

B.  It is assumed in the absence of experimental evidence to the contrary that the form of the scattering distribution is dependent on gas, surface, and incident angle only and is independent of the speed of the incident molecules within the range of speeds possessed by molecules of gases at ordinary temperatures. This implies that the form of the distribution is independent of the distribution of speeds in the incident ray. It may very well be that this assumption will be proved inaccurate by later experiment. It is introduced here simply to help provide a model for the calculations.

C.  It is assumed for this calculation that the incident gas is so rarefied that the motion of the impinging molecules is essentially unaltered by those scattered from the surface in question. The velocity distribution of the impinging molecules will be taken to be the Maxwell distribution with superimposed mass velocity.

D.  The definition of f will again be stated, i.e., that

$$f = \frac{G_i - G_r}{G_i} \qquad (4.1)$$

where $G_i$ is the magnitude of the net tangential momentum brought up to the surface per unit time by all incident molecules and $G_r$ is the magnitude of the tangential momentum imparted by the surface to the issuing molecules per unit time.

At this point two alternate assumptions relating to the mode

of energy accommodation at the surface must be introduced. Calcu-
lations made on the basis of each of these assumptions will be pre-
sented.

E-1 It is assumed that molecules issuing in any particular direction
from the scattering surface possess the distribution in speed which
they would have had had they issued from a body of gas in thermal
equilibirum at the surface. It follows that the thermal accommodation
coefficient has the value 1.

E-2 Consider again the form of the scattering distribution of sec-
tion 3.0. As was more fully discussed in that section, the scatter-
ing shells (represented in Figures 29 through 32) show a hemispheric
shape as the "back scattering" section. The distortions from the cosine
scattering sphere take the form of bulges protruding from the "for-
ward scattering" hemisphere. It is assumed that those molecules con-
tributing to the bulging deviation from the cosine scattering sphere
have been perfectly elastically scattered and so possess the same
distribution in speed as before impact. The remainder, i.e., all
those contributing to the cosine scattering sphere are assumed to
possess the distribution in speed given by assumption (E-1). Thus,
for the purpose of this calculation, the great majority of molecules
are assumed to have been diffusely scattered with accommodation coef-
ficient 1 while the remainder are assumed to have been specularly
reflected from tilted surface elements. This is a special case of
the modified Maxwell hypothesis discussed earlier in this report.

## 4.2 Calculation of f Under Terms of Assumption E-1

First consider the quantity of tangential momentum incident on
the surface element. For a representation of surface and coordinate
system, see Figure 41. Let the element of surface be placed at the
origin of coordinates. Let the magnitude of the mass velocity be
$U$ . Let this mass velocity be directed along the positive $X$ axis.
Consider those molecules so directed as to strike the surface from
below. (This choice of coordinates is dictated by convenience since
$C_z$ will be positive for those molecules striking the plate and $C_x$
and $C_y$ will be positive for molecules having a line of flight di-
rected into the first octant). $C_x$, $C_y$, and $C_z$ are the x, y, and
z components of the total molecular velocity relative to the fixed

coordinate system.

The number of molecules of all velocities striking unit area per unit time can be expressed as

$$N_i = m A \int_0^{\infty} \int_{-\infty}^{\infty} \int_{-\infty}^{\infty} C_z F_U \, dC_x \, dC_y \, dC_z \qquad (4.2)$$

where $F_u$ is the Maxwell distribution with superimposed mass velocity,

$$F_U = e^{-\beta^2 \left\{ (C_x - U)^2 + C_y^2 + C_z^2 \right\}} \qquad (4.3)$$

where n is the molecule number density of the gas, $A = \dfrac{\beta^3}{\pi^{3/2}}$, $\beta = \dfrac{1}{V_m} = \sqrt{\dfrac{m}{2kT}}$, and $V_m$ is the most probable speed. Each molecule brings up to the surface a component of the tangential momentum in the direction of the x axis having the value $m\, C_x$. Thus the total x component of tangential momentum brought up to a unit area of surface per unit time by molecules of all velocities is given by

$$G_i = m n A \int_0^{\infty} \int_{-\infty}^{\infty} \int_{-\infty}^{\infty} C_z C_x F_U \, dC_x \, dC_y \, dC_z \qquad (4.4)$$

Integration yields

$$G_i = \frac{m n \bar{C} U}{4} = \frac{m n V_m U}{2\sqrt{\pi}} \qquad (4.5)$$

The calculation of $G_r$, the magnitude of the net tangential momentum transferred from the surface to the issuing molecules, requires a little more work since in some fashion the direct experimental data must be applied. Consider the expression

$$G_r = \int_{C_i, \theta_i, \phi_i, C_r, \theta_r, \phi_r} m \, N_i(C_i, \theta_i, \phi_i) \, P_i(C_i, \theta_i, \phi_i, C_r, \theta_r, \phi_r) \qquad (4.6)$$

$$\times C_r \cos\phi_r \sin\theta_r \, dC_i \, dC_r \, d\omega_i \, d\omega_r$$

Here $P_1(c_i, \theta_i, \phi_i, c_r, \theta_r, \phi_r)$ is a distribution function denoting the probability per unit solid angle and speed range that a molecule with incident speed $C_1$ and direction $\theta_i$, $\phi_i$ will be scattered with speed $C_r$ in direction $\theta_r$, $\phi_r$. Here also $N_i(c_i, \theta_i, \phi_i)$ represents the number of incident molecules per unit speed range and solid angle having the speed $C_1$ and incident direction $\theta_i$, $\phi_i$ striking unit surface area per unit time. Thus Eq. (4.6) states that the net tangential momentum transferred from the surface in the x direction per unit time can be represented by the integral over all speeds and directions of the number per unit time of molecules incident with given speed and direction multiplied by the probability that these molecules will be scattered with a given speed and direction multiplied by the x component of that speed and also by the molecular mass.

Now consider how (4.6) may be specialized by application of the assumptions. By the terms of assumption (E-1) $G_r$ must be determined by the same speed distribution in a particular direction as that holding for molecules issuing from a gas in equilibrium at the temperature of the surface. However, this implies that this distribution in speed is independent of the probability that an issuing molecule will take a given direction as determined from the measured flux distributions of scattering from a real surface. The issuing distribution in speed is also assumed by (E-1) to be independent of the incident speed distribution. Under the terms of assumption B the probability that an issuing molecule will take a given direction is also assumed to be independent of the incident speed. Thus the probability distribution function P may be rewritten as

$$P_1(c_i, \theta_i, \phi_i, c_r, \theta_r, \phi_r) = P_2(\theta_i \, \phi_i \, \theta_r \, \phi_r) P_3(c_r, \theta_r, \phi_r)$$

It will be shown at a later point in this section that $P_3$ is independent of the issuing direction, i.e., $P_3 = P_3(c_r)$.

It will be recalled that the representative scattering shells (see section 3.3 and Figure 42) give scattering information with respect to a primed coordinate system with the $X'$ coordinate axis oriented along the incident ray. From these shells a probability

distribution function of the form P ($\Theta_i, \Theta', \phi'$) can be computed. The function P ($\Theta_i, \Theta', \phi'$) is assumed (assumption A) to be independent of the orientation of $x'$ axis in the scattering surface and hence independent of $\phi_i'$. A change of variables can now be introduced. Letting $\phi' = \phi_r + \phi_i$ and $\Theta' = \Theta_r$, $P_2$ can be rewritten as

$$P_2(\Theta_i, \phi_i, \Theta_r, \phi_r) = P_2(\Theta_i, \Theta_r, \phi_r + \phi_i) = P_2(\Theta_i, \Theta', \phi')$$

and equation (4.6) becomes

$$G_r = \int_{c_i, \Theta_i, \phi_i, c_r, \Theta', \phi'} N_i(c_i, \Theta_i, \phi_i) P_3(c_r) P_2(\Theta_i, \Theta', \phi') \cos(\phi' - \phi_i)$$
$$\times \sin^2\Theta' \sin\Theta_i \, dc_i \, dc_r \, d\Theta_i \, d\phi_i \, d\Theta' \, d\phi' \qquad (4.7)$$

in which the angular integrations are now to be carried out over the variables $\Theta_i, \phi_i, \Theta', \phi'$.

The probability distribution $P_2$ may be expressed in terms of the measured flux distributions as

$$P_2(\Theta_i, \Theta', \phi') = \frac{A(\Theta_i, \Theta', \phi')}{\int_0^{2\pi}\int_0^{\pi/2} A(\Theta_i, \Theta', \phi') \sin\Theta' \, d\Theta' \, d\phi'} \qquad (4.8)$$

where $A(\Theta_i, \Theta', \phi')$ is the beam signal amplitude in arbitrary units, and hence is proportional to the molecule number flux through unit area of the unit scattering hemisphere in the direction $\Theta', \phi'$ i.e., $A(\Theta_i, \Theta', \phi') = K N(\Theta_i, \Theta', \phi')$ where K is a constant of proportionality.

The terms in the primed coordinates may be collected after expansion of $\cos(\phi' - \phi_i)$. The integral over the primed coordinates may be written

$$\int_0^{2\pi}\int_0^{\pi/2} P_2(\Theta_i, \Theta', \phi')(\cos\phi'\cos\phi_i + \sin\phi'\sin\phi_i) \sin^2\Theta' \, d\Theta' \, d\phi'$$

$$= \frac{\int_0^{2\pi}\int_0^{\pi/2} A(\Theta_i, \Theta', \phi')(\cos\phi'\cos\phi_i + \sin\phi'\sin\phi_i \sin^2\Theta' \, d\Theta' \, d\phi'}{\int_0^{2\pi}\int_0^{\pi/2} A(\Theta_i, \Theta', \phi') \sin\Theta' \, d\Theta' \, d\phi'} \qquad (4.9)$$

It should be noted that the scattering shells are symmetric about the $X'$ axis, i.e., $A(\theta_i, \theta', \phi') = A(\theta_i, \theta', -\phi')$, an even function in $\phi'$ about $\phi' = 0$. Hence the portion of the integral (4.9)

$$\int_0^{2\pi}\int_0^{\pi/2} A(\theta_i, \theta', \phi')\sin\phi'\sin\phi_i\sin^2\theta'd\theta'd\phi'$$

must have the value zero.

The remainder of (4.9) may be written as

$$\cos\phi_i \frac{\int_0^{2\pi}\int_0^{\pi/2} A(\theta_i, \theta', \phi')\cos\phi'\sin^2\theta'd\theta'd\phi'}{\int_0^{2\pi}\int_0^{\pi/2} A(\theta_i, \theta', \phi')\sin\theta'd\theta'd\phi'}$$

$$= \cos\phi_i\, g_r(\theta_i) \qquad\qquad (4.10)$$

The integrals of $g_r(\theta_i)$, (defined by equation (4.10) must be evaluated numerically. Details of the numerical integration are given in Appendix B and a plot of the results is shown in Figure 44.

The evaluation of $P_3(C_r)$ must be considered more fully at this point. Consider a coordinate system $\xi, \eta, \zeta$ immersed in a body of gas at rest having molecule number density $n_f$. The number of molecules per unit time crossing unit area of the $\xi, \eta$ plane into solid angle $d\Omega$ making angle $\psi$ with the $\zeta$ axis and having speed lying within the range $C_f$ to $C_f + dC_f$ is given by

$$N_{f\,dC_f\,d\Omega} = m_f A_f C_f^2 e^{-\beta_f^2 C_f^2} C_f\cos\psi\,dC_f\,d\Omega$$

Then the probability per unit solid angle that a molecule will have a speed $C_f$ lying within unit speed range will be

$$P(C_f) = \frac{m_f A_f e^{-\beta_f^2 C_f^2} C_f^3 \cos\psi}{\int_0^\infty m_f A_f e^{-\beta_f^2 C_f^2} C_f^3 \cos\psi\,dC_f}$$

If this fictitious gas is assumed to be thermal equilibrium with the surface then

$$P(C_f) = P_3(C_r) = \frac{e^{-\beta_r^2 C_r^2} C_r^3}{\int_0^\infty e^{-\beta_r^2 C_r^2} C_r^3\,dC_r}$$

An integration of $P(C_r) C_r dC_r$ over all speeds may be performed immediately such that

$$\int_0^\infty P(C_r) C_r \, dC_r = \overline{\overline{C}}_r = \frac{3\sqrt{\pi}}{4\,\beta_r} \tag{4.11}$$

Equation (4.7) may now be rewritten as

$$G_r = \int_{C_i, \Theta_i, \phi_i} m \, N_i(C_i, \Theta_i, \phi_i) \, \overline{C}_r \, g_r(\Theta_i) \cos\phi_i \sin\Theta_i$$
$$\times dC_i \, d\Theta_i \, d\phi_i \tag{4.12}$$

Equation (4.12) may be looked at in a very direct and intuitive fashion. A review of the integral of Eq. (4.10) defining $g_r$ ( $\Theta_i$ ) will show that the quantity $m\overline{C}_r g_r(\Theta_i)$ might be thought of as being the magnitude of the mean $X'$ component of tangential momentum per molecule transferred from unit area of the surface per unit time in the primed coordinate system by molecules incident at angle $\Theta_i$ . Multiplication by $\cos\phi_i$ , the angle made by the $X'$ axis with the x axis of the original coordinate system, gives the value of the aforementioned momentum in the x direction of the original coordinate system. Multiplication of this quantity by the number of molecules incident per unit time of all speeds from all directions and an integration overall vairables yields the total magnitude of tangential momentum transferred from the surface.

To return to the original argument, if the integrand of equation (4.2) is put into polar coordinate form, there results, as the number of molecules incident on the surface per unit time from direction $\Theta_i$ and $\phi_i$ in the intervals $d\Theta_i$ and $d\phi_i$ having the speed $C_i$ in the range $d C_i$, the expression

$$N_i(C_i, \Theta_i, \phi_i) dC_i \, d\Theta_i \, d\phi_i = m \, A \, C_i^3 \sin\Theta_i \cos\Theta_i$$
$$\times e^{-\beta^2\left\{(C_i \sin\Theta_i \cos\phi_i - U)^2 + C_i^2 \sin^2\Theta_i \sin^2\phi_i + C_i^2 \cos^2\Theta_i\right\}} \, dC_i \, d\Theta_i \, d\phi_i \tag{4.13}$$

which reduces to

$$N_i(c_i\theta_i\phi_i)\,dc_i\,d\phi_i\,d\phi_i = m\,A\,c_i^3\,\sin\theta_i\cos\theta_i$$

$$\times e^{-\beta^2\left\{c_i^2 - 2c_iU\sin\theta_i\cos\phi_i + U^2\right\}}\,dc_i\,d\theta_i\,d\phi_i$$

Then

$$G_r = \frac{m\,m\,3\sqrt{\pi}\,A}{4\beta_r}\int_0^{2\pi}\int_0^{\pi/2}\int_0^{\infty} c_i^3\,g_r(\theta_i)\cos\theta_i\,\sin\theta_i\cos\phi_i$$

$$\times e^{-\beta^2\left\{c_i^2 - 2c_iU\sin\theta_i\cos\phi_i + U^2\right\}}\,dc_i\,d\theta_i\,d\phi_i \qquad (4.14)$$

Performing the indicated integrations over $C_i$ and $\phi_i$ we have,

$$G_r(\theta_i) = \frac{m\,m\,3\sqrt{\pi}\,e^{\frac{b^2}{2}-s^2}}{16\beta_r\beta}\cos\theta_i\,\sin\theta_i\,g_r(\theta_i)$$

$$\times \left[(3b+2b^3)I_0\left(\frac{b^2}{2}\right) + (b+2b^3)I_1\left(\frac{b^2}{2}\right)\right]$$

$$\qquad (4.15)$$

where $b = s\,\sin\theta_i$ and $I_0$ and $I_1$ are modified Bessel functions and $s(s = \frac{U}{V_m})$ is the molecular speed ratio.

The details of the integration above are given in Appendix A and $\dfrac{G_r(\theta_i)}{m\,m\,g_r(\theta_i)\,V_m\,V_{mr}}$ is plotted as a function of $\theta_i$ for $s = 0.1$, $1.0$, $2.0$, and $10.0$ as given in Figure 43.

The final integration over $\theta_i$ must be performed numerically of course. One can observe immediately, however, that for $g_r(\theta_i) = 0$ (diffuse reflection) $G_r$ will equal 0 and $f = 1$.

Thus, subject to the limitations of the data and of the assumptions, $f$ can be calculated for any molecular speed ratio, $s$, from the direct measurement of the scattered flux. Such calculations were carried out for the case of the unpolished glass surface for values of $s = 0.1$, $1.0$, $2.0$, and $10.0$ and $\beta_r = \beta$. A plot of the resultant findings showing the behavior of $f$ as a function of $s$ is shown in Figure 45.

## 4.3 Calculation of f under Terms of Assumption E-2

The main work of this section is again the calculation of $G_{r2}$, the magnitude of the tangential momentum transferred from the gas to the surface under the terms of assumption E-2. With the exception of this latter assumption, all assumptions are as outlined in section 4.1. The same flow situation is also assumed. $G_i$ will remain as calculated in Eq. 4.5.

Consider now again how the probability distribution function of Eq. (4.6) might be appropriately specialized. According to the terms of assumption E-2 two alternate classes of gas-surface interaction occur. The scattered molecules may be either diffusely scattered according to the cosine distribution with speed distribution as in assumption E-1 or they may be specularly scattered from tilted surface elements. The total probability distribution may be represented as the sum of the probability distributions for these two alternate events. Eq. 4.6 may be rewritten as follows:

$$G_{r2} = \int_{C_i,\Theta_i,\phi_i,C_r,\Theta_r,\phi_r} m\, N_i(C_i,\Theta_i,\phi_i)\left\{ P_{1D}(C_i,\Theta_i,\phi_i,C_r,\Theta_r,\phi_r)C_r \right.$$

$$\left. + P_{1S}(C_i\Theta_i\phi_i\,C_r\,\Theta_r\,\phi_r)C_r \right\}\cos\phi_r \sin^2\Theta_r \sin\Theta_i$$

$$\times\, dC_i\,d\Theta_i\,d\phi_i\,dC_r\,d\Theta_r\,d\phi_r \tag{4.16}$$

The subscript D identifies the probability function associated with the diffusely scattered molecules while the subscript S identifies that associated with the specularly scattered molecules.

By the same arguments as were employed in section 4.2, $P_{1D}(C_i,\Theta_i,\phi_i,C_r,\Theta_r,\phi_r)$ can be specialized to the form $P_{2D}(\Theta_i,\Theta',\phi')$ $\times P_{3D}(C_r)$ where $\phi' = \phi_r + \phi_i$ and $\Theta' = \Theta_r$ as before. The probability distribution function $P_{1S}(C_i,\Theta_i,\phi_i,C_r,\Theta_r,\phi_r)$ can be specialized immediately to the form $P_{2S}(\Theta_i,\Theta',\phi')$ since the angular flux distribution is assumed to be independent of $C_i$ (assumption B) and for these molecules $C_r$ can have only the value $C_i$. Thus equation 4.16 can be rewritten as

$$G_{r2} = \int_{C_i,\Theta_i,\phi_i,C_r,\Theta',\phi'} m\, N_i(C_i,\Theta_i,\phi_i)\left\{ P_{2D}(\Theta_i,\Theta',\phi')P_{3D}(C_r)C_r \right.$$

$$\left. + P_{2S}(\Theta_i,\Theta',\phi')C_i \right\}\cos(\phi'-\phi_i)\sin^2\Theta' \tag{4.17}$$

$$\times\, \sin\Theta_i\,dC_i\,d\Theta_i\,d\phi_i\,dC_r\,d\Theta'\,d\phi'$$

Recalling again assumption (E-2), it can be seen that $A(\Theta_i, \Theta', \phi')$, the beam signal amplitude ( $A(\Theta_i, \Theta', \phi') = K N(\Theta_i, \Theta', \phi')$ as before), can be written

$$A(\Theta_i, \Theta', \phi') = A_D \cos\Theta' + A_S(\Theta_i, \Theta', \phi')$$

where $A_D$ is a constant representing the diameter of the assumed diffuse scattering sphere and $A_S(\Theta_i, \Theta', \phi')$ are the amplitude differences between this sphere and the total amplitudes of the specular bulges. From the data then, $P_{2D}(\Theta_i, \Theta', \phi')$ can be found as indicated below:

$$P_{2D}(\Theta_i, \Theta', \phi') = \frac{A_D \cos\Theta'}{\int_0^{2\pi}\int_0^{\pi/2} A(\Theta_i, \Theta', \phi') \sin\Theta'\, d\Theta'\, d\phi'} \qquad (4.18)$$

while $P_{2S}(\Theta_i, \Theta', \phi')$ becomes

$$P_{2S}(\Theta_i, \Theta', \phi') = \frac{A_S(\Theta_i, \Theta', \phi')}{\int_0^{2\pi}\int_0^{\pi/2} A(\Theta_i, \Theta', \phi') \sin\Theta'\, d\Theta'\, d\phi'} \qquad (4.19)$$

Extracting the integrals over the primed coordinates which apply to $P_{2S}$ from 4.17, we have

$$\frac{\int_0^{2\pi}\int_0^{\pi/2} A_D\cos\Theta'\{\cos\phi'\cos\phi_i + \sin\phi'\sin\phi_i\} \sin^2\Theta'\, d\Theta'\, d\phi'}{\int_0^{2\pi}\int_0^{\pi/2} A(\Theta_i, \Theta', \phi') \sin\Theta'\, d\Theta'\, d\phi'} \qquad (4.20)$$

which has the value zero.

The remainder of the integration over the primed coordinates may be written

$$\frac{\int_0^{2\pi}\int_0^{\pi/2} A_S(\Theta_i, \Theta', \phi')\{\cos\phi'\cos\phi_i + \sin\phi'\sin\phi_i\} \sin^2\Theta'\, d\Theta'\, d\phi'}{\int_0^{2\pi}\int_0^{\pi/2} A(\Theta_i, \Theta', \phi') \sin\Theta'\, d\Theta'\, d\phi'} \qquad (4.21)$$

For the same reasons of symmetry as before, the integration over the second section of the numerator (i.e. over the section

$A_S(\Theta_i, \Theta', \Phi')\sin\Phi'\sin\Phi_i$ ) makes no contribution to the total values of the integral. Further, we can add $A_D\cos\Theta'$ to $A_S(\Theta_i, \Theta', \Phi')$ without changing the value of the integral. Thus the expression 4.21 can be re-expressed as

$$\cos\Phi_i\frac{\displaystyle\int_0^{2\pi}\int_0^{\pi/2}A(\Theta_i\,\Theta'\,\Phi')\cos\Phi'\sin^2\Theta'\,d\Theta'd\Phi'}{\displaystyle\int_0^{2\pi}\int_0^{\pi/2}A(\Theta_i,\Theta',\Phi')\sin\Theta'\,d\Theta'd\Phi'} \qquad (4.22)$$

$$= \cos\Phi_i\, g_r(\Theta_i)$$

The $g_r(\Theta_i)$ as defined here is the same as that defined by Eq. 4.10 of the previous section.

Equation 4.17 may now be rewritten as

$$G_{r2} = \int_{c_i,\Theta_i,\Phi_i} N_i(c_i,\Theta_i,\Phi_i)\,c_i\,g_r(\Theta_i)\cos\Phi_i\sin\Theta_i\,dc_i\,d\Theta_i\,d\Phi_i$$
$$(4.23)$$

If now the function $N_i$ $(c_i,\Theta_i,\Phi_i)$ is expressed in polar coordinate form as in equation 4.13, and if the integrand of 4.23 is multiplied by $\dfrac{\sin\Theta_i}{\sin\Theta_i}$ $G_{r2}$ becomes

$$G_{r2} = \int_{c_i,\Theta_i,\Phi_i}\left(\frac{g_r(\Theta_i)}{\sin\Theta_i}\right)\left[mn\,A\,c_i^4\,e^{-\beta^2\left\{c_i^2-2c_i U\sin\Theta_i\cos\Phi_i+U^2\right\}}\right.$$
$$\left.\times\cos\Phi_i\sin^2\Theta_i\cos\Theta_i\right]dc_i\,d\Theta_i\,d\Phi_i$$
$$(4.24)$$

or

$$G_{r2} = \int_0^{\pi/2}\frac{g_r(\Theta_i)}{\sin\Theta_i}\,G_i(\Theta_i)\,d\Theta_i \qquad (4.25)$$

where $G_i$ ( $\Theta_i$ ) is the integral over $c_i$ and $\Phi_i$ of the quantity within the brackets of Eq. (4.24). Although this grouping might appear rather arbitrary it is justified by the fact that $G_i(\Theta_i)$ has an interesting physical interpretation since the function represents

the net x component of momentum incident on the surface per unit time, unit area and unit polar angle at angle $\Theta_i$ resulting from molecules of all speeds coming from all azimuth angles.

The result of integration over $C_1$ and $\phi_i$ can be written in the form

$$G_i(\Theta_i) = m n V_m^2 \cos\Theta_i \sin^2\Theta_i e^{-s^2}$$

$$\times \left[ (S' + 1)(b^3 + 2b) \right] \quad (4.26)$$

where

$$S' = S \frac{b e^{b^2}}{2\sqrt{\pi}} \quad, \quad b = s \sin\Theta_i \quad, \quad s = \frac{U}{V_m}$$

and

$$S = \int_0^{2\pi} \cos\phi_i \, ERF(b\cos\phi_i) \, e^{-b^2 \sin^2\phi_i} \, d\phi_i \quad (4.27)$$

Details of the integration may be found in Appendix C and a plot of $S'$ may be found in Figure 46 giving $S'$ for values of b from 0 to 10. Also $\frac{G_i(\Theta_i)}{m n V_m^2}$ has been plotted as a function of $\Theta_i$ for s = 0.1, 1.0, 2.0, and 10.0; see Figure 47.

Thus again, subject to the limitations of the assumptions, f can be calculated for any molecular speed ratio. Such calculations were performed for the unpolished glass surface for s = 0.1, 1.0, 2.0, and 10.0 and a plot of the results is shown in Figure 45. The final integration over $\Theta_i$ in the evaluation of $G_{r2}$ had to be performed numerically, of course.

## 4.4 Calculation of f for Pure Specular Reflection at Grazing Incidence

A consideration of Figure 47 will show that molecules incident at angles close to grazing, play an increasingly important part in the momentum transfer to the surface as the molecular speed ratio increases. It has already been argued that at some incident angle very close to grazing a condition of pure specular reflection may set in. (i.e., the reflected molecule has direction $\phi_i$ and $\pi - \Theta_i$

and has speed $C_r = C_i$). All molecules at some angle $\Theta_0$ on to 90°
will be assumed to be specularly reflected for the purpose of this
speculative calculation while all molecules incident form $0°$ to $\Theta_0$
will be assumed to be diffusely reflected according to the cosine law
and thus contribute nothing to the momentum transfer from the surface.
f for this situation can be very simply formulated as

$$ f = \frac{1 - \int_{\Theta_0}^{\frac{\pi}{2}} G_i(\Theta_i) \, d\Theta_i}{G_i} \qquad (4.28) $$

where the tangential momentum transferred from the surface is equal
in magnitude to $G_i(\Theta_i)$ integrated from $\Theta_0$ to $\frac{\pi}{2}$. Calculations
of f were performed for $\Theta_0$ assuming various values from 85° to
90° and for s, the molecular speed ratio taking on the values s = 0.1,
1.0, 2.0 and 10.0. The results of these calculations are plotted in
Figure 48.

## 4.5 Discussion

Figure 45 shows the behavior of f for variations of the para-
meter s for both assumed cases of molecular interaction E-1 and E-2.
The diverging behavior of these plots lends plausibility to the
intuition which had originally led to assumptions E-1 and E-2; namely
that these assumptions were bracketing assumptions and that more com-
plete knowledge of the scattering probability distribution function
would probably lead to values of f for this surface lying in be-
tween these extremes.

It is possible that the relative validity of assumptionsE-1 and
E-2 leading to the divergent results above might be assessed by the
performance of a rotating cylinder experiment at molecular speed
ratios of 2 or more. Unfortunately, such an experiment would be
difficult to perform because of the high peripheral speeds involved
and the delicate drag measurements necessary to resolve the rather
small differences in f. A much more reasonable approach would be,
as suggested in section 3.4, to introduce a velocity selector into
the path of the scattered molecules in a molecular beam experiment
and measure directly the reflected speed distributions.

It is interesting to note that neither calculation based on the alternate assumptions (E-1) and (E-2) yielded values of f nearly low enough for agreement with the reported value of f = 0.89 for air on glass. Such a value is clearly beyond the limit of error of these present experiments since it could only result from much larger forward distortions of the scattering shells. Millikan, in arriving at his value of f (above) re-examined the earlier work of Knudsen and of Warburg on slip in glass capillaries. Warburg worked with air on glass while Knudsen confined his investigations to $H_2$, $O_2$ and $CO_2$. It is barely possible that the somewhat higher pressures at which these early experiments were performed has some effect on the adsorbed gas layer thickness, which in turn may have allowed more "specular" scattering. It is also likely that some errors could be expected as a result of using the findings of experiments on gases other than air to make predictions for the air-glass surface interaction. However, no explanation has been found which properly accounts for the discrepancy between Millikan's results and that of this report.

The results of the calculation of section 4.4 are also quite interesting since they serve to show the importance of the gas-surface behavior at near glancing angles of incidence in determining the overall momentum transfer. These results also serve to show the importance of extending the molecular beam scattering experiments to include measurements at angles extremely close to glancing. It need hardly be stated that an engineering surface which exhibited some considerable degree of specular reflection at a few degress from glancing incidence would find immediate application in high altitude, high speed aerodynamics.

It is hoped that the calculations of this section will suggest a new approach to the problems of evaluating the boundary conditions for rarefied gas flows. It seems possible that the old concepts of a constant f and a constant $\propto$, the energy transfer counterpart of f, might profitably be supplanted by the more general scattering probability function.

## 5.0 SUMMARY

A molecular beam apparatus was used to investigate the scattering of air and $N_2$ molecules from surfaces of polished low carbon steel,

etched low carbon steel, polished aluminum, unpolished window glass, and polished window glass. A beam of molecules was directed against the surfaces at representative angles of incidence. Polar flux distributions of the scattered molecules were measured by a movable detector. An ionization gage beam detector system was devised to accomplish this measurement.

Spatial polar plots of these measured flux distributions were found to approximate closely the form of the cosine scattering distribution for the cases of the steel and aluminum surfaces. Similar plots in the case of the glass surfaces were found to have well defined but small bulging deviationsfrom the cosine scattering shape on the side away from the incident beam. These findings did not serve to distinguish the degree of elasticity of the interaction since both elastic and inelastic interaction models would serve to produce pure cosine scattering, and only a small degree of elasticity would suffice in some models to account for the observed deviation from cosine scattering. Among others, a modified Maxwell model would seem to satisfy the available data. In this, a fraction of the incident molecules undergo a diffuse scattering, being more or less accomodated in energy to the surface, while the remainder are specularly reflected from tilted surface elements.

In order to illustrate one aerodynamic application of scattering data obtained by molecular beam techniques, a procedure was devised for the computation of the coefficient of specular reflection, f, and values of this coefficient were calculated for the case of an unpolished glass surface oriented tangentially to the direction of mass motion in a free molecule flow. These values were calculated as a function of the parameter s, the molecular speed ratio. If all scattered molecules are assumed to possess the distribution in speed in a particular direction which they would have had had they issued from a gas in equilibrium at the temperature of the surface, f takes on values of $\sim$ 0.97 as s approaches 0 to $\sim$ 0.99 at s = 10. Alternatively, if the modified Maxwell surface interaction model is assumed, f takes on values of $\sim$ 0.97 as s approaches 0 to $\sim$ 0.93 at s = 10. These values do not agree with the published value of f of 0.89 for air on glass. This lack of agreement could not be accounted for by a consideration of experimental errors.

A speculative calculation was performed showing the effect on f for molecular speed ratios of 0.1, 1.0, 2.0, and 10.0, in the case where

a condition of pure specular reflection occurs from source angle, $\Theta_o$, close to grazing incidence on to 90° incidence. f was shown to have the value $0.5$ for $s = 10$ and $\Theta_o = 85°$.

Three points of departure for further experimental work were discussed. A. The substitution of mercury diffusion pumps for the present oil diffusion pumps would remove one important source of surface contamination. B. Higher resolution experiments using a slit-form beam geometry would yield interesting data on the behavior of the scattering at incident angles close to grazing. C. A velocity selector introduced into the scattered beam would afford a means of determining the relative validity of the assumptions leading to the computed values of f. This device would also afford a means of studying in detail the energy exchange between gas and surface. This latter work would provide a valuable basis for a better physical understanding of the basic scattering mechanisms.

## ACKNOWLEDGEMENT

# REFERENCES

1) A. Kundt,
   E. Warburg
      – "Über Reibung und Wärmeleitung, verdünnter Gase", Phil. Mag. 50, (1875)

2) L. B. Loeb
      – "Kinetic Theory of Gases", McGraw-Hill Publishing Co. (1934)

3) S. A. Schaaf,
   P. L. Chambre
      – "The Flow of Rarefied Gases", High Speed Aerodynamics and Jet Propulsion Vol. 4, Princeton University Press.

4) J. C. Maxwell
      – "Scientific Papers", Vol. 2, p 708

5) M. Knudsen
      – "Die molikulare Wärmeleitung der Gase und der Akkommodations koefficient", Ann. Physik, Vol. 34, (1911) pp 593-656.

6) R. G. Fraser
      – "Molecular Rays", Cambridge University Press (1931).

7) I. Estermann,
   O. Stern
      – "Beugung von Molekularstrahlen", Z. Physik, Vol. 61, (1930) p 95.

8) F. Knauer,
   O. Stern
      – "Über die Reflexion von Molekularstrahlen", Z. Physik, Vol. 53, (1929) p 779.

9) R. W. Wood
      – "Law of Reflection of Gas Molecules", Phil. Mag. Vol. 30 (1915) p 304.

10) M. Knudsen
      – "Das Cosinasgesetz in der Kinetischen Gastheorie", Ann. Physik, Vol. 48 (1915) p 1113.

11) R. A. Millikan
      – "Coefficients of Slip in Gases and the Law of Reflection of Molecules from the Surfaces of Solids and Liquids", Phys. Rev. Vol. 21, (1923) p 217.

12) E. Blankenstein — "Coefficient of Slip and Momentum Transfer in $H_2$, He, air and $O_2$" Phys. Rev. Vol. 22 (1923) p 582.

13) S. F. Chiang — "Drag on a Rotating Cylinder at Low Pressures", Inst. of Engr. Res., Univ. of Calif., Eng. Projs. Rept. HE-150-85 (1951) (also Ph.D. thesis).

14) M. Knudsen — "Kinetic Theory of Gases", Methuen, (1934) London.

15) R. N. Oliver, M. Farber — "Experimental Determination of Accommodation Coefficients as Function of Temperature for Several Metals on Gases", Jet Propulsion Lab., Calif. Inst. of Tech., Memorandum No. 9-19 (1950).

16) M. L. Weidmann — "Thermal Accommodation Coefficients", Trans. ASME, 68, p 57 (1946).

17) J. K. Roberts — "The Exchange of Energy Between Gas Atoms and Solid Surfaces", Proc. Roy. Soc. (London) A 129 p 146 (1930) and A 135 p 135 (1932).

18) W. C. Michels — "Accommodation Coefficients of Helium and Argon against Tungsten", Phys. Rev. Vol. 40, (1932) p 472.

19) J. B. Taylor — "Reflection of Beams of Alkali Metals from Crystals", Phys. Rev. Vol. 35 (1930) p 375.

20) A. Ellet, H. F. Olson — "The Reflection of Atoms by a Crystal", Phys. Rev. Vol. 31 (1928) p 643.

21) A. Ellet, H. F. Olson, H. A. Zahl — "The Reflection of Atoms from Crystals", Phys. Rev. Vol. 34 (1929) p 493.

22) H. A. Zahl — "Reflection of Cd and Zn Atoms from NaCl Crystals", Phys. Rev. Vol. 36, (1930) p 893.

23) T. H. Johnson — "Reflection of H Atoms from Li F Crystals", Jo. Frank. Inst. Vol. 210, (1930) p 135.

24) I. Estermann, R. Frisch, O. Stern — "Monochromasierung der de Broglie - Wellen von Molekularstrahlen", Z. Physik, Vol. 73, (1931) p 348.

25) G. J. Maslach — "A Precision Manometer for Low Pressures", Inst. of Engr. Res. Univ. of Calif. Eng. Projs. Rept. HE-150-75, (1950).

26) F. C. Hurlbut — "Instrumentation for Molecular Beam (Part 2 Progress on Development of a Molecular Beam Ionization Gage Detector)", Inst. of Engr. Res., Univ. of Calif., Engr. Projs. Rept. HE-150-52, (1949).

27) F. C. Hurlbut — "An Experimental Investigation of Flow through Short Tubes for Large Molecular Mean Free Path", Inst. of Engr. Res., Univ. of Calif. Engr. Projs. Rept. HE-150-54, (1949).

28) F. C. Hurlbut — "A Molecular Beam Investigation of Free Molecule Flow Through Short Tubes", Inst. of Engr. Res., Univ. of Calif. Eng. Projs. Rept. HE-150-94 (1951).

29) R. T. Bayard, D. Alpert — "Extensions of the Low Pressure Range of the Ionization Gage", RSI 21 (1950), p 571.

30) M. L. Greenough,
W. E. Williams,
J. K. Taylor

\- "Regulated Low Voltage Supply for Electrolysis and Other Uses", RSI Vol. 22 (1951) p 484.

31) U. J. Childs

\- "The Childs' Custom Built Amplifier", Rad. and Television News, Vol. 46 (1951) p 37.

32) A. Q. Nier,
E. P. Ney,
M. G. Ingraham

\- "A Null Method for the Comparison of Two Ion Currents in a Mass Spectrometer", RSI 18 (1947) p 294.

33) G. L. Mellen

\- "Radium Type Vacuum Gage", Electronics, April 1946.

34) B. Baule

\- "Theoretische Behandlung der Erscheinungen in Verdunnten Gasen", Ann. Physik 44 (1914) p 145.

35) H. A. Zahl,
A. Ellet

\- "Reflection of Mercury from Alkali Halide Crystals", Phy. Rev. Vol. 38 (1931) 977.

36) F. C. Hurlbut

\- "Molecular Beam Model 2", Inst. of Engr. Res. Univ. of Calif. Engr. Projs. Rept. HE-150-79, (1951).

## APPENDIX A

To integrate over $C_i$ and $\phi_i$

$$G_r = \frac{mm\, 3\sqrt{\pi}\, A}{4\,\beta_r} \int_0^{2\pi} \int_0^{\pi/2} \int_0^{\infty} C_i^3\, g_r(\theta_i) \cos\theta_i \sin\theta_i \cos\phi_i$$

$$\times\, e^{-\beta^2 \{C_i^2 - 2C_i U \sin\theta_i \cos\phi_i + U^2\}} \qquad \text{(A-1)}$$
$$dC_i\, d\theta_i\, d\phi_i \qquad \text{(Eq. 4.14 = A-1)}$$

let $P = 2U \sin\theta \cos\phi$

and $\dfrac{P\beta}{2} = \dfrac{U}{V_m} \sin\theta \cos\phi = b \cos\phi$

Making the above substitution, completing the square in the exponent, and letting $\dfrac{mm\, 3\sqrt{\pi}\, A \cos\theta \sin\theta\, g_r(\theta)}{4\,\beta_r} = M$

there results

$$G_r(\theta)\,d\theta = M\,d\theta \int_0^{2\pi} \cos\phi\, d\phi\, e^{-\beta^2(U^2 - \frac{P^2}{4})} C^3\, e^{-\beta^2(C - \frac{P}{2})^2}\, dC$$

Integration over $C$ yields

$$G_r(\theta)\,d\theta = M\,d\theta \int_0^{2\pi} \cos\phi\, e^{-\beta^2(U^2 - \frac{P^2}{4})} \left[ \frac{P\sqrt{\pi}}{8\,\beta^3} \left\{ 1 + \mathrm{ERF}\left(\frac{P\beta}{2}\right) \right\} \right.$$

$$\left. + \left(\frac{P^2}{4} + \frac{1}{\beta^2}\right) \frac{1}{2\beta^2} \left\{ e^{-\frac{P^2\beta^2}{4}} + \sqrt{\pi}\, \frac{P\beta}{2}\left[ 1 + \mathrm{ERF}\left(\frac{P\beta}{2}\right) \right] \right\} \right] d\phi \qquad \text{(A-2)}$$

Multiplying out and collecting terms it was found that the integrals over $\phi$ not equal to zero are:

$$\frac{3\sqrt{\pi}}{4\,\beta^4} \int_0^{2\pi} \cos^2\phi\, e^{b^2 \cos^2\phi}\, d\phi$$

$$= \frac{3\pi^{3/4}}{4\,\beta^4} e^{\frac{b^2}{2}} b \left[ I_0\left(\frac{b^2}{2}\right) + I_1\left(\frac{b^2}{2}\right) \right] \qquad \text{(A-3)}$$

and

$$\frac{b^3\sqrt{\pi}}{4\,\beta^4} \int_0^{2\pi} \cos^4\phi\, e^{b^2 \cos^2\phi}\, d\phi$$

$$= \frac{\pi^{3/4}\, b^3}{4\,\beta^4} e^{\frac{b^2}{2}} \left[ I_0\left(\frac{b^2}{2}\right) + \left(1 - \frac{1}{b^2}\right) I_1\left(\frac{b^2}{2}\right) \right] \qquad \text{(A-4)}$$

$I_0\left(\frac{b^2}{2}\right)$ and $I_1\left(\frac{b^2}{2}\right)$ are the zeroth and first order modified Bessel functions of the first kind.

A final collection of terms yields the result of Eq. 4.15:

$$G_r(\theta_i) = \frac{m\,n\,3\sqrt{\pi}\,e^{\frac{b^2}{2} - s^2}}{16\,\beta_r\,\beta} \cos\theta_i\,\sin\theta_i\,g_r(\theta_i)$$

$$\times\left[(3b+2b^3)I_0\left(\frac{b^2}{2}\right) + (b+2b^3)I_1\left(\frac{b^2}{2}\right)\right]$$

## APPENDIX B

In order to perform the indicated integration of Eq. 4.11 i.e.

$$\int_0^{2\pi} \int_0^{\pi/2} A(\theta_i, \theta', \phi') \cos\phi' \sin^2\theta' \, d\theta' \, d\phi'$$

and

$$\int_0^{2\pi} \int_0^{\pi/2} A(\theta_i, \theta', \phi') \sin\theta' \, d\theta' \, d\phi'$$

the indicated integrations must be replaced by summations and the summation carried out over the surface of a unit hemisphere. Thus the flux through a surface element is approximated by $A_m(\theta_i, \theta', \phi') \Delta a_m$ where

$$\sum_{m=0}^{b} \Delta a_m = a = 2\pi \, (\text{UNITS})^2$$

A simple integration scheme was devised in which the total unit hemisphere was divided into 414 elementary surfaces of approximately equal area. Since the scattering distributions were assumed symmetrical about the incident plane, just half of this number were employed in the actual integration. Since all scattering shells were regarded as spherical on the incident ray side, this section of the integration was performed only once. For a representation of the division of the unit hemisphere surface see Figure 49.

The $A_m(\theta_i, \theta', \phi')$ were taken from the representations of the scattering shells at the centerpoint of each elementary area. The resultant $g_r(\theta_i)$ are illustrated in Figure 44.

A table of the $\Delta a_m$ of this integration scheme follows:

| BOUNDING POLAR ANGLES OF SPHERICAL ZONE | NUMBER OF ELEMENTARY SURFACES IN SPHERICAL ZONE | AREA OF SURFACE ELEMENT |
|---|---|---|
| 90° - 85° | 36 | 0.015212 |
| 85° - 80° | 36 | 0.015048 |
| 80° - 75° | 36 | 0.014866 |
| 75° - 70° | 36 | 0.014520 |
| 70° - 65° | 36 | 0.014068 |
| 65° - 60° | 36 | 0.013503 |
| 60° - 55° | 36 | 0.012843 |
| 55° - 50° | 36 | 0.012083 |

| BOUNDING POLAR ANGLES OF SPHERICAL ZONE | NUMBER OF ELEMENTARY SURFACES IN SPHERICAL ZONE | AREA OF SURFACE ELEMENT |
|---|---|---|
| 50° – 40° | 36 | 0.024586 |
| 40° – 30° | 36 | 0.017455 |
| 30° – 20° | 30 | 0.015425 |
| 20° – 10° | 18 | 0.015752 |
| 10° – 0° | 6 | 0.015909 |

## APPENDIX C

To evaluate the net incident tangential momentum $G_i(\theta_i)$ as a function of $\theta_i$ where

$$G_i(\theta_i) = \frac{m\,m\,\beta^3}{\pi^{3/2}}\sin^2\theta_i\cos\theta_i \int_0^{2\pi}\int_0^\infty c_i^+ \cos\phi_i$$

$$\times\, e^{-\beta^2\{c_i^2 - 2c_i U \sin\theta_i\cos\phi_i + U^2\}}\, dc_i\, d\phi_i \qquad (C-1)$$

(From Eqs. 4.24 and 4.25)

let $P = U\sin\theta\cos\phi$

and $\dfrac{P\beta}{2} = \dfrac{U}{V_m}\sin\theta\cos\phi = b\cos\phi$

as in Appendix A.

Making the above substitution, completing the square in the exponent and letting

$$\frac{m\,m\,\beta^3}{\pi^{3/2}}\sin^2\theta\cos\theta = M'$$

there results

$$G_i(\theta) = M'\int_0^{2\pi}\int_0^\infty \cos\phi\, e^{-\beta^2\left(U^2 - \frac{P^2}{4}\right)} c^4 e^{-\beta^2\left(c - \frac{P}{2}\right)^2}\, dc\, d\phi$$

Integration over C yields

$$G_i(\theta) = M'\int_0^{2\pi}\cos\phi\, e^{-\beta^2\left(U^2 - \frac{P^2}{4}\right)}$$

$$\times\left[\frac{1}{2\beta^2}\left(\frac{P^2}{4} + \frac{3}{2\beta^2}\right)\frac{\sqrt{\pi}}{2\beta}\left[1 + \mathrm{ERF}\left(\frac{P\beta}{2}\right)\right]\right.$$

$$\left. + \frac{P}{2}\left(\frac{P^2}{4} + \frac{5}{2\beta^2}\right)\frac{1}{2\beta^2}\left\{e^{-\frac{P^2\beta^2}{4}} + \sqrt{\pi}\left(\frac{P\beta}{2}\right)\left[1 + \mathrm{ERF}\left(\frac{P\beta}{2}\right)\right]\right\}\right]d\phi \qquad (C-2)$$

Multiplying out and collecting terms the integrals over $\phi$ not equal to zero were found to be:

$$\frac{b^3}{2\beta^6}e^{-s^2}\int_0^{2\pi}\cos^4\phi\, d\phi = \frac{3\pi b^3 e^{-s^2}}{8\beta^6} \qquad (C-3)$$

$$\frac{5b}{4\beta^6}e^{-s^2}\int_0^{2\pi}\cos^2\phi\, d\phi = \frac{5\pi b e^{-s^2}}{4\beta^6} \qquad (C-4)$$

$$\frac{3\sqrt{\pi}}{8\beta^6}e^{-s^2+b^2}\int_0^{2\pi}\cos\phi\,\mathrm{ERF}(b\cos\phi)e^{-b^2\sin^2\phi}\, d\phi$$

$$= \frac{3\sqrt{\pi}}{8\beta^6}e^{-s^2+b^2}\, S' \qquad (C-5)$$

$$\frac{3\sqrt{\pi}\, b^2 e}{2\beta^5}^{-s^2+b^2}\int_0^{2\pi} \cos^3\phi\, ERF(b\cos\phi)\, e^{-b^2\sin^2\phi}\, d\phi$$

$$= \frac{3\sqrt{\pi}\, b^2}{2\beta^5} e^{-s^2+b^2}\left\{\frac{1}{2b^2}\left[(2b^2-1)\mathcal{S}' + 2b\sqrt{\pi}\, e^{-b^2}\right]\right\} \qquad (C\text{-}6)$$

$$\frac{\sqrt{\pi}\, b^4}{2\beta^5} e^{-s^2+b^2}\int_0^{2\pi} \cos^5\phi\, ERF(b\cos\phi)\, e^{-b^2\sin^2\phi}\, d\phi$$

$$= \frac{\pi b^4}{2\beta^5} e^{-s^2+b^2}\left\{\mathcal{S}'\left[1-\frac{1}{b^2}+\frac{3}{4b^4}\right]+\pi e^{-b^2}\left[\frac{5}{4b}-\frac{3}{2b^3}\right]\right\} \qquad (C\text{-}7)$$

Integrations (C-6) and (C-7) proceed by parts from (C-5). A collection and cancellation of terms yields

$$G_i(\theta) = \frac{M'}{\beta^5} e^{-s^2}\left[\sqrt{\pi}\, e^{b^2}\mathcal{S}'\left(\frac{b^4}{2}+b^2\right)+\pi b^3 + 2\pi b\right]$$

If now $\mathcal{S}'$ is defined such that $\mathcal{S}' = \dfrac{b e^{b^2}\mathcal{S}'}{2\sqrt{\pi}}$

a final substitution yields the results of Eq. 4.26:

$$G_i(\theta_i) = \frac{m\, n\, V_m^2 \cos\theta_i \sin^2\theta_i\, e^{-s^2}}{\sqrt{\pi}}\left[(\mathcal{S}'+1)(b^3+2b)\right] \qquad (C\text{-}8)$$

There remains the task of evaluating $\mathcal{S}$ or $\mathcal{S}'$. This integral did not appear reducible to previously tabulated functions. A numerical integration was accomplished as shown below:

In $\quad \mathcal{S}' = \int_0^{2\pi} \cos\phi\, ERF(b\cos\phi)\, e^{-b^2\sin^2\phi}\, d\phi$

let $\quad X = b\cos\phi \quad , \quad d\phi = -\dfrac{dX}{\sqrt{b^2-X^2}}$

The appropriate transformation of the limits and an integration by parts makes possible the expression of $\mathcal{S}'$ as

$$\mathcal{S}' = \frac{2e^{-b^2}}{b}\sqrt{\pi}\left[b^2+\frac{4}{\sqrt{\pi}}\int_0^b \sqrt{b^2-X^2}\, ERF(X)\, e^{X^2}\, dX\right]$$

applying the definition of $\mathcal{S}'$ there results

$$\mathcal{S}' = b^2 + \frac{4}{\sqrt{\pi}}\int_0^b \sqrt{b^2-X^2}\, ERF(X)\, e^{X^2}\, dX \qquad (C\text{-}9)$$

In this form $\mathcal{S}'$ was computed for values of $b$ sufficient for the

further computation of $\dfrac{G_i(\theta_i)}{m_m V_m^2}$. A table of the computed values of $S'$ and $\log S'$ follows and a plot of these values is given in Fig. 46.

| b | $S'$ | $\log S'$ |
|---|------|-----------|
| 0 | 0.0000 | $-\infty$ |
| 0.005 | 0.00249 | -2.6038 |
| 0.1 | 0.01005 | -1.9978 |
| 0.15 | 0.02276 | -1.6428 |
| 0.2 | 0.04081 | -1.3892 |
| 0.25 | 0.06449 | -1.1905 |
| 0.3 | 0.09417 | -1.0261 |
| 0.35 | 0.13032 | -0.8850 |
| 0.4 | 0.17351 | -0.7607 |
| 0.45 | 0.22446 | -0.6489 |
| 0.5 | 0.28402 | -0.5466 |
| 0.55 | 0.35322 | -0.4520 |
| 0.6 | 0.43330 | -0.3632 |
| 0.65 | 0.52571 | -0.2792 |
| 0.7 | 0.63219 | -0.1992 |
| 0.75 | 0.75480 | -0.1222 |
| 0.8 | 0.89598 | -0.0477 |
| 0.85 | 1.05864 | 0.0248 |
| 0.9 | 1.24023 | 0.0956 |
| 0.95 | 1.46284 | 0.1652 |
| 1.0 | 1.71331 | 0.2338 |
| 1.25 | 3.772 | 0.5766 |
| 1.5 | 8.478 | 0.9283 |
| 1.75 | 20.37 | 1.309 |
| 2.0 | 53.58 | 1.729 |
| 4.0 | $8.891 \times 10^6$ | 6.949 |
| 10.0 | $2.69 \times 10^{43}$ | 43.43 |

## TABLE I
## COEFFICIENT OF SPECULAR REFLECTION f

| GAS | SURFACE | f | REFERENCE |
|-----|---------|---|-----------|
| air | machined brass | 1.00 | 11 |
| $CO_2$ | machined brass | 1.00 | 11 |
| air | old shellac | 1.00 | 11 |
| $CO_2$ | old shellac | 1.00 | 11 |
| air | Hg | 1.00 | 11 |
| air | oil | 0.90 | 11 |
| $CO_2$ | oil | 0.92 | 11 |
| $H_2$ | oil | 0.93 | 11 |
| air | glass | 0.89 | 11 |
| He | oil | 0.87 | 11 |
| air | fresh shellac | 0.79 | 11 |
| air | $Ag_2O$ | 0.98 | 12 |
| He | $Ag_2O$ | 1.00 | 12 |
| $H_2$ | $Ag_2O$ | 1.00 | 12 |
| $O_2$ | $Ag_2O$ | 0.99 | 12 |
| air | oil on machined aluminum | 0.90 | 13 |

## TABLE II
### THERMAL ACCOMMODATION COEFFICIENTS $\alpha$

| GAS | SURFACE | $\alpha$ | REFERENCE |
|---|---|---|---|
| $H_2$ | bright Pt. | 0.32 | 14 |
| $H_2$ | black Pt. | 0.74 | 14 |
| $O_2$ | bright Pt. | 0.81 | 14 |
| $O_2$ | black Pt. | 0.93 | 14 |
| $N_2$ | Pt | 0.50 | 15 |
| $N_2$ | tungsten | 0.35 | 15 |
| air | flat laquer on bronze | 0.88 - 0.89 | 16 |
| air | polished bronze | 0.91 - 0.94 | 16 |
| air | machined bronze | 0.89 - 0.93 | 16 |
| air | etched bronze | 0.93 - 0.95 | 16 |
| air | polished cast iron | 0.87 - 0.93 | 16 |
| air | machined cast iron | 0.87 - 0.88 | 16 |
| air | etched cast iron | 0.89 - 0.96 | 16 |
| air | polished aluminum | 0.87 - 0.95 | 16 |
| air | machined aluminum | 0.95 - 0.97 | 16 |
| air | etched aluminum | 0.89 - 0.97 | 16 |
| He | tungsten | 0.025 - 0.057 | 17 |
| He | nickel not flashed | 0.20 | 17 |
| He | nickel flashed | 0.085 | 17 |
| He | tungsten flashed | 0.17 | 18 |
|  |  | 0.12 | 15 |
| He | tungsten not flashed | 0.53 | 18 |
| argon | tungsten flashed | 0.82 | 18 |
|  |  | 0.46 | 18 |
| argon | tungsten not flashed | 1.00 | 18 |

## TABLE III

### SUMMARY OF MOLECULE-SURFACE SCATTERING INVESTIGATIONS

| INVESTIGATOR | GAS | SURFACE | OBSERVATION TECHNIQUE | OBSERVATIONS | REF. |
|---|---|---|---|---|---|
| R. W. Wood | Hg, Cd | Glass | Condensation on cooled bulb | Diffuse scattering | 9 |
| M. Knudsen | Hg | Glass | Condensation on cooled bulb | Diffuse scattering | 10 |
| J. B. Taylor | Li, K, Cs | LiF, NaCl | Surface ionization detector | Diffuse scattering | 19 |
| A. Ellet and H. F. Olson | Hg, Cd | NaCl | Condensation on cooled bulb | Specular reflection of large fraction of total incident beam. | 20 |
| | Na | NaCl | Condensation in cooled bulb | Diffuse scattering | |
| | H | NaCl | Reduction of $W O_3$ | Specular reflection | |
| A. Ellet, H. F. Olson, H. A. Zahl | Cd | NaCl | Double crystal molecular beam with disc velocity selector. Condensation detector. Fixed crystal angles of 45°. | Specular reflection of 17% of beam from first crystal, 100% of these from second crystal. 83% of parent crystal beam diffusely scattered. Velocity selection of first crystal was observed. | 21 |
| H. A. Zahl | Zn | NaCl | Apparatus as above | 95% specular reflection of incident beam observed from both crystals. No observed velocity selection. | 22 |
| T. H. Johnson | H | LiF | Reduction of $Mo\ O_3$ | A specular maximum was found containing 90% of the parent beam. Diffraction maxima contained the remaining 10%. | 23 |

## TABLE III - CONTINUED

| INVESTIGATOR | GAS | SURFACE | OBSERVATION TECHNIQUE | OBSERVATIONS | REF. |
|---|---|---|---|---|---|
| F. Knauer and O. Stern | $H_2$, He | Speculum metal | Pirani Gage | Specular reflection observed at entrance and exit angles $10^{-3}$ radian from glancing. Diffuse reflection observed elsewhere. | 8 |
| I. Estermann and O. Stern | $H_2$, He | LiF | Pirani gage | Observed diffraction maxima at position calculated on basis of de Broglie wavelength of incident beam and crystal grating space. | 7 |
| I. Estermann, R. Frisch and O. Stern | He | LiF | Pirani gage detector with double crystal molecular beam and disc velocity selector. Variable crystal angles. | Observed diffraction maxima at position calculated as above. Diffracted molecules in maxima were monochromatic in de Broglie wavelength. | 24 |
| H. A. Zahl and A. Ellet | Hg | NaCl | Ionization gage | Observed smeared out specular scattering at all incident angles. | 35 |

LINES A B N LIE IN INCIDENT PLANE
LINES T C N LIE IN PLANE OF OBSERVATION
INCIDENT ANGLE $\theta$ MEASURED IN B O N
POLAR OBSERVATION ANGLE $\theta'$ MEASURED IN N O T
AZIMUTH OBSERVATION ANGLE $\phi'$ MEASURED IN C O A

INCIDENT ANGLE
ROTATION AXIS

TEST
SURFACE

BLOCK OF
TEST MATERIAL

A

N

AXIS OF
INCIDENT
BEAM

$\theta$

B

O

B

$\theta'$

C

$\phi'$

N

T

A

NORMAL TO
TEST SURFACE

DETECTOR
GAGE
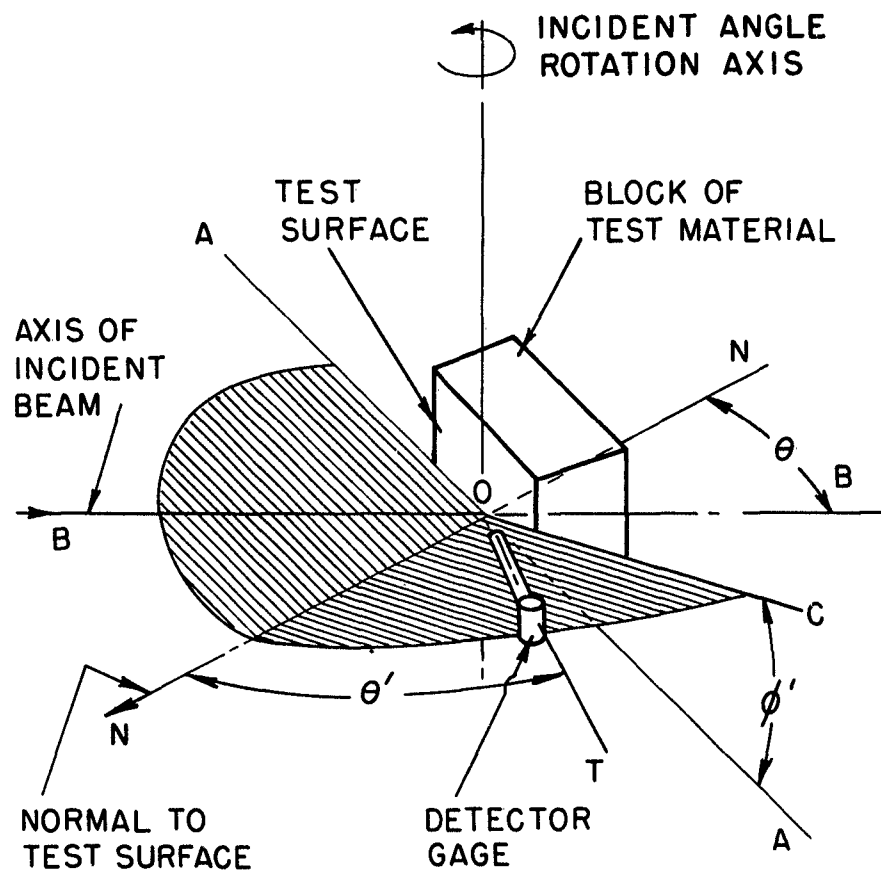
FIG. I GEOMETRY OF SCATTERING EXPERIMENT

HYD 6530-150-0

FIG. 2 SCHEMATIC OF MOLECULAR BEAM MODEL 2 VACUUM SYSTEM

A-1 INCH FULTON SYLPHON
     VACUUM VALVE

B-2 INCH FULTON SYLPHON
     VACUUM VALVE

C-6 INCH DISTILLATION PRODUCTS
     QUARTER SWING VACUUM VALVE

DETECTOR VACUUM SHELL $10^{-6}$ MM. PRESSURE

SOURCE VACUUM SHELL

1.65 INCH I.D. ALL LINES

REFRIGERATED TRAP

~1 MICRON PRESSURE

MCF. 700 OIL DIFFUSION PUMP

MC 275 OIL DIFFUSION PUMP

MB 100 BOOSTER PUMP

~40 MICRON PRESSURE

CENCO MEGAVAC

1½ HORSE POWER KINNEY MECHANICAL PUMP

HYD 6531-150-0

| | | | | |
|---|---|---|---|---|
| ① | SOURCE REGION VACUUM SHELL | | ⑤ | EMISSION REGULATOR CHASSIS |
| ② | DETECTOR REGION VACUUM SHELL | | ⑥ | MONITOR ION GAGE SUPPLY |
| ③ | SOURCE PRESSURE OIL MANOMETER | | ⑦ | PIRANI GAGE SUPPLY |
| ④ | DIFFERENCE AMP- LIFIER CHASSIS | | ⑧ | STRIP CHART RECORDER |

FIG. 3  MOLECULAR  BEAM  APPARATUS

HYD 6532-150-0
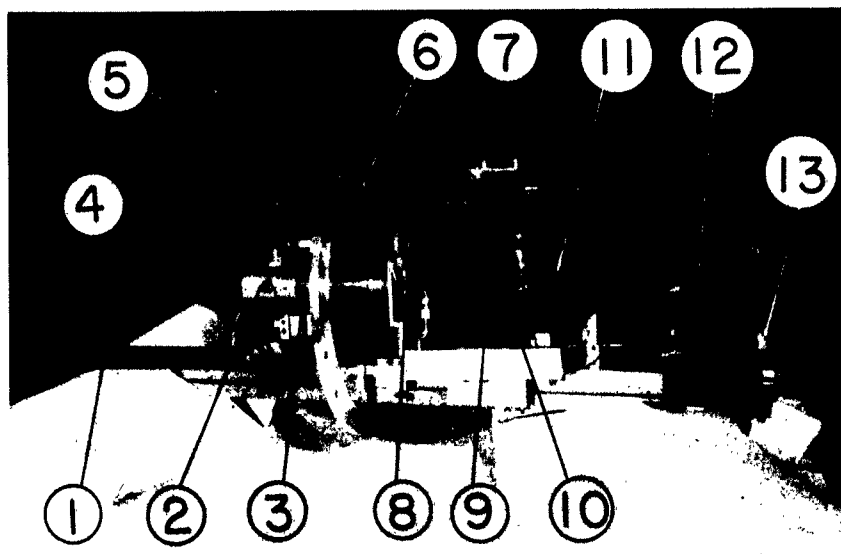
1. OPTICAL BENCH
2. SOURCE GAS INLET
3. SOURCE ORIFICE HOLDER
4. MANOMETER LINE
5. CENTRAL SUPPORT FLANGE
6. DEFINING ORIFICE
7. SHUTTER
8. SECONDARY DEFINING SLIT
9. TEST SURFACE
10. DETECTOR ENTRANCE TUBE
11. DETECTOR GAGE
12. COMPARATOR GAGE
13. APRON

FIG. 4  OPTICAL BENCH WITH BEAM FORMING AND DETECTING EQUIPMENT

HYD 6533-150-0
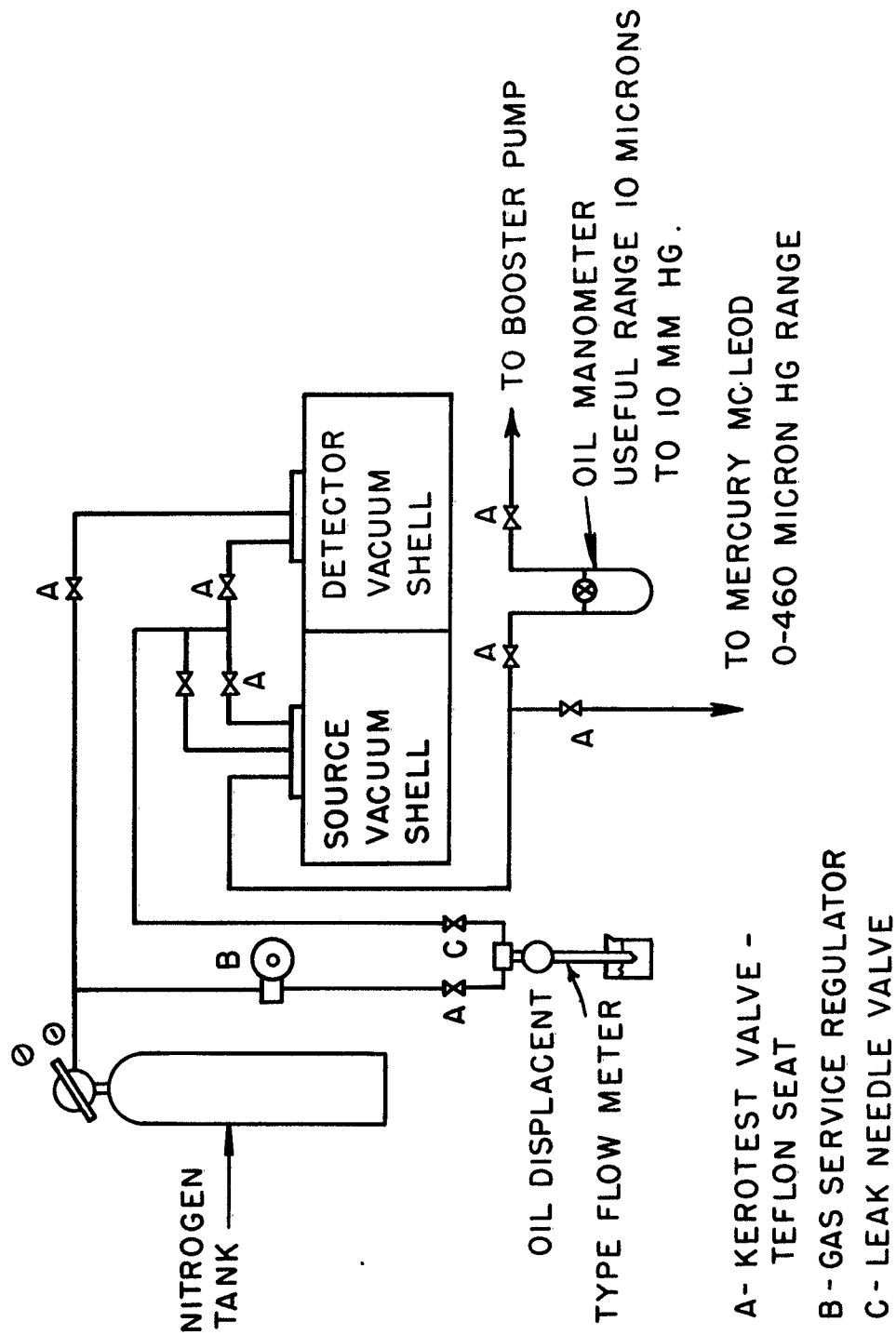
FIG. 5 SCHEMATIC OF SOURCE GAS AND CALIBRATION SYSTEM

A - KEROTEST VALVE – TEFLON SEAT

B - GAS SERVICE REGULATOR

C - LEAK NEEDLE VALVE

HYD 6534-150-0

POLAR ANGLE ROTATION AXIS

AZIMUTH ANGLE
ROTATION AXIS

CARRIAGE

OPTICAL
BENCH

TYPICAL OBSERVATION
LINE

BEAM AXIS

NORMAL TO TEST
SURFACE

INCIDENT ANGLE
ROTATION AXIS
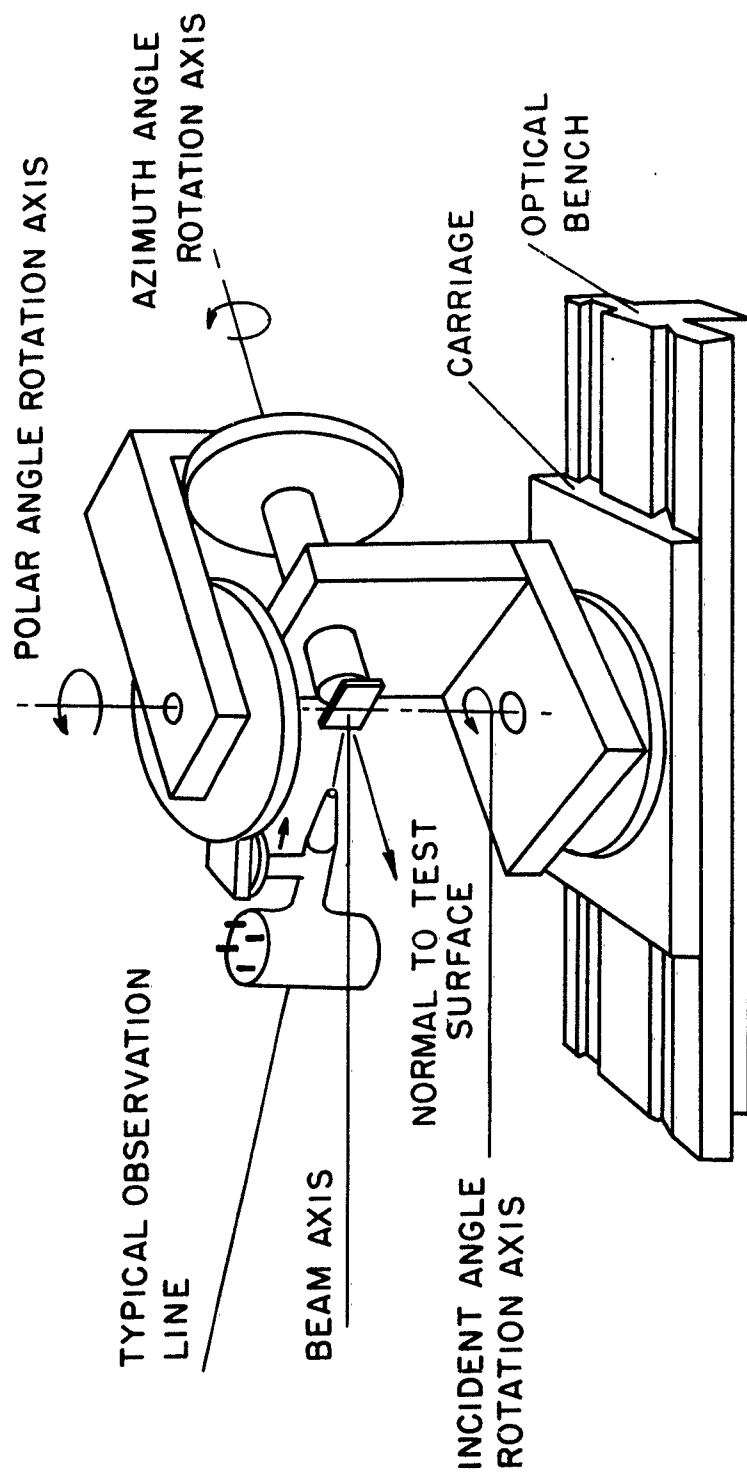
FIG.6 SCHEMATIC OF BASIC ROTATION ELEMENTS
OF DETECTOR MECHANISM

HYD 6535-150-0

GAGE WITH TAPERED
ENTRANCE TUBE

DETECTION GAGE

ENTRANCE AREA $A_3$

$A_2$ = AREA AT $\lambda$

DEFINING
ORIFICE

SHUTTER

TEST
SURFACE

$\theta$

R

$\lambda$

SOURCE
ORIFICE

AREA $A_1$

SCATTERED BEAM DETECTION

$AREA_{3b}$

AREA $A_{3a}$

DIRECT BEAM DETECTION
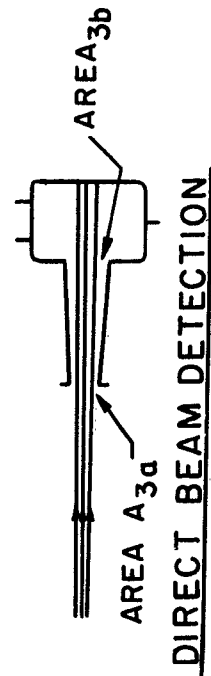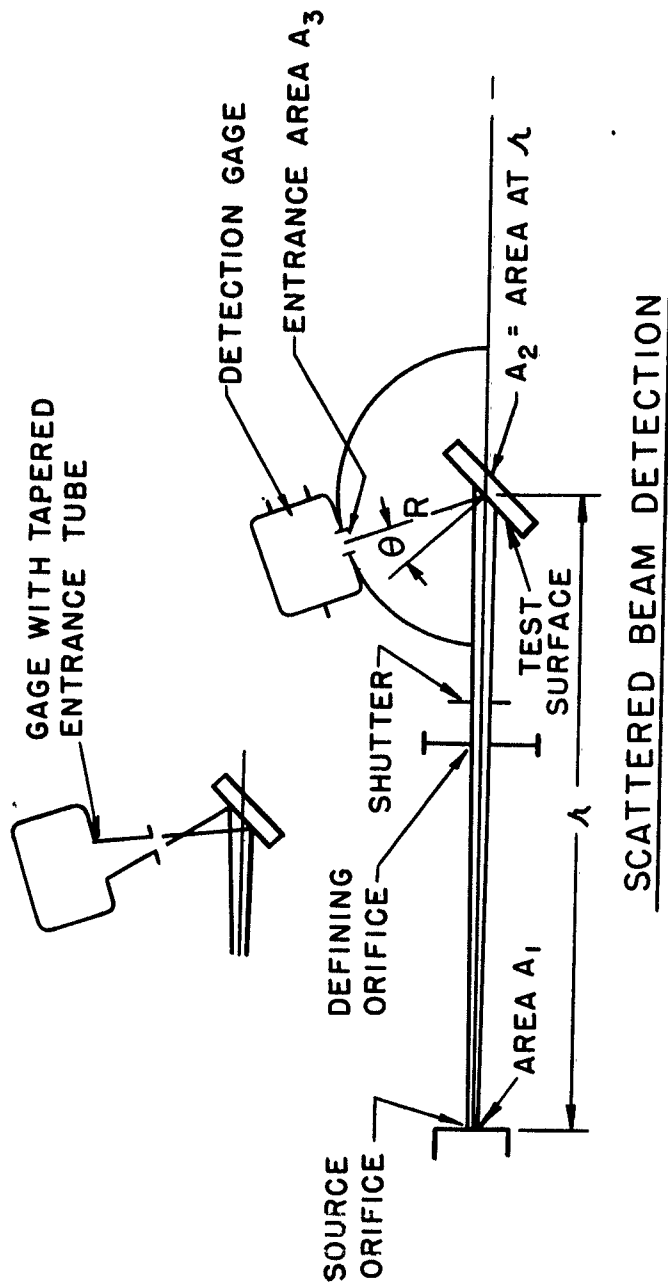
FIG. 7 SCHEMATICS FOR ESTIMATION OF BEAM
PRESSURE INCREMENT IN DETECTOR GAGE

HYD 6536-150-0
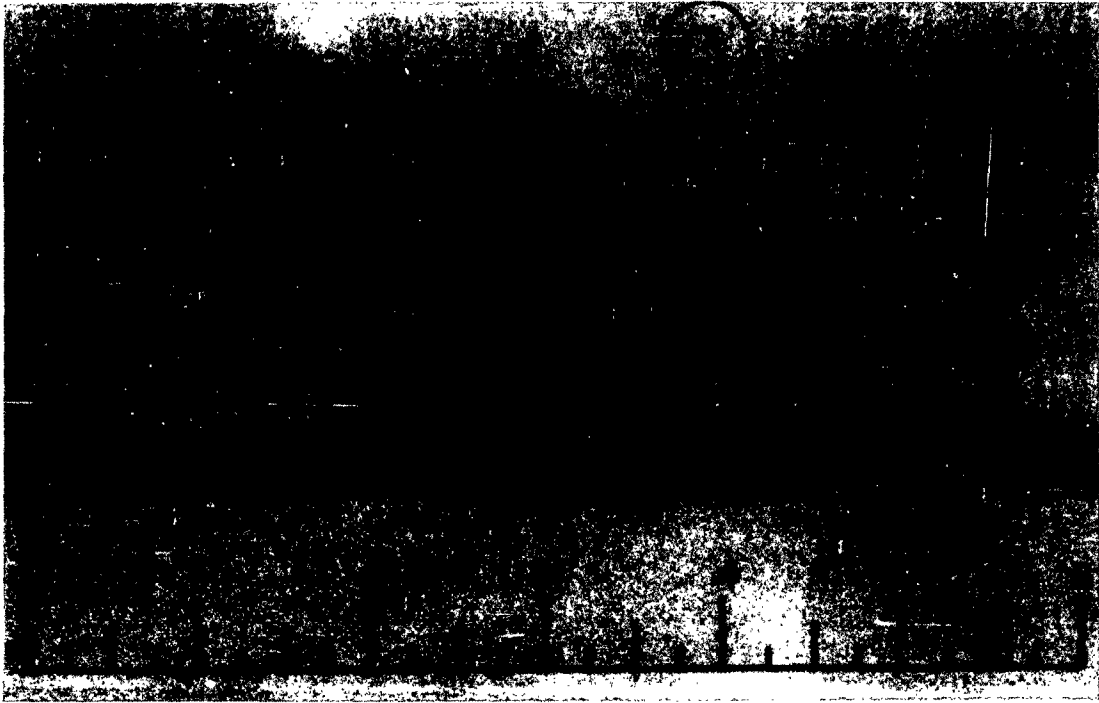
| | | | | |
|---|---|---|---|---|
| ① | SPUTTERING SHIELDS | | ④ | GRID |
| ② | FILAMENT SUPPORT POINTS | | ⑤ | HOUSEKEEPER SEAL |
| ③ | ION COLLECTOR | | ⑥ | GAGE ENTRANCE |

FIG. 8  IONIZATION GAGE-MOLECULAR
BEAM DETECTOR

HYD 6537-150-0

DIFFERENCE AMPLIFIER

POSITIVE REGULATED POWER SUPPLY

NEGATIVE REGULATED POWER SUPPLY

STRIP CHART RECORDER

PRE-AMPLIFIER

DETECTOR ANODE LEAD

COMPARATOR ANODE LEAD

BASE PRESSURE MONITOR, ION GAGE POWER SUPPLY AND METERING CIRCUIT

DETECTOR GAGE FILAMENT LEAD

GRID LEAD

COMPARATOR GAGE FILAMENT LEAD

GRID LEAD

INTERLOCK LEAD

INTERLOCK LEAD

DETECTOR ADMISSION REGULATOR

COMPARATOR ADMISSION REGULATOR

LOW VOLTAGE REGULATED POWER SUPPLY

HIGH VOLTAGE REGULATED POWER SUPPLY

ARROW POINTS INDICATE SIGNAL OR POWER TRANSFER DIRECTION

FIG. 9 SCHEMATIC OF MOLECULAR BEAM DETECTION SYSTEM

HYD 6538-150-0

FIG. 10 BLOCK DIAGRAM OF EMISSION REGULATOR

HYD 6539-150-0

FIG. 11  MOLECULAR BEAM ION GAGE REGULATOR

HYD 6540-150-0

CHASSIS CONNECTIONS:

A1 — C1    A3 — LINE
A2 — C12   A4 — LINE
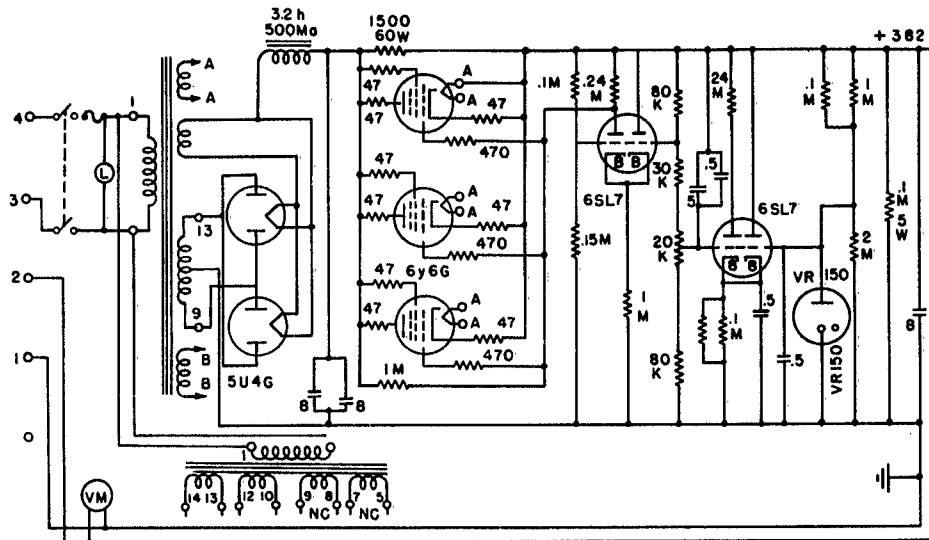


FIG. 12 a
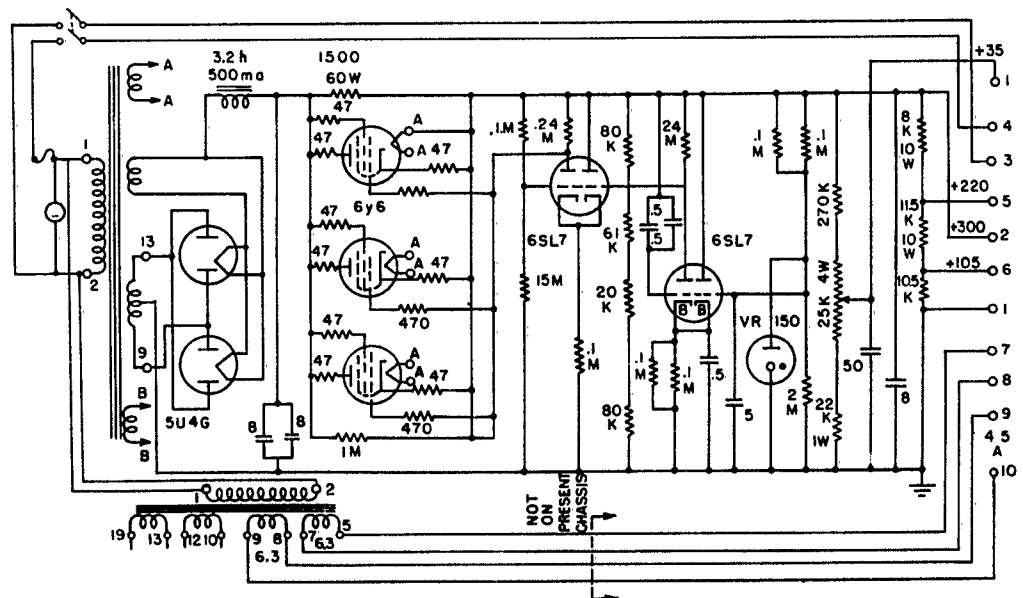


CHASSIS B

300 V POWER SUPPLY

CHASSIS CONNECTIONS:

B1 - C1    B4 - LINE
B2 - C2    B5 - C5
B3 LINE    B6 - C6

FIG. 12 b

HYD 6541 - 150 - 0
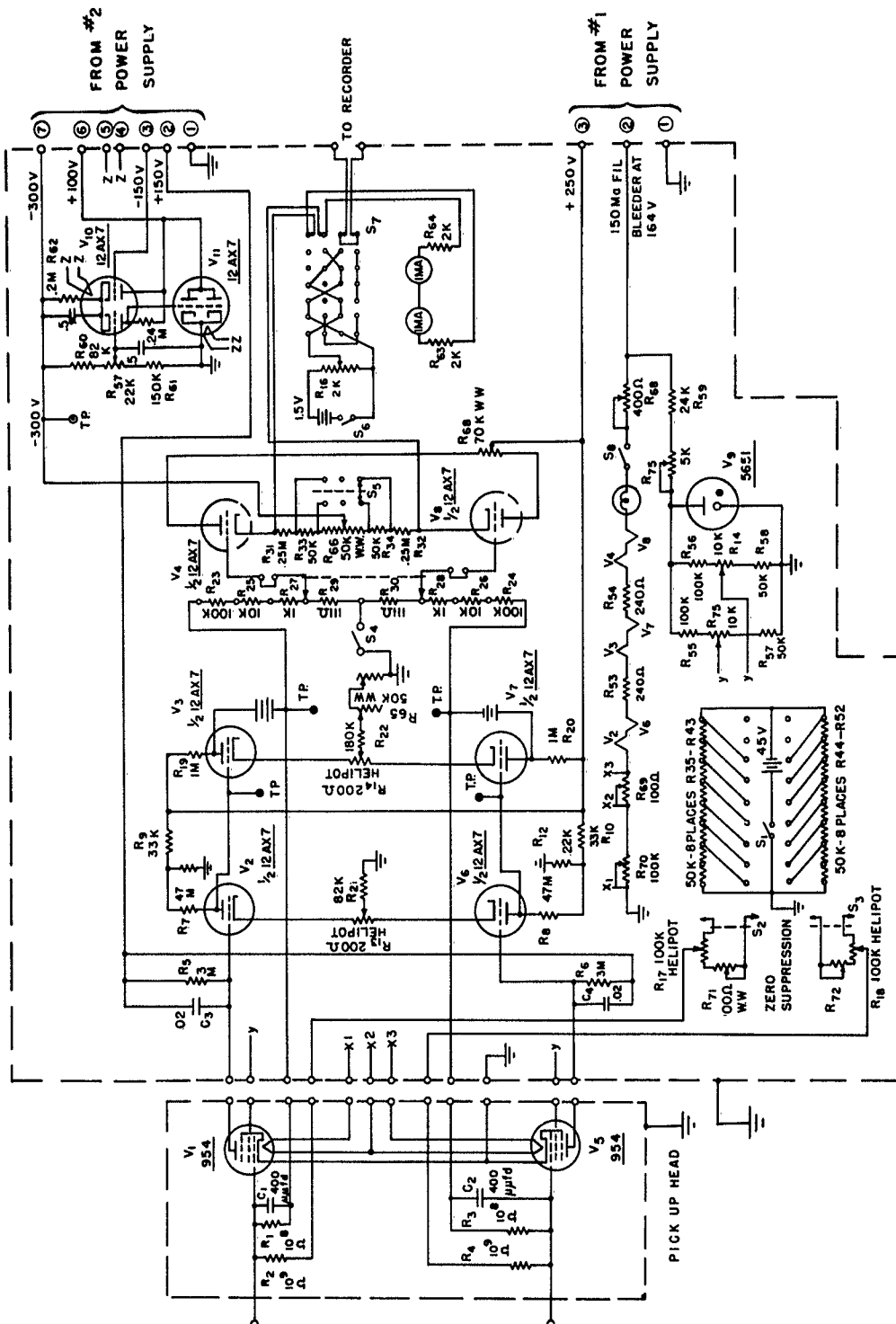
FIG. 13 MOLECULAR BEAM DIFFERENCE AMPLIFIER

HYD 6542-150-0

POWER SUPPLY #1

MODIFIED D150753 TYPE SCR 545A STANDARD POWER SUPPLY
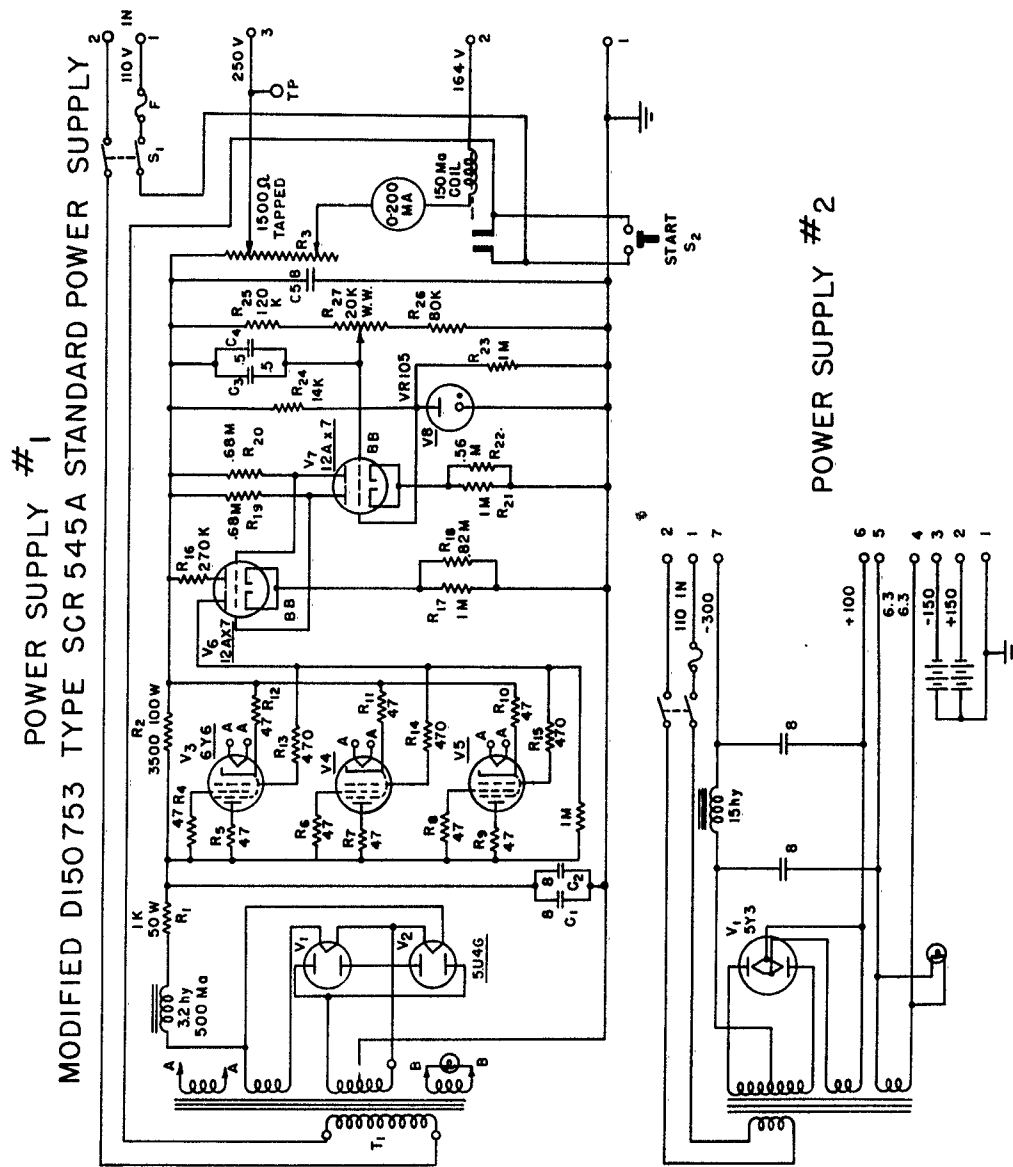
POWER SUPPLY #2

FIG 14

POWER SUPPLIES MOLECULAR BEAM DIFFERENCE AMPLIFIER

HYD 6543-150-0
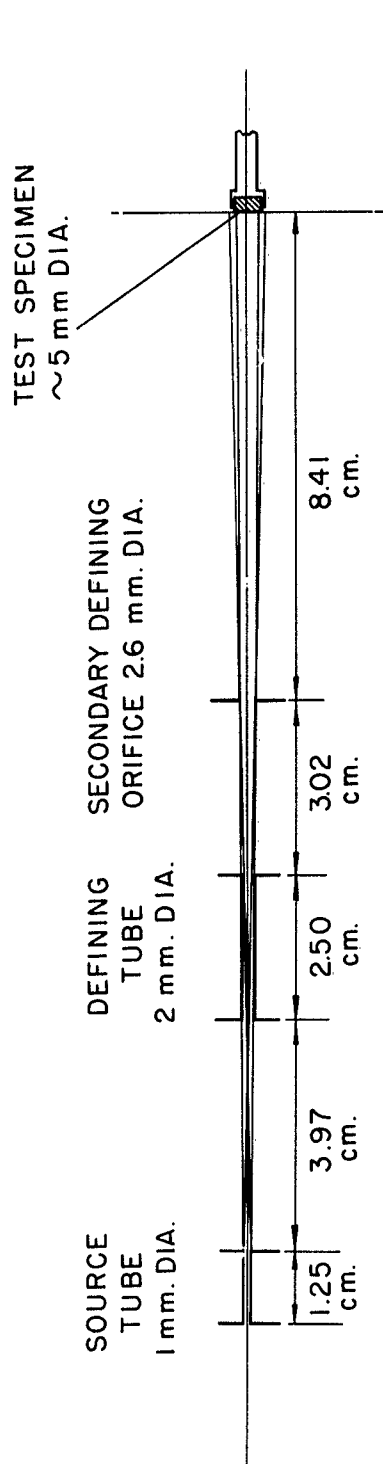
BEAM GEOMETRY – METAL SURFACES

TEST SPECIMEN ~5 mm DIA.

SECONDARY DEFINING ORIFICE 2.6 mm. DIA.

DEFINING TUBE 2 mm. DIA.

SOURCE TUBE 1 mm. DIA.

8.41 cm.

3.02 cm.

2.50 cm.

3.97 cm.

1.25 cm.
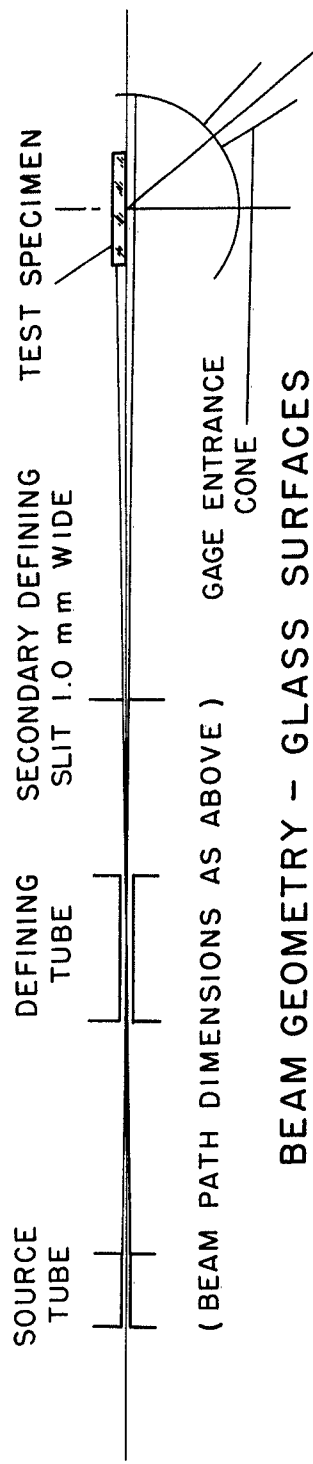
BEAM GEOMETRY – GLASS SURFACES

TEST SPECIMEN

SECONDARY DEFINING SLIT 1.0 mm WIDE

DEFINING TUBE

SOURCE TUBE

GAGE ENTRANCE CONE

( BEAM PATH DIMENSIONS AS ABOVE )

FIG. 15   EXPERIMENT BEAM GEOMETRIES

HYD 6544-150-0
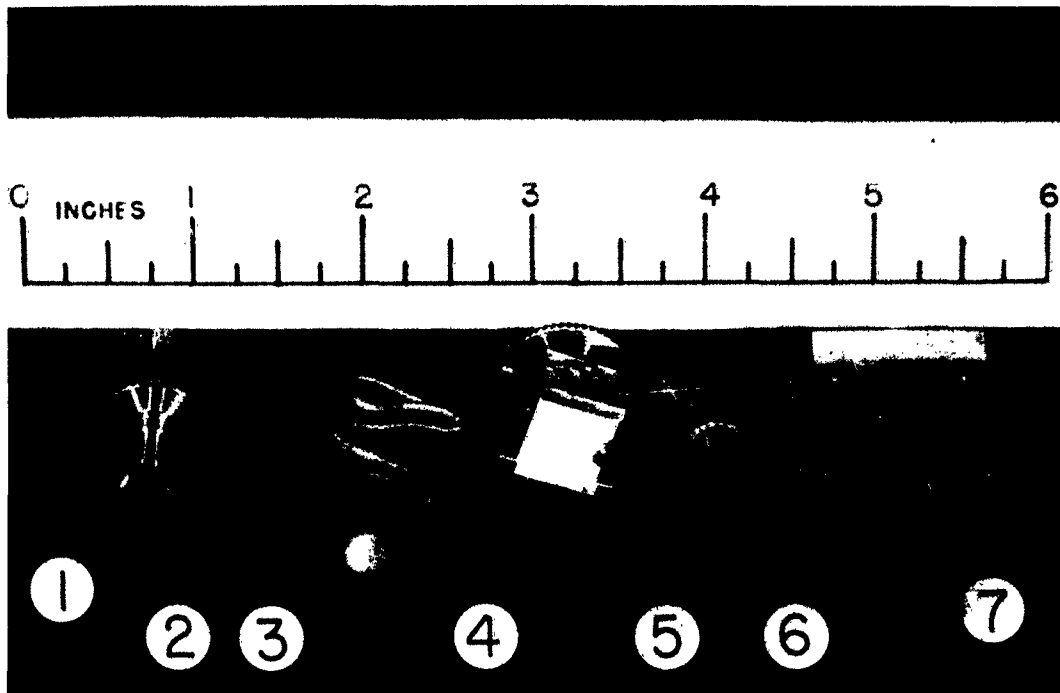
1. SPECIMEN HOLDER METAL SURFACES

5. ETCHED CRS SURFACE

2. POLISHED CRS SURFACE

6. SPECIMEN HOLDERS GLASS SURFACES

3. POLISHED ALUMINUM SURFACE

7. UNPOLISHED GLASS SURFACE

4. POLISHED GLASS SURFACE

FIG. 16 TEST SURFACES & HOLDERS

HYD 6545-150-0
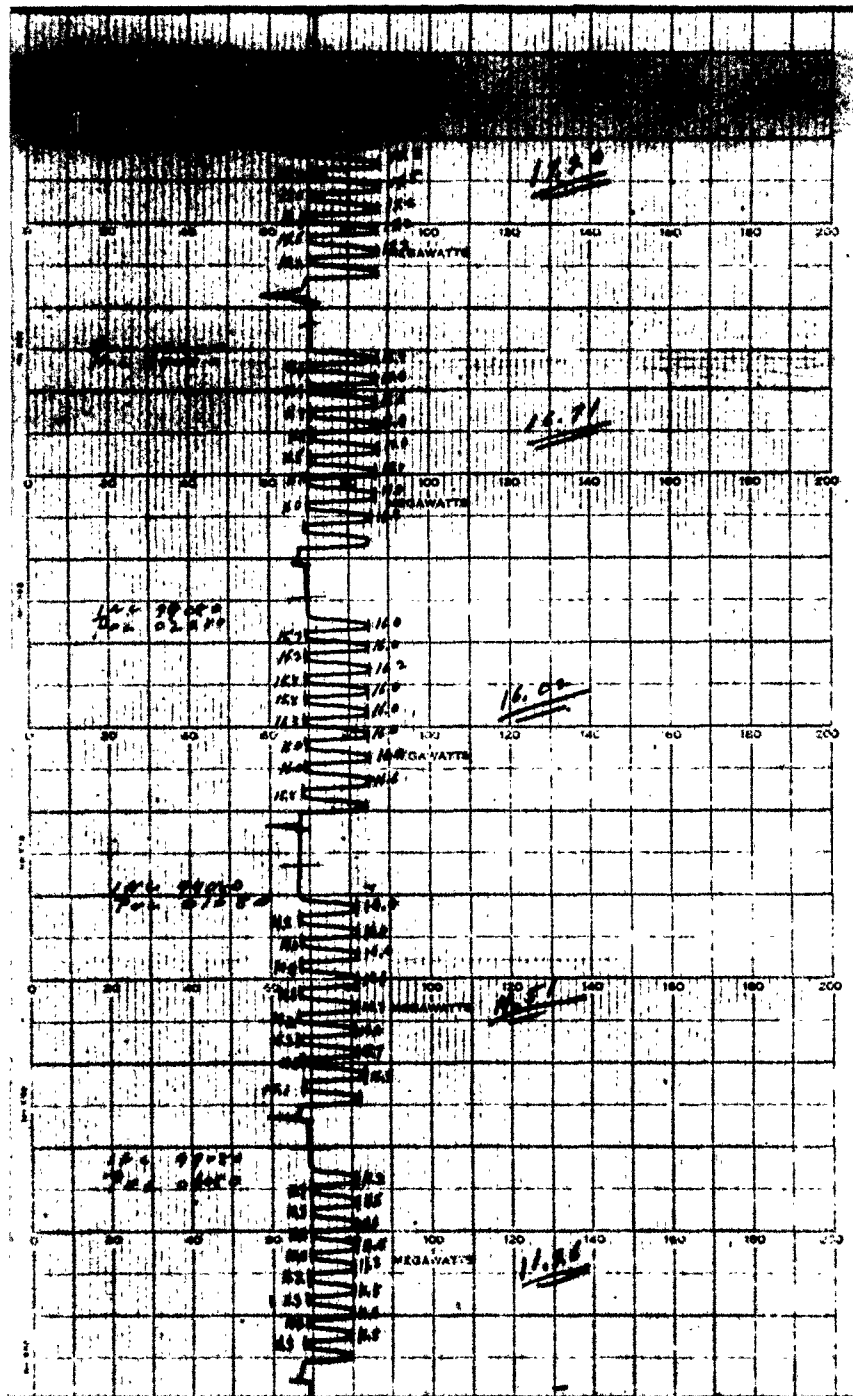
FIG. 17 RAW DATA RECORD
(FROM RUN OF JULY 22, 1953)

INC ANGLE 0.00°
AZ ANGLE 0.00°

o-FEB. 15, 1953
□-FEB. 17, 1953

INC. ANGLE 0.00°
AZ. ANGLE 19.57°

◇-FEB. 21, 1953

FIG. 18  SCATTERING PLOT- POLISHED STEEL SURFACE

25.11°

INC ANGLE 25.11°
AZ. ANGLE 0.00°

o-FEB. 15, 1953
□-FEB. 17, 1953

INC. ANGLE 25.11°
AZ. ANGLE 19.57°

◇-FEB. 21, 1953
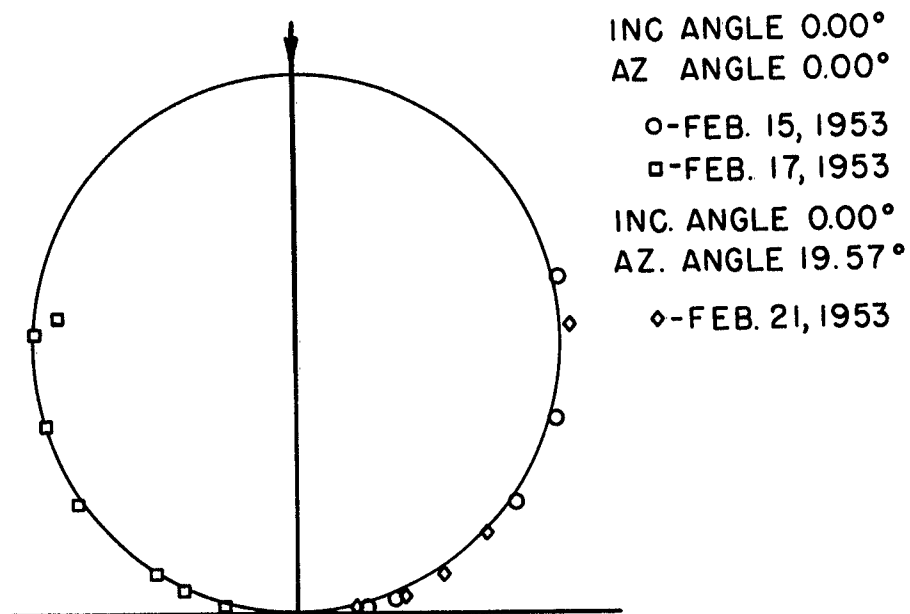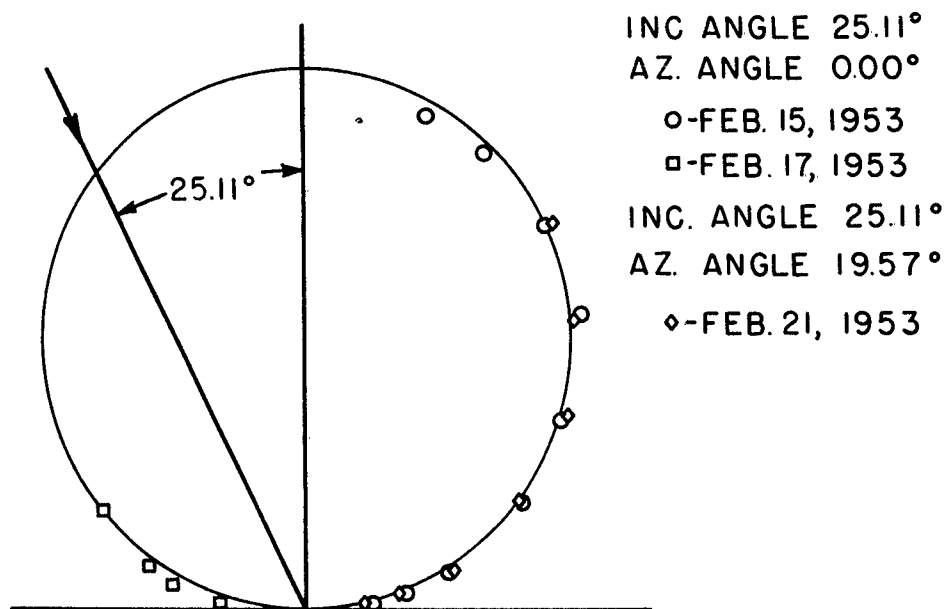
FIG.19  SCATTERING PLOT- POLISHED STEEL SURFACE

HYD 6547-150-0

FIG.20 SCATTERING PLOT-POLISHED STEEL SURFACE

INC. ANGLE 53.65°
AZ. ANGLE 15.94°

□-FEB. 26,1953

INC. ANGLE 53.65°
AZ. ANGLE 0.00°

O-FEB. 27, 1953



FIG. 21 SCATTERING PLOT - POLISHED STEEL SURFACE

INC. ANGLE 71.83°
AZ. ANGLE 15.94°

◇-FEB. 26, 1953

INC. ANGLE 74.42°
AZ. ANGLE 15.94°

□-FEB. 24, 1953

INC. ANGLE 71.83°
AZ. ANGLE 00.0°

O FEB. 27, 1953

HYD 6548-150-0

INC ANGLE  0.00°
AZ ANGLE  0.00°
UNHEATED SPECIMEN
o – MARCH 23, 1953
HEATED SPECIMEN
□ – APRIL 7, 1953
UNHEATED SPECIMEN
△ – APRIL 8, 1953

FIG. 22  SCATTERING PLOT-ALUMINUM SURFACE



INC ANGLE 25.11°
AZ ANGLE 0.00°
UNHEATED SPECIMEN
o – MARCH, 23, 1953
HEATED SPECIMEN
□ – APRIL 7, 1953
UNHEATED SPECIMEN
△ – APRIL 8, 1953

FIG. 23  SCATTERING  PLOT-ALUMINUM SURFACE

HYD 6549-150-0

INC. ANGLE 53.65°
AZ. ANGLE 0.00°

UNHEATED SPECIMEN
o-MARCH 23, 1953
HEATED SPECIMEN
□-APRIL 7, 1953
UNHEATED SPECIMEN
△-APRIL 8, 1953

53.65°

FIG. 24 SCATTERING PLOT- POLISHED
ALUMINUM SURFACE

INC. ANGLE 71.83°
AZ. ANGLE 0.00°

UNHEATED RUN
o-MARCH 23, 1953

71.83°

FIG. 25 SCATTERING PLOT- POLISHED
ALUMINUM SURFACE

HYD 6550-150-0

INC ANGLE 0.00°
AZ ANGLE 0.00°
□ MAY 16, 1953

INC ANGLE 0.00°
AZ ANGLE 19.57°
○ MAY 23, 1953

FIG. 26 SCATTERING PLOT UNPOLISHED
GLASS SURFACE
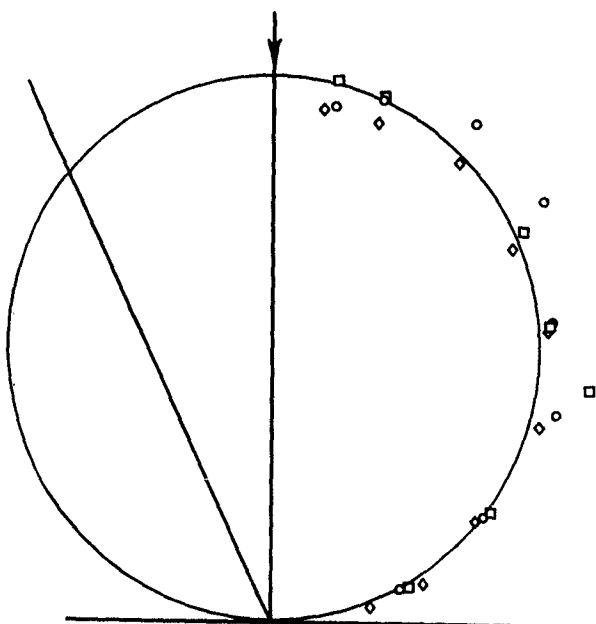
INC ANGLE 25.11°
AZ ANGLE 0.00
○ MAY 16, 1953
◇ MAY 5, 1953

INC ANGLE 25.11°
AZ ANGLE 19.57°
□ MAY 17, 1953

FIG. 27 SCATTERING PLOT UNPOLISHED
GLASS SURFACE

HYD 6551-150-0
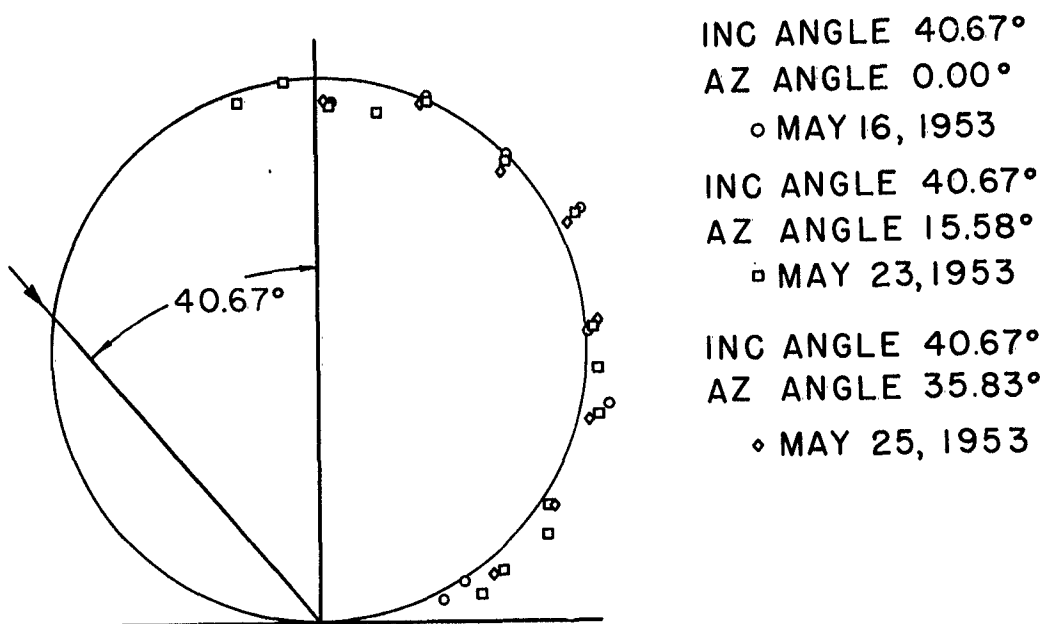
FIG. 28 SCATTERING PLOT UNPOLISHED
GLASS SURFACE

INC ANGLE 40.67°
AZ ANGLE 0.00°
o MAY 16, 1953
INC ANGLE 40.67°
AZ ANGLE 15.58°
▫ MAY 23, 1953

INC ANGLE 40.67°
AZ ANGLE 35.83°
◇ MAY 25, 1953



FIG. 29 SCATTERING PLOT UNPOLISHED
GLASS SURFACE

INC ANGLE 53.65°
AZ ANGLE 0.00°
o MAY 16, 1953
▫ JUNE 18, 1953

$\theta'$
95° & 85°
75°
65°
55°
45°
35°
25°
15°
5° & 0°

HYD 6552-150-0

INC ANGLE 66.63°
AZ ANGLE 0.00°
° JUNE 20, 1953
$\phi'$
—90°
—85°
—70°
—65°
—55°
—45°
—35°
—25°
—15°
—5°
—0°

66.63°
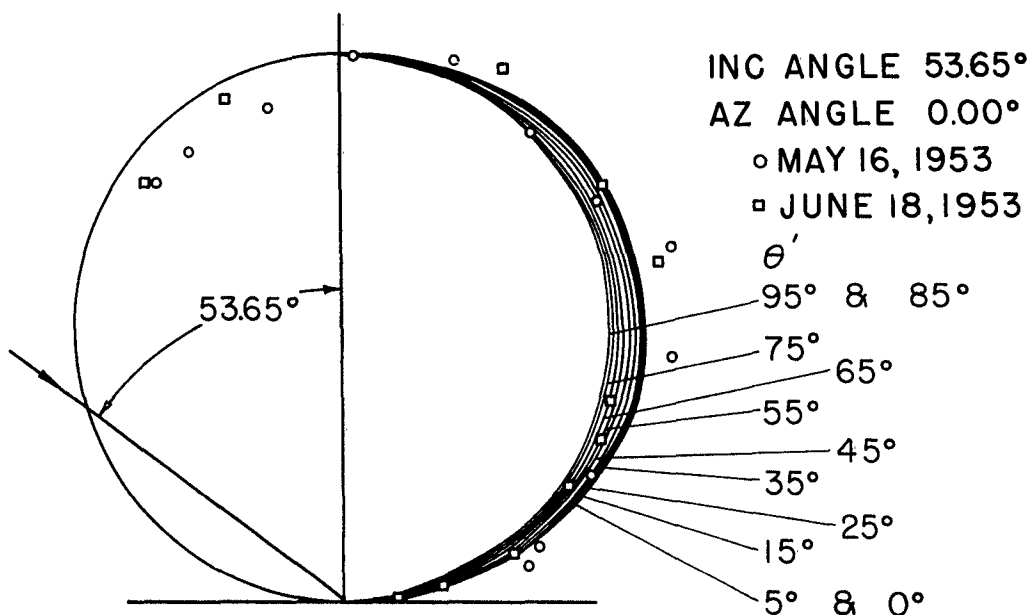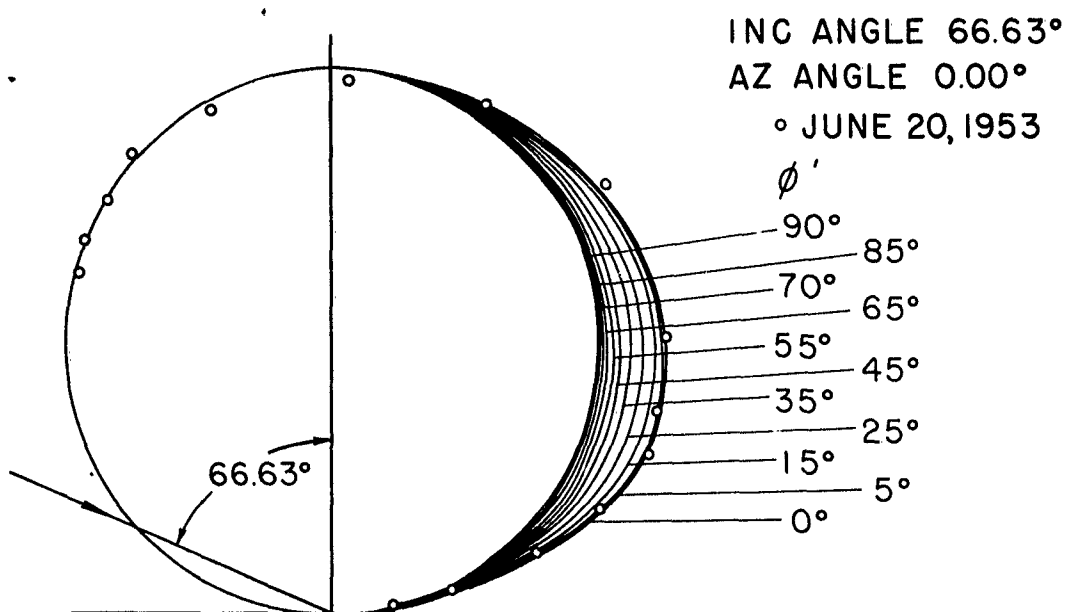
FIG 30  SCATTERING PLOT UNPOLISHED
GLASS SURFAFE



INC ANGLE 79.62°
AZ ANGLE 0.00°
° JUNE 21, 1953
INC ANGLE 79.62°
AZ. ANGLE 15.58°
□ MAY 23, 1953
$\phi'$
—90°, 85° & 80°
—65°
—55°
—45°
—35°
—25°
—15°
—5°
—0°

79.62°
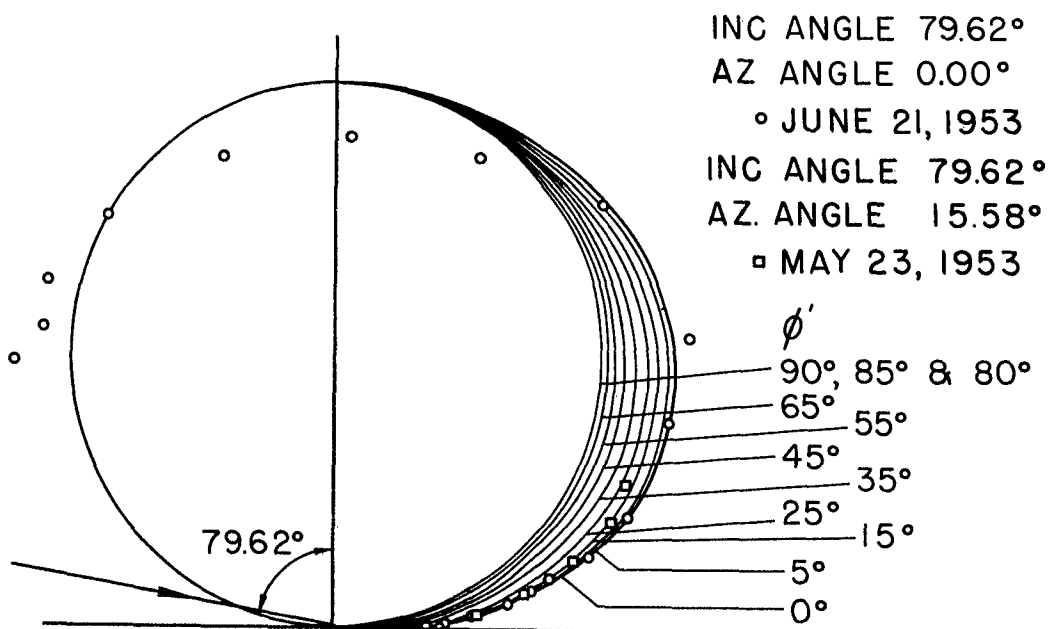
FIG. 31  SCATTERING PLOT UNPOLISHED
GLASS SURFACE

HYD 6553-150-0

INC ANGLE 84.82°
AZ. ANGLE 0.00°
JUNE 21, 1953

$\phi'$

90° & 85°
75°
65°
55°
45°
35°
25°
15°
5°
0°

84.82°
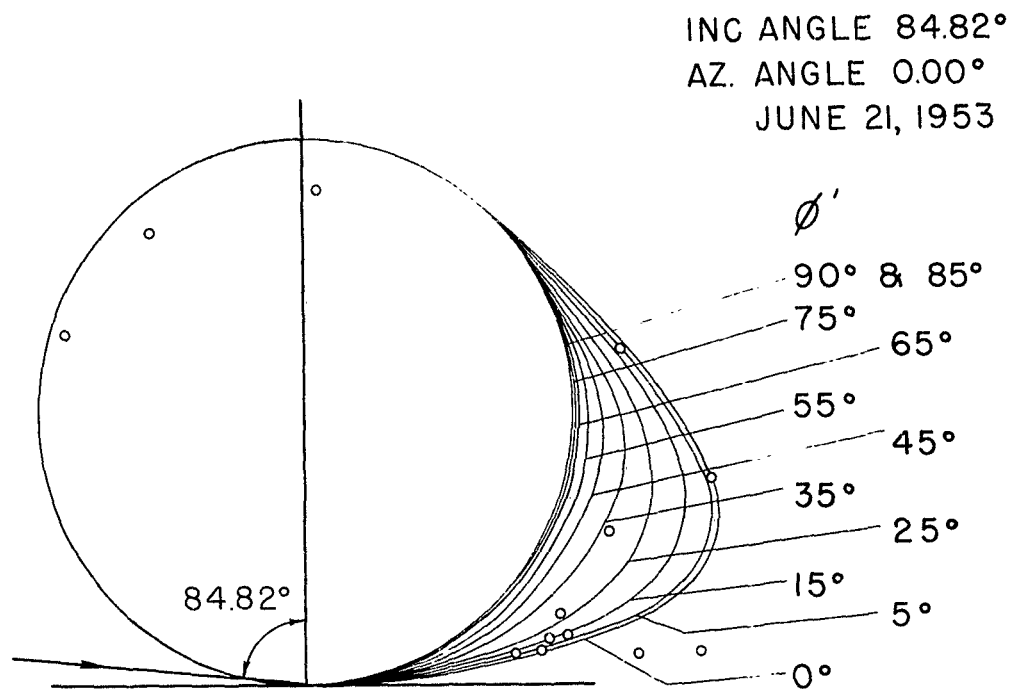
FIG. 32 SCATTERING PLOT UNPOLISHED
GLASS SURFACE

HYD 6554-150-0
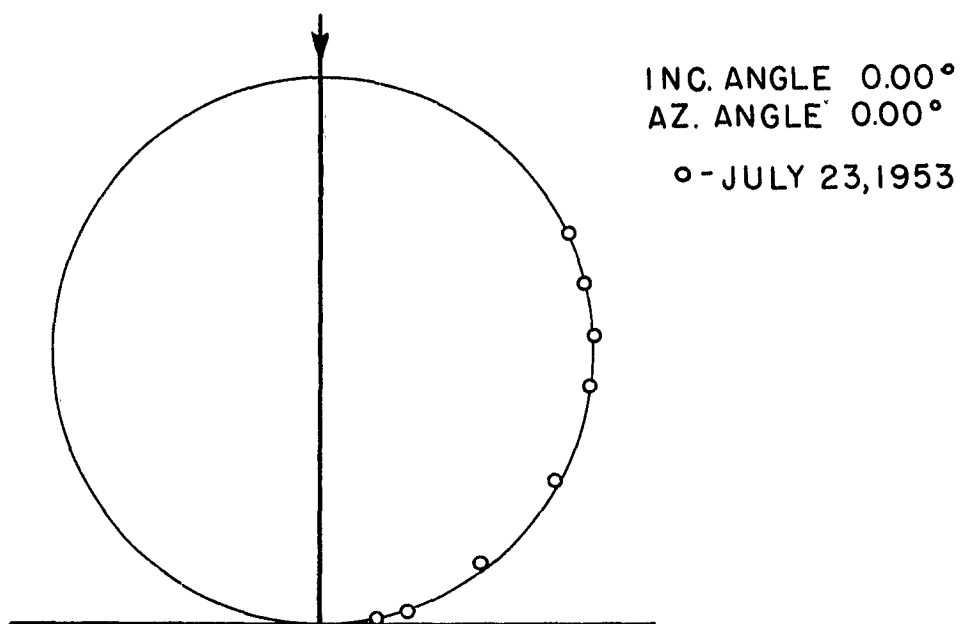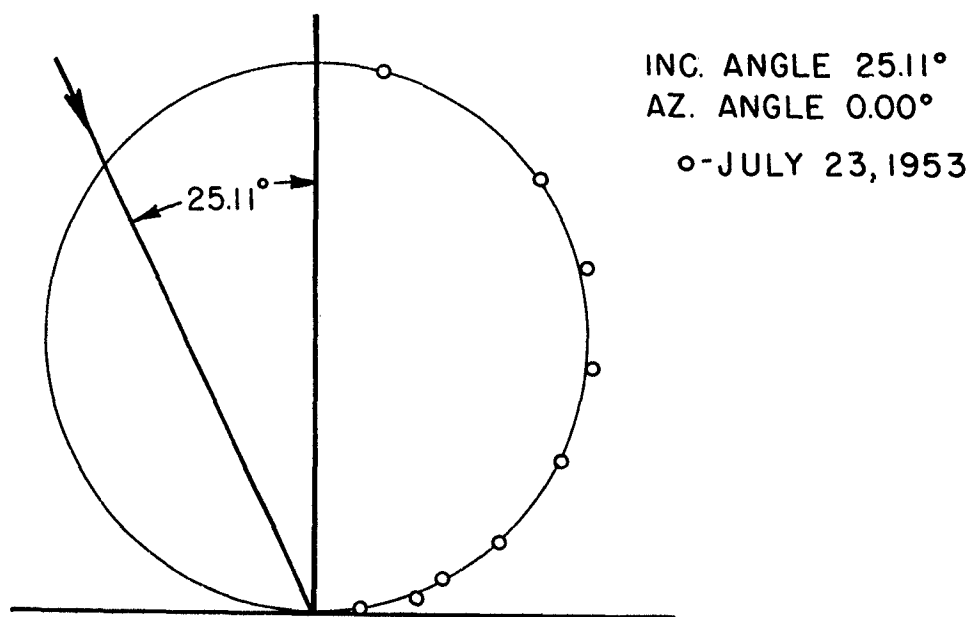
INC. ANGLE  0.00°
AZ. ANGLE  0.00°

○-JULY 23,1953

FIG.33  SCATTERING PLOT- POLISHED
GLASS SURFACE



INC. ANGLE 25.11°
AZ. ANGLE 0.00°

○-JULY 23,1953

25.11°

FIG. 34  SCATTERING PLOT- POLISHED
GLASS SURFACE

HYD 6555-150-0

INC. ANGLE 40.07°
AZ. ANGLE 0.00°

o – JULY 23, 1953

40.07°

FIG. 35 SCATTERING PLOT – POLISHED
GLASS SURFACE

INC. ANGLE 56.25°
AZ. ANGLE 0.00°

o – JULY 23, 1953

56.25°
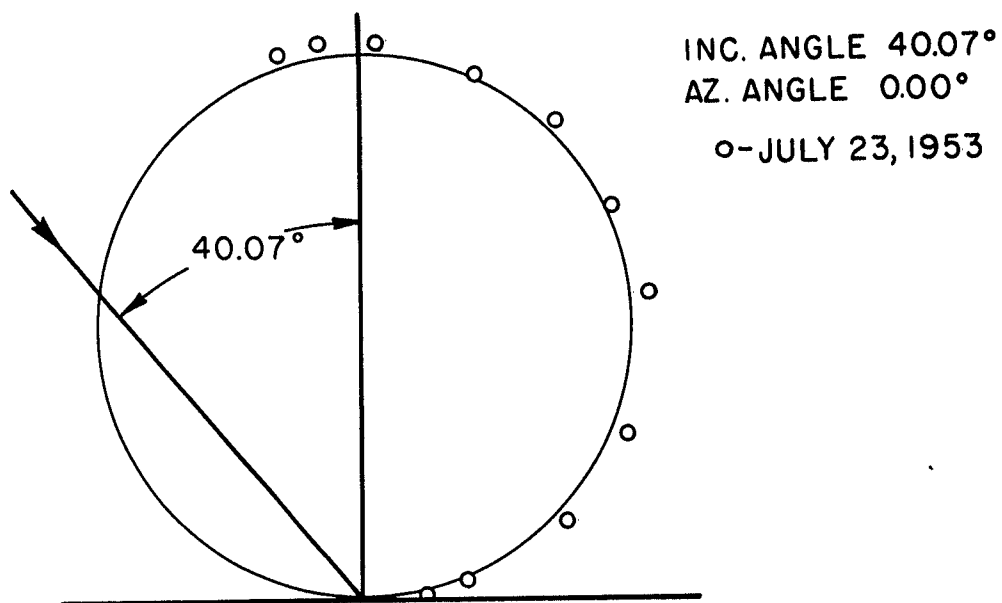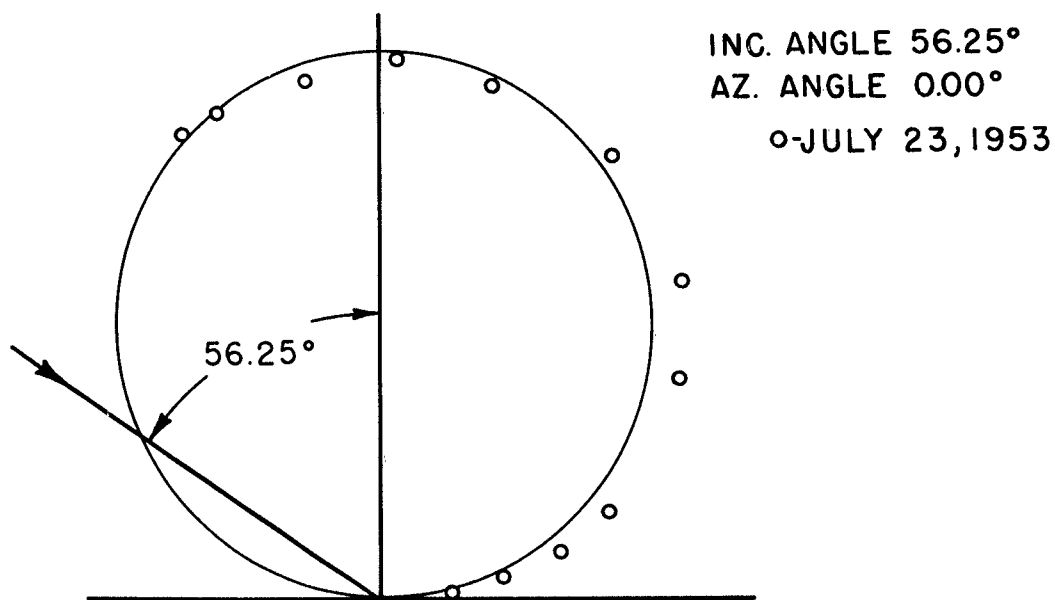
FIG. 36 SCATTERING PLOT – POLISHED
GLASS SURFACE

HYD 6556-150-0
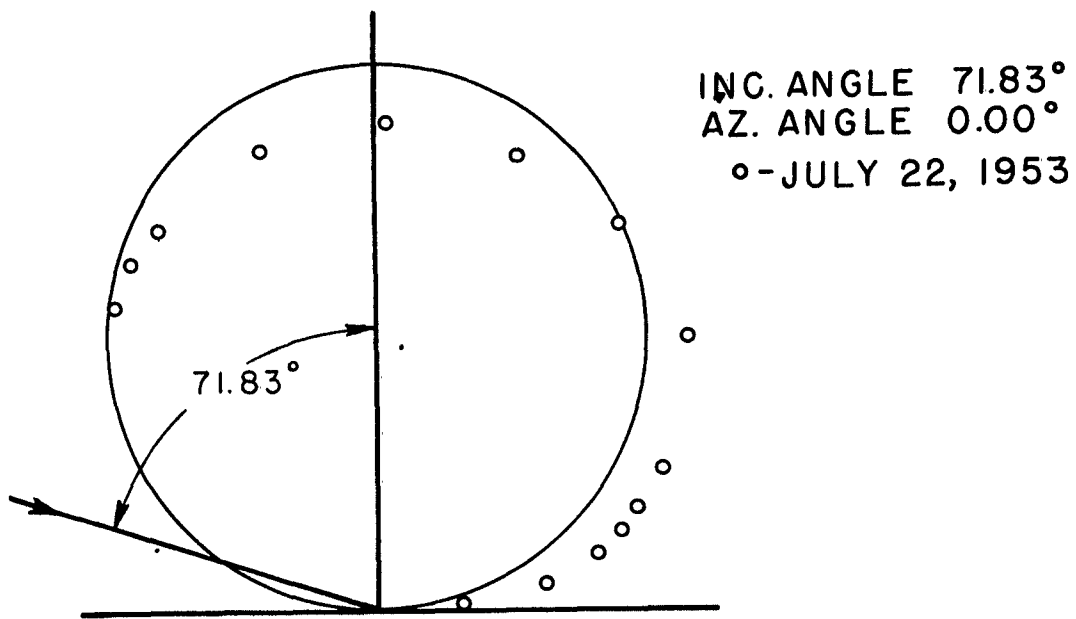
INC. ANGLE 71.83°
AZ. ANGLE 0.00°
o - JULY 22, 1953

71.83°

FIG. 37 SCATTERING PLOT - POLISHED
GLASS SURFACE



INC. ANGLE 79.62°
AZ. ANGLE 0.00°
o - JULY 22, 1953

79.62°

FIG. 38 SCATTERING PLOT - POLISHED
GLASS SURFACE

HYD 6557 - 150 - 0

INC. ANGLE 84.81°
AZ. ANGLE 0.00°
o - JULY 23, 1953

84.81°

TO 18.79
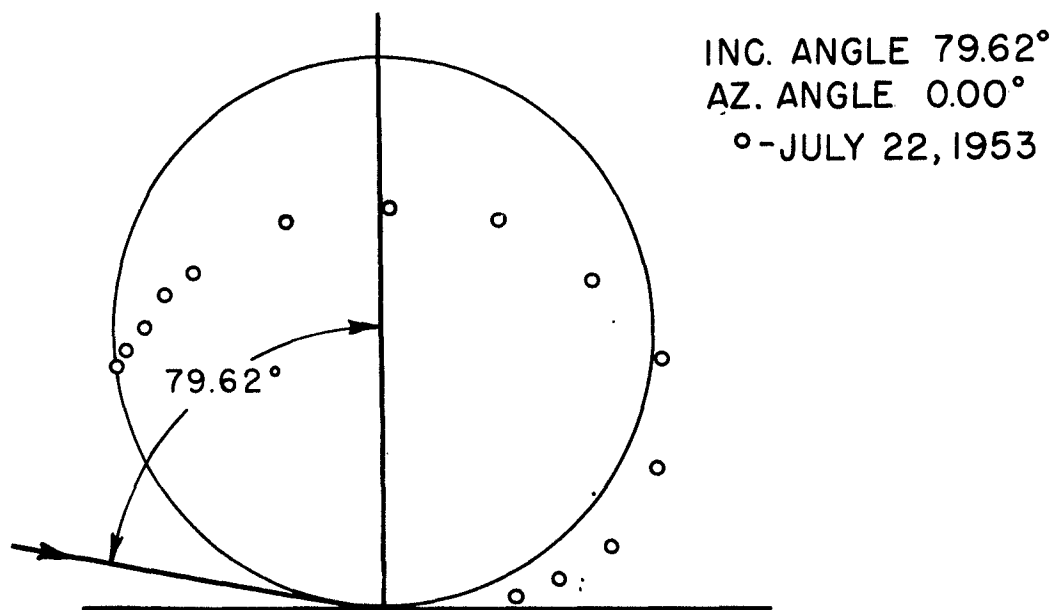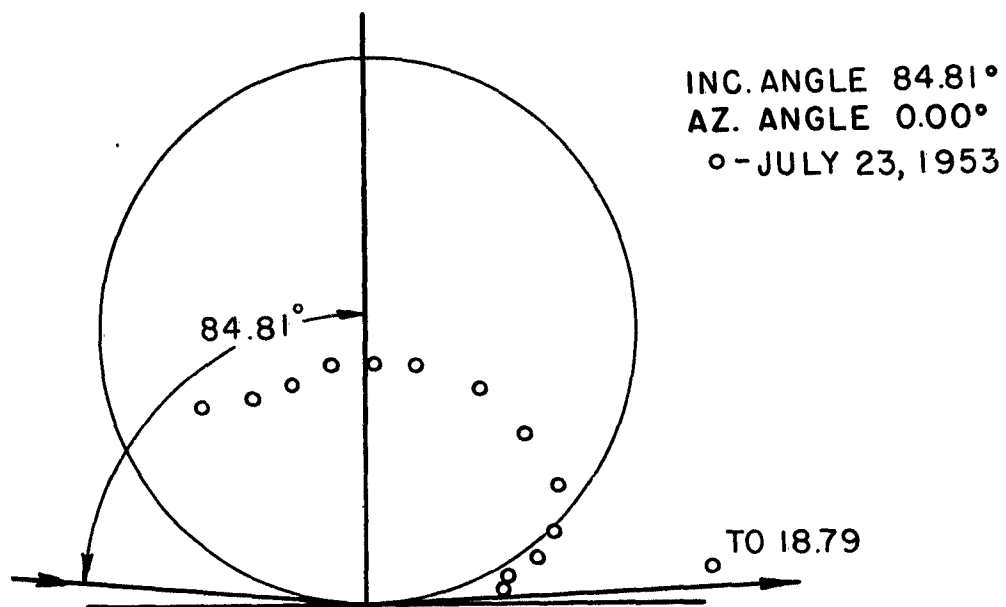
FIG. 39 SCATTERING PLOT - POLISHED
GLASS SURFACE



INC. ANGLE 90.00°
AZ. ANGLE 0.00°
o - JULY 23, 1953

TO 34 88
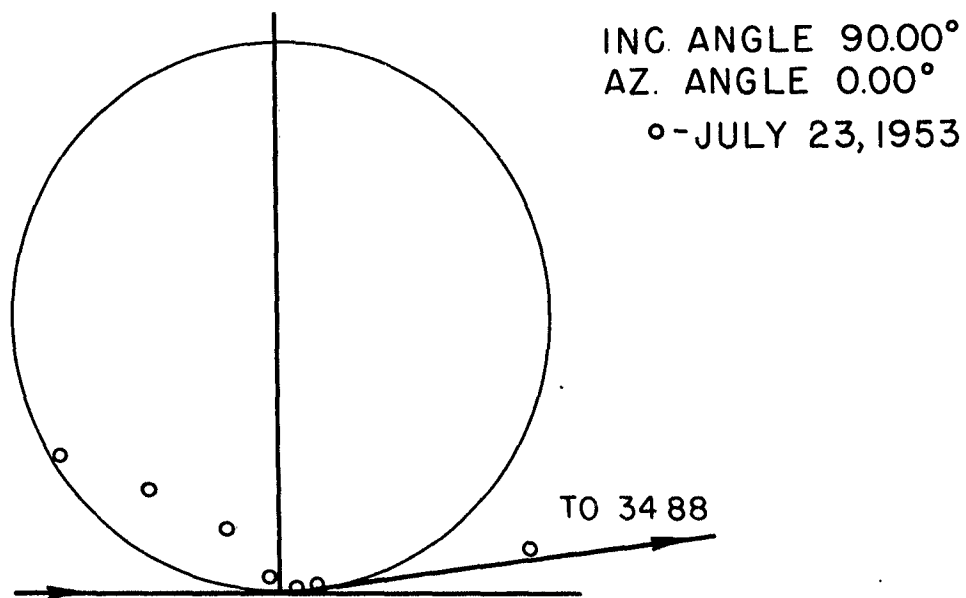
FIG. 40 SCATTERING PLOT - POLISHED
GLASS SURFACE

HYD 6558-150-0
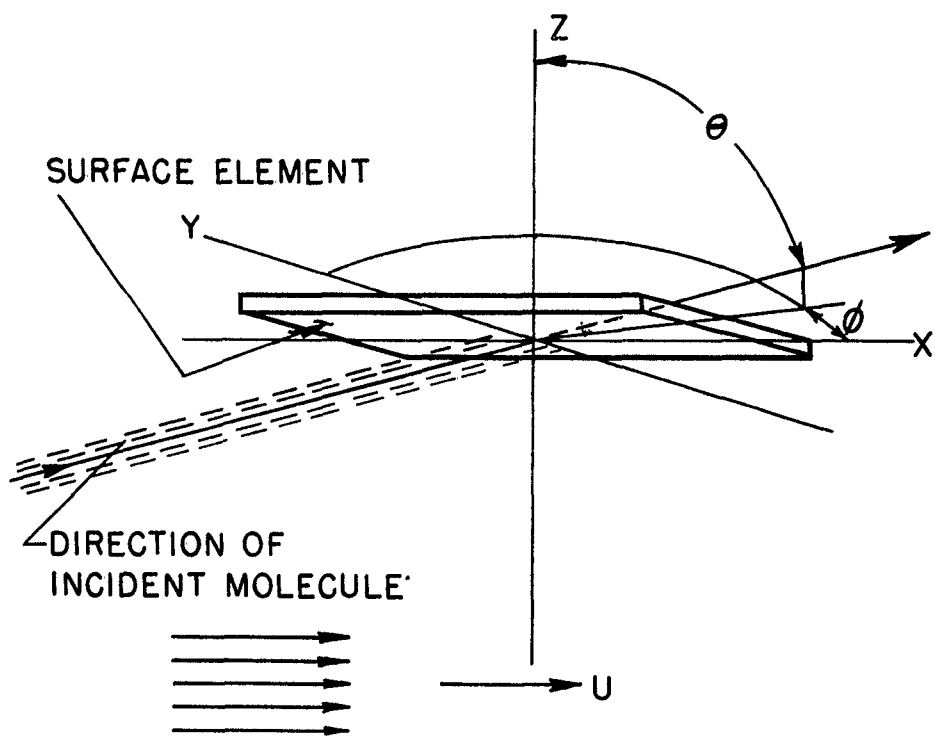
FIG.41 COORDINATE SYSTEM - INCIDENT
MOMENTUM CALCULATIONS
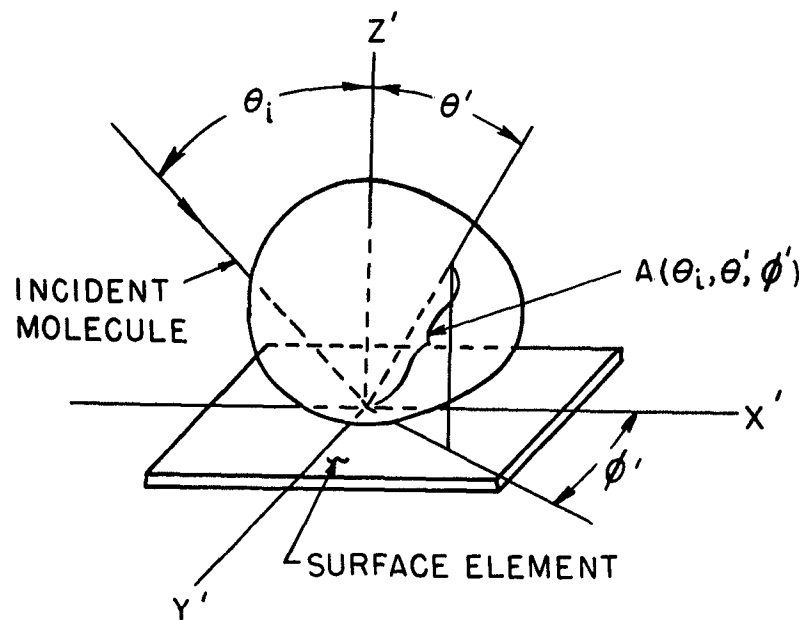
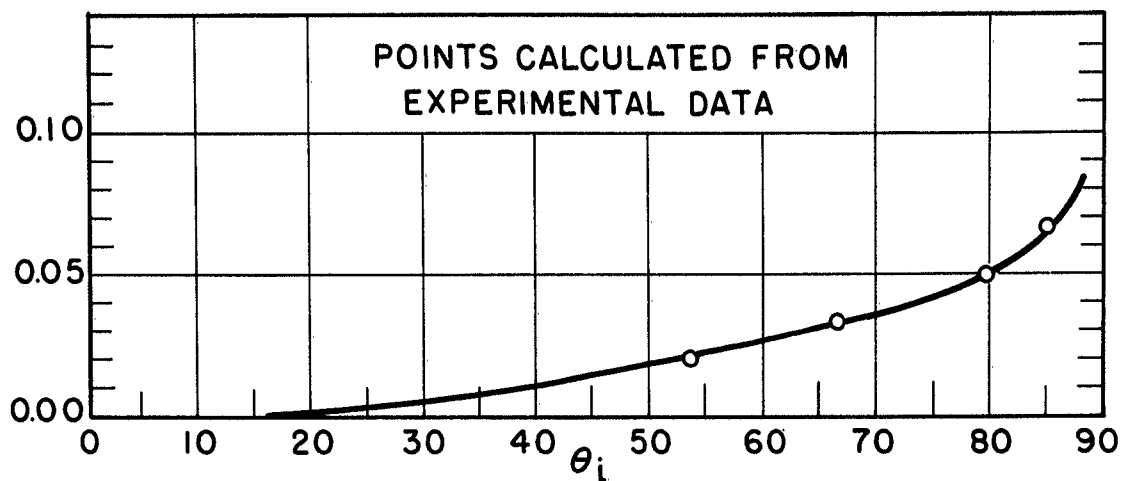FIG. 42    COORDINATE SYSTEM —
ISSUING MOMENTUM CALCLATIONS

HYD 6560-150-0
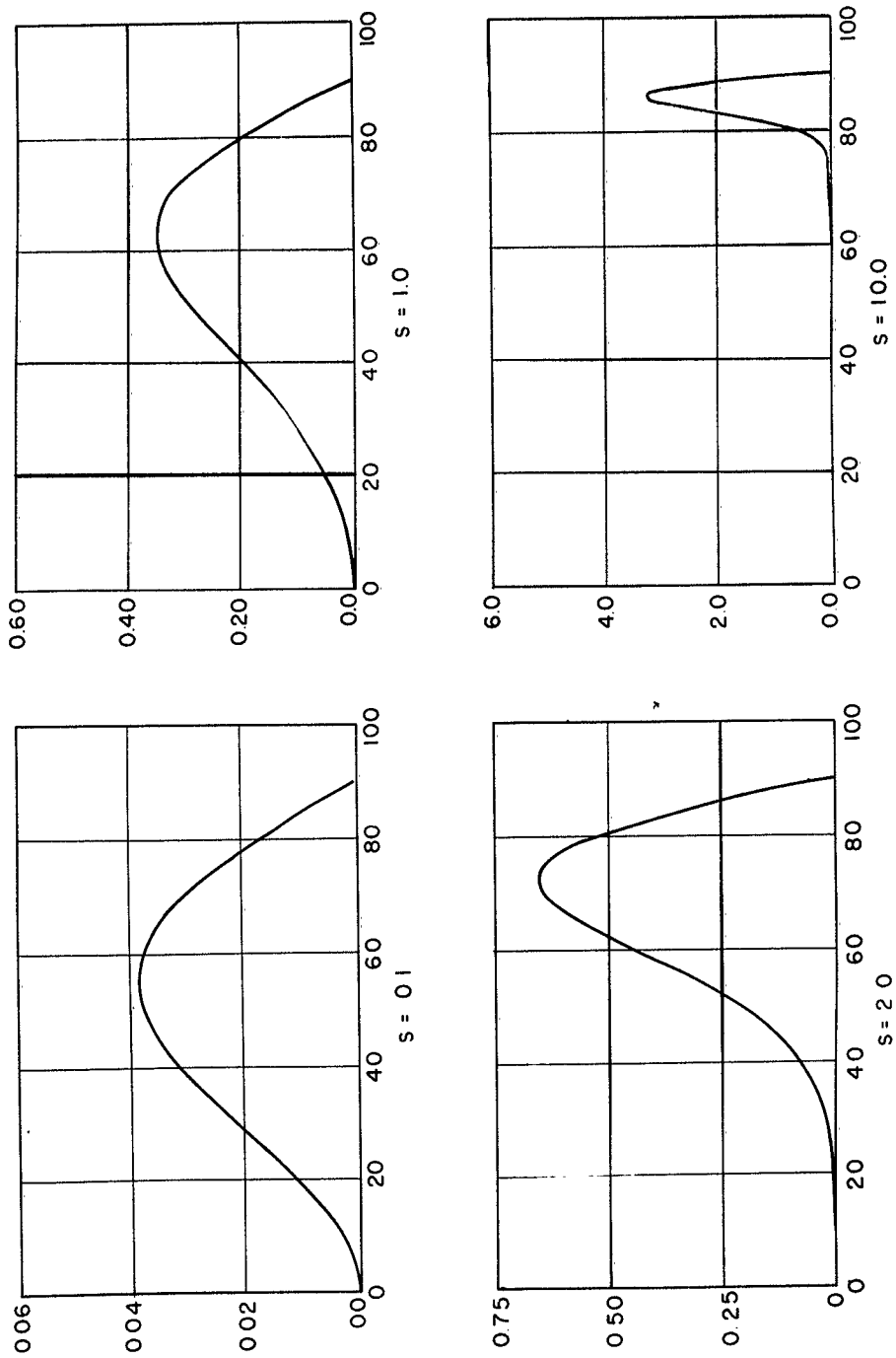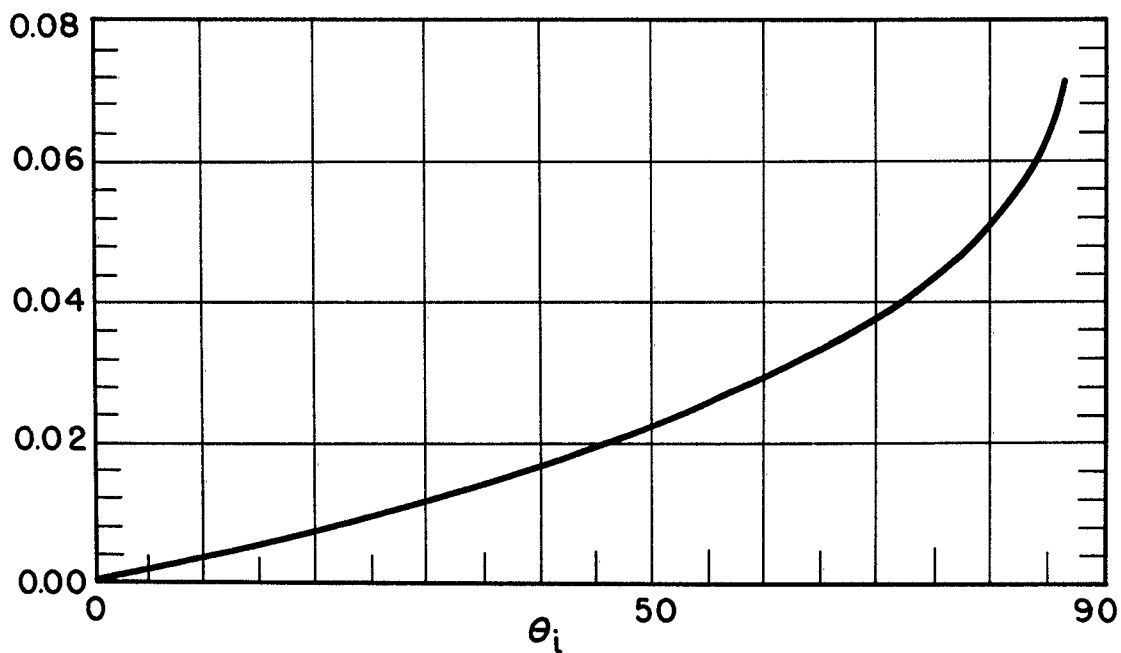
FIG. 43    $\dfrac{Gr(\theta_i)}{nm \, gr(\theta_i) \, Vm \, Vmr}$    AS A FUNCTION OF $\theta_i$ FOR $s = 0.1$, $1.0$, $2.0$ AND $10.0$

POINTS CALCULATED FROM
EXPERIMENTAL DATA

$gr(\theta_i)$ AS A FUNCTION OF $\theta_i$
FOR NITROGEN ON UNPOLISHED GLASS

$$\frac{gr(\theta_i)}{\sin\theta_i}$$ AS A FUNCTION OF $\theta_i$
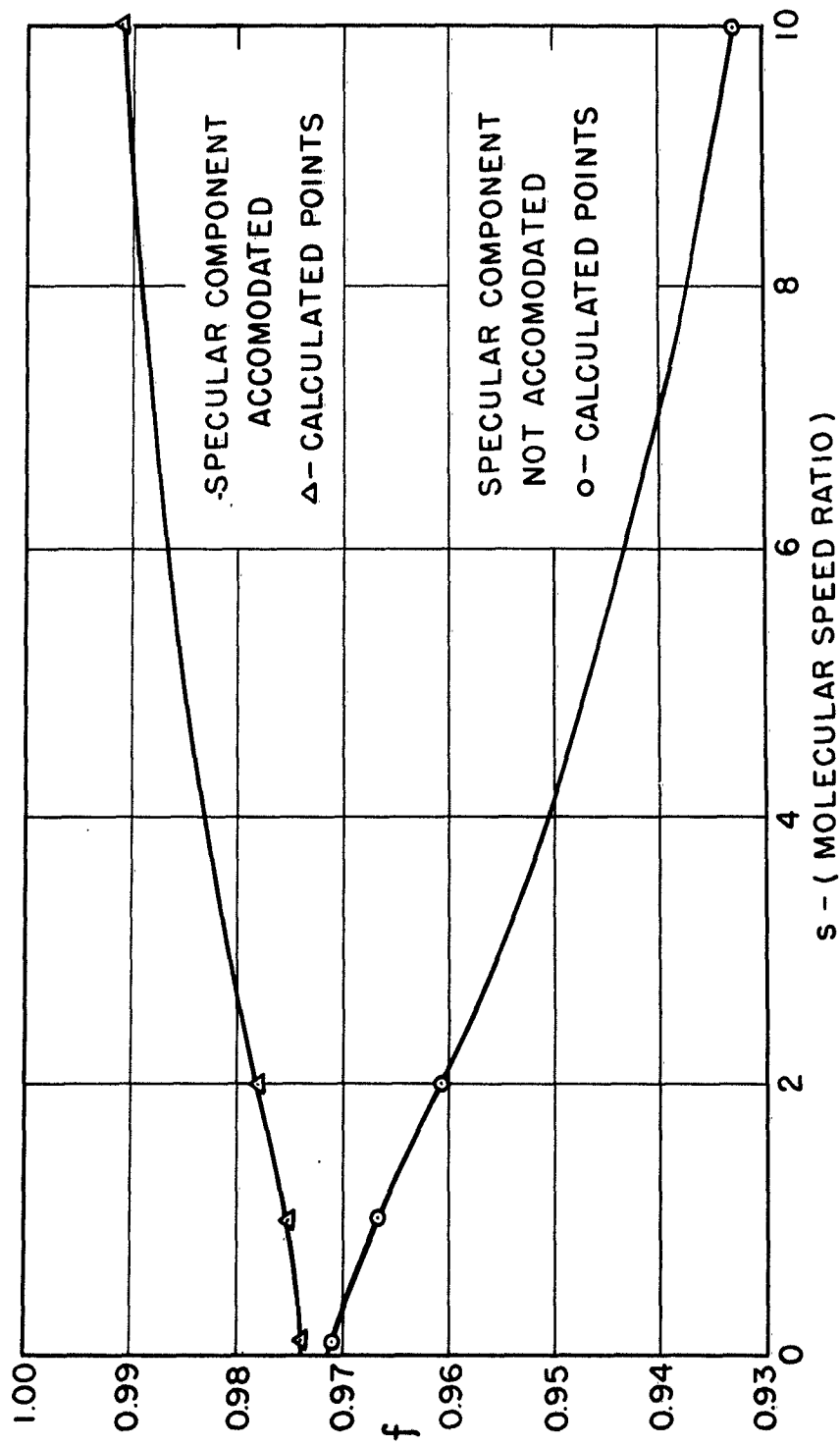FOR NITROGEN ON UNPOLISHED GLASS

FIG. 44

FIG. 45    f (COEFFICIENT OF SPECULAR REFLECTION) AS A
FUNCTION OF s (MOLECULAR SPEED RATIO) FOR
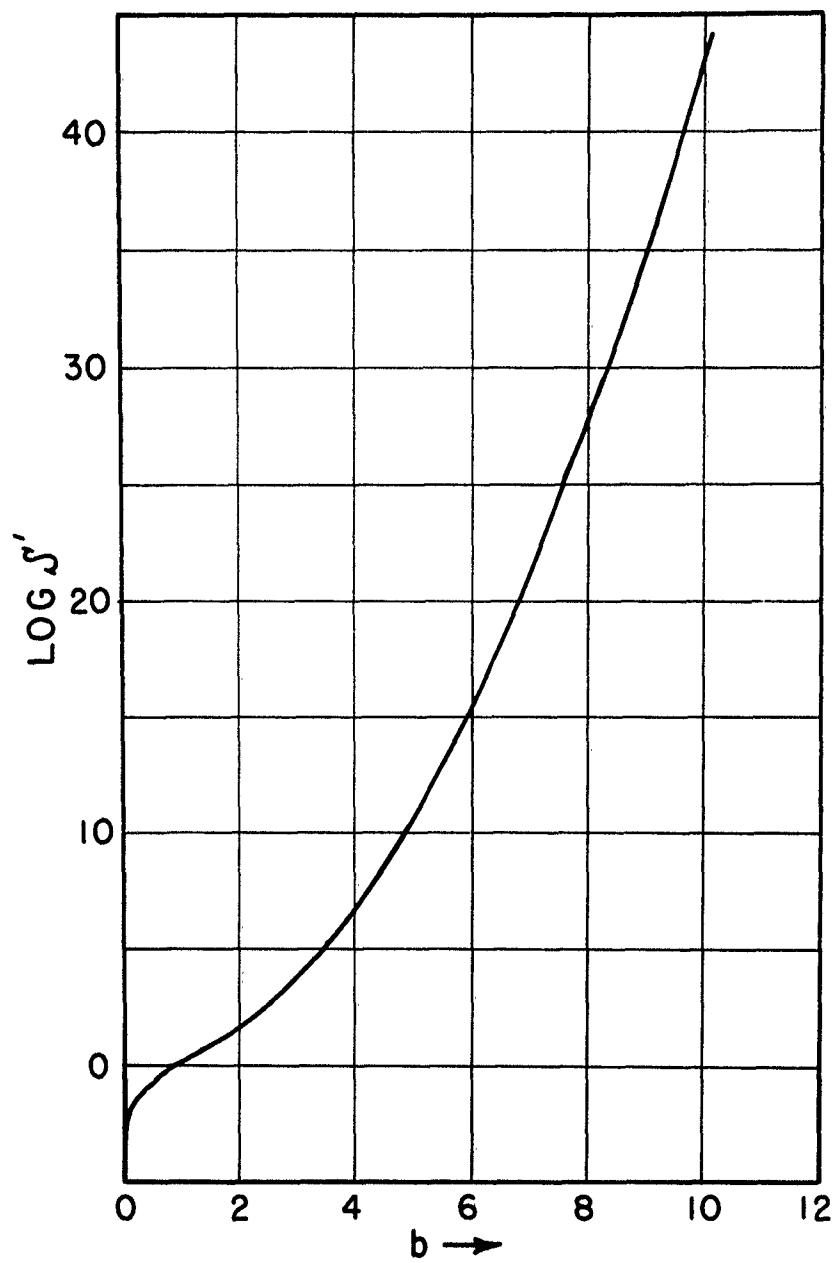NITROGEN ON UNPOLISHED GLASS

HYD 6563-150-0

FIG. 46 PLOT OF LOG $\mathcal{S}''$ AS A FUNCTION OF b
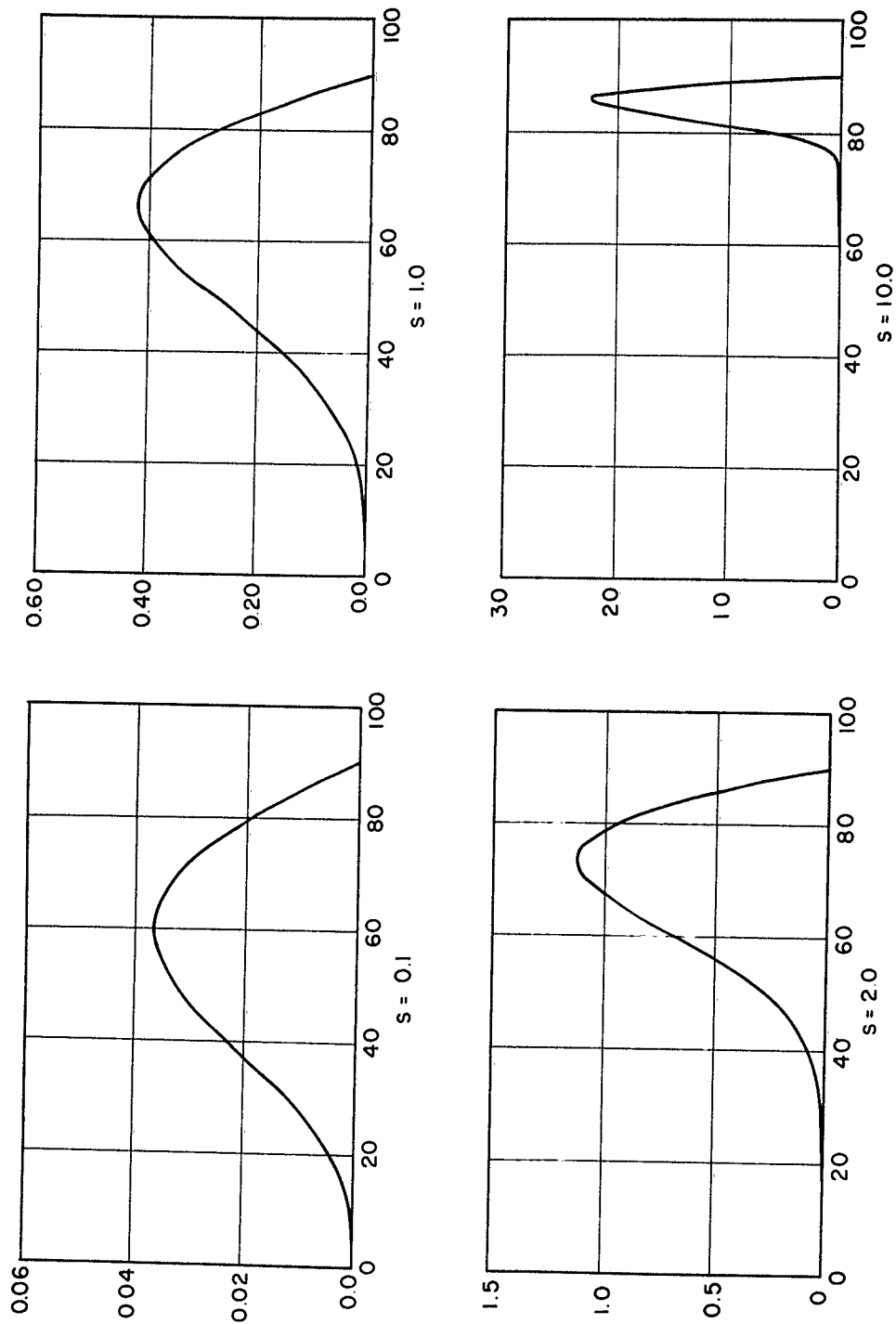
$$\frac{G_i(\theta_i)}{m\,n\,V\,m^2}$$ AS A FUNCTION OF $\theta_i$ FOR $s = 0.1, 1.0, 2.0,$ AND $10.0$
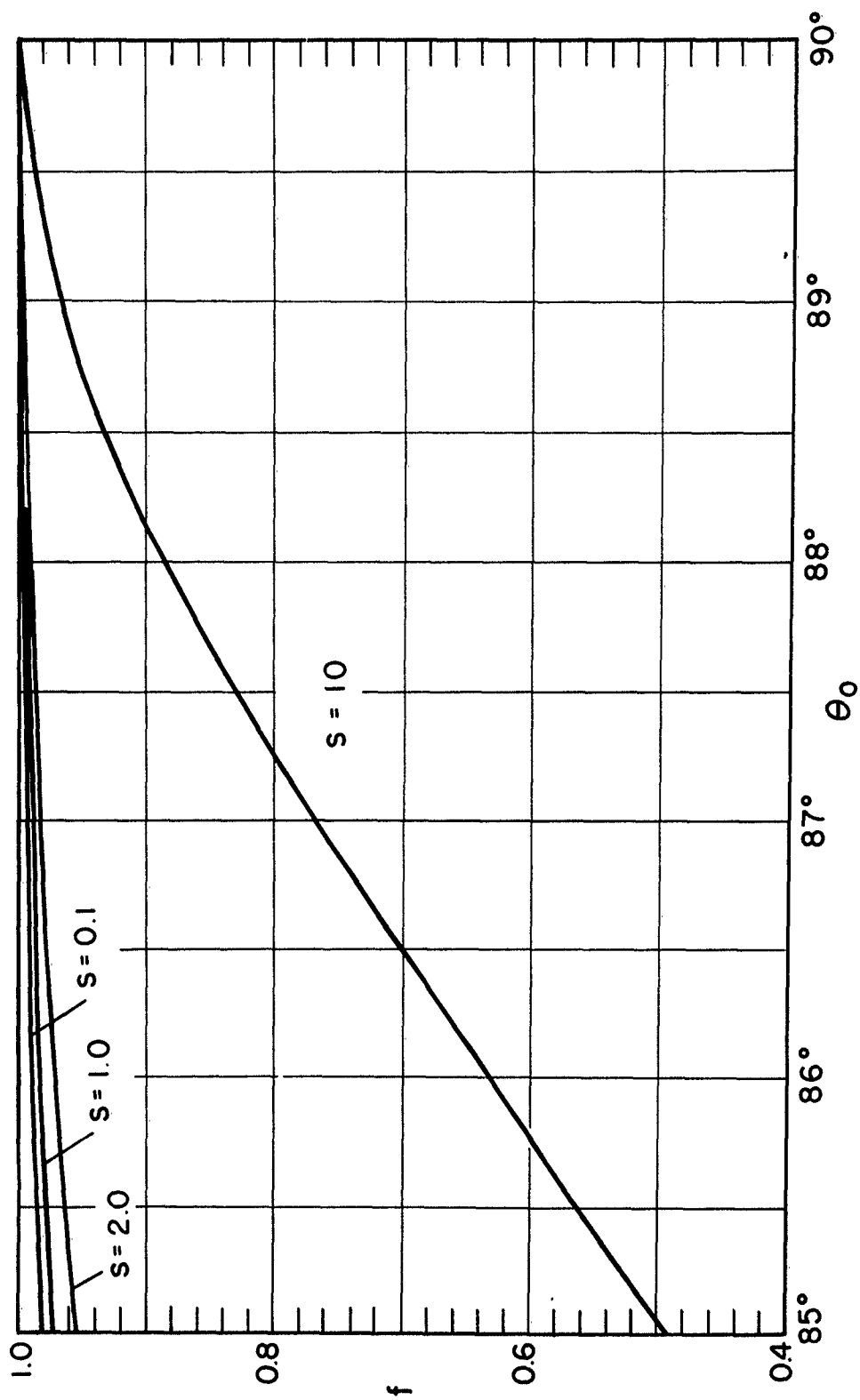
FIG. 47

FIG. 48 f AS A FUNCTION OF $\theta_o$ FOR VARIOUS
MOLECULAR SPEED RATIOS (s)
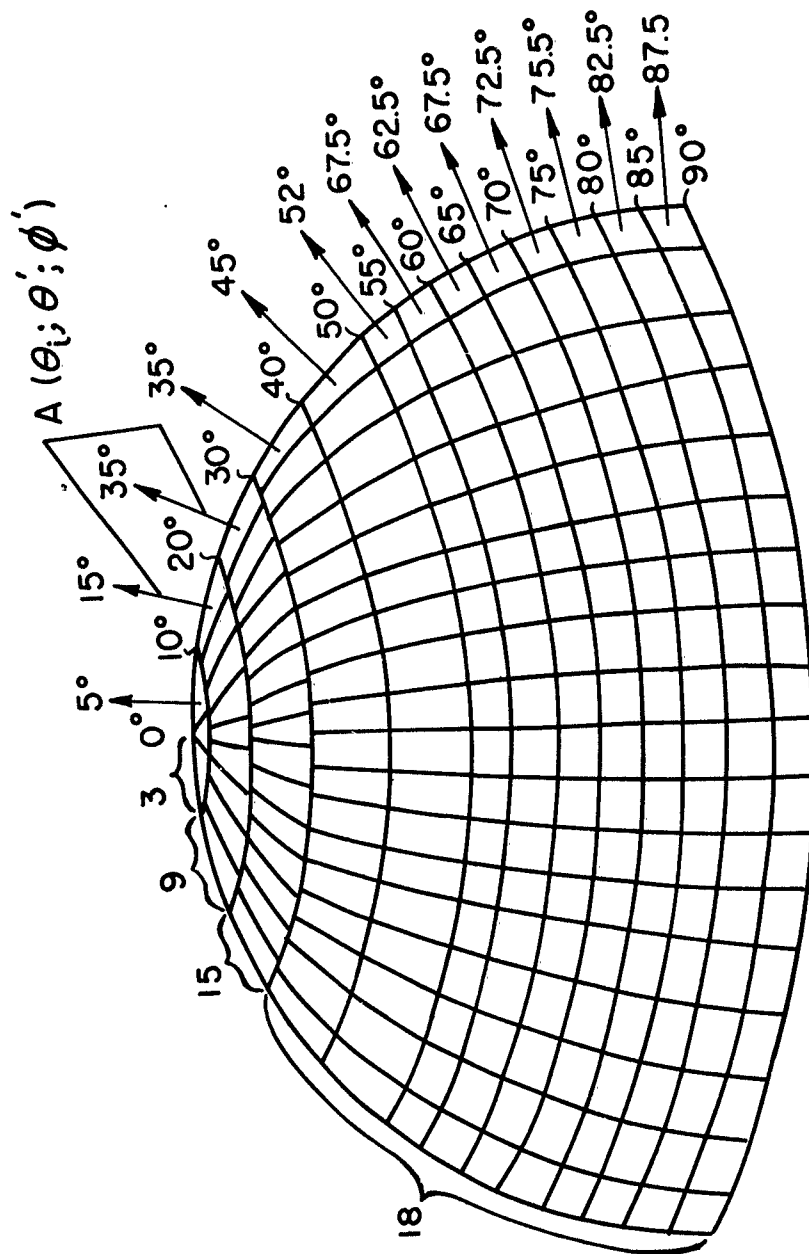
HYD 6566-150-0

FIG. 49 DIAGRAM OF UNIT HEMISPHERE AREA DIVISION FOR ISSUING MOMENTUM CALCULATIONS

HYD 6567-150-0

## DISTRIBUTION LIST FOR ONR TECHNICAL REPORTS

Director, Aeronautical Res, NACA, 1724 F St. NW, Wash. 25, D. C. (1)

Commanding General, Air Res. and Development Command, PO Box 1395, Baltimore (2)
    Maryland, Attn: OSR(RDRF)

Dr. Morton Alperin, Western Regional Office, Hdqrs, Air Res. & Development (1)
    Command, PO Box 2035, Pasadena 2, Calif.

Director, Ames Aeronautical Lab., NACA, Moffett Field, Calif. (1)

Applied Physics Lab., Johns Hopkins Univ., 8621 Georgia Ave, Silver Sprg, Md.(1)

Armed Forces Special Weapons Project, The Pentagon, Wash., 25, D. C. (1)

Commanding General, AF Cambridge Res. Cen., 230 Albany St, Attn: Dr. H. D. (1)
    Edwards, Geophysics Div., Cambridge 39, Mass.

Commanding Officer, Arnold Engr. Devel. Center, Tullahoma, Tenn., Attn: (1)
    ACGT, ACR & AEMCL

Mr. C. K. Bauer, Hermes Proj., General Electric Co, Schenectady 5, N.Y. (1)

Dr. Seymour Bogdonoff, James Forrestal Res. Cen, Princeton Univ, Princeton, (1)
    N. J.

Prof. W. S. Bradfield, Dept. of Aeronautical Engr. Univ. of Minnesota (1)
    Minneapolis, Minn.

Chief, Bureau of Aeronautics, Dept. of the Navy, Wash., 25, D.C. - Attn: (1)
    Aero and Hydro Branch

Chief, Bureau of Aeronautics, Dept. of the Navy, Wash. 25, D.C. - Attn: (1)
    Research Division

Bureau of Aeronautics Representative, USN, Central District, Wright-Patter- (1)
    son AFB, Dayton, Ohio, Attn: WCOWS-3, James G. Law.

Chief, Bureau of Ordnance, Dept. of the Navy, Wash. 25, D.C. - Attn: Re9a (1)

Dr. Francis H. Clauser, Johns Hopkins Univ. Dept. of Aeronautical Engr., (1)
    Baltimore 18, Md.

Commanding Officer and Director, David Taylor Model Basin, Wash. 7, D.C. - (1)
    Attn: Technical Library

Chief of Naval Res., Dept. of the Navy, Wash. 25, D.C. - Attn: Code 438 (3)

Chief of Staff, Hdqrs USAF, Directorate of Research and Development, Wash. (1)
    D.C. - Attn: AFDRD-AC2

Chief, Documents Service Center, Armed Services Technical Information (2)
    Agency, Knott Bldg., Dayton 2, Ohio (1 reproducible copy)

Prof. Fred S. Eastman, Univ. of Wash., Dept. of Aero. Engr., Seattle 5, Wash.(1)

Dr. I. Estermann, Code 419, Office of Naval Research, Wash., D.C. (1)

Prof. K. O. Friedrichs, New York Univ. Inst. for Math. and Mechs., 45 (1)
    Astor Place, New York, N. Y.

Director, Jet Propulsion Lab., Calif. Inst. of Tech., Pasadena, Calif. (1)

Dr. J. M. Jones, Engr. Res. Inst., Univ. of Mich., Ann Arbor, Mich. (1)

Prof. A. Kantrowitz, Graduate School of Aeronautical Engr., Cornell Univ. (1)
    Ithaca, New York.

Dr. J. Kaplan, Dept. of Physics, Univ. of Calif. at Los Angeles, L.A., Calif.(1)

Prof. J. H. Keenan, Mass. Inst. of Tech., Mechanical Engr. Dept, Cambridge (1)
    Mass.

Prof. M. Z. Krzywoblocki, Univ. of Illinois, Urbana, Illinois      (1)

Dr. A. M. Kuethe, Dept. of Aero. Engr., Univ. of Mich, Ann Arbor, Mich.      (1)

Dr. A. R. Kuhlthau, Univ. of Virginia, Dept. of Physics, Charlottesville, Va.(1)
    VIA:  Naval Inspector of Ordnance, Applied Physics Lab., Johns Hopkins
        Univ., Silver Spring, Md.

Director, Langley Memorial Aeronautical Lab., NACA, Langley Field, Virginia      (1)

Prof. Lester Lees, Dept. of Aero. Engr., Calif. Inst. of Tech., Pasadena      (1)

Director, Lewis Flight Propulsion Laboratory, NACA, Cleveland, Ohio      (1)

Prof. H. Lewy, Applied Math. Group, Math. Dept., Univ. of Calif., Berkeley      (1)

Dr. James E. Lipp, The Rand Corp., 1500 Fourth St., Santa Monica, Calif.      (1)

Prof. J. R. Markham, Mass. Inst. of Tech., Cambridge 39, Mass.      (1)

Dr. C. B. Millikan, Guggenheim Aeronautical Lab., Calif. Inst. of Tech.      (1)
    Pasadena, California

Dr. Henry T. Naganatsu, Director, Hypersonic Wind Tunnel, Calif. Inst. of      (1)
    Tech., Pasadena 4, Calif.

Commanding Officer, U.S. Naval Ordnance Test Station, Inyokern, China Lake      (1)
    Calif. - Attn:  Technical Library

Director, Naval Research Lab., Wash. 20, D. C. - Attn:  Code 2020      (9)

Commander, Naval Ordnance Lab., White Oak, Silver Spring 19, Md, Attn:      (1)
    Aeroballistic Res. Dept.

Director, Office of Naval Research, 346 Broadway, New York 13, N. Y.      (1)

Director, Office of Naval Research, 844 North Rush St., Chicago 11, Ill.      (1)

Director, Office of Naval Research, 1000 Geary St., San Francisco 9, Calif.      (2)

Director, Office of Naval Research, 1030 East Green St., Pasadena 1, Calif.      (1)

Officer in Charge, Office of Naval Research, Navy #100, FPO, New York, N.Y.      (3)

Radiation Lab., Univ. of Calif., Berkeley 4, Calif. - Attn:  R. Wakerling      (1)

Chairman, Research and Development Board, The Pentagon, Wash. 25, D.C.      (1)
    Attn:  Information Requirement Board, Room 3D-1075

Mr. R. H. Shick, Consolidated Vultee Aircraft Corp., San Diego 12, Calif.      (1)

Mr. Joseph Sternberg, Ballistics Res. Lab., Ordnance Dept. Aberdeen, Md.      (1)

Sverdrup & Parcel, Inc., Consulting Engrs., Syndicate Trust Bldg, St. Louis      (1)

Dr. Theodore Theodorsen, Univ. of Maryland, Bldg. J, Rm. 314, College Pk, Md.(1)

Dr. F. L. Wattendorf, A.G.A.R.D. of NATO, APO 58, c/o PM, New York      (1)

Western Coordination Office, NACA, 7660 Beverly Blvd. L. A., 36, Calif.      (1)

Dr. E. P. Williams, Missiles Div., Rand Corp., 1500 Fourth St., Santa      (1)
    Monica, California

Wright Air Development Center, Wright-Patterson Air Force Base, Dayton, Ohio (2)
    Attn: WCRRS-3 (1)          Attn: MCIDXE (1)

Dr. J. H. Marchant, Div. of Engr., Brown Univ., Providence 12, Rhode Island  (1)